MASTERARBEIT | MASTER'S THESIS

Titel | Title

The impact of leaving group variation on the stability and anticancer potential of 4-phenyl-thiazole rhodium(III) complexes.

verfasst von | submitted by

Claudia Heufler BSc

angestrebter akademischer Grad | in partial fulfilment of the requirements for the degree of

Master of Science (MSc)

Wien | Vienna, 2025

Studienkennzahl lt. Studienblatt | Degree programme code as it appears on the student record sheet:	UA 066 862
Studienrichtung lt. Studienblatt | Degree programme as it appears on the student record sheet:	Masterstudium Chemie
Betreut von | Supervisor:	Assoz. Prof. Mag. Dr. Christian Kowol
Mitbetreut von | Co-Supervisor:	Dipl.-Ing. Dr. Wolfgang Kandioller

A zia Leda.

Acknowledgments

I would like to thank Dr. Dipl.-Ing. Wolfgang Kandioller for being a great supervisor and for his guidance throughout this internship and my previous studies at the University of Vienna. The work in his group has shaped both my skillset and my view on research overall. I would also like to thank Assoc. Prof. Dr. Christian Kowol for allowing me to work in this group and providing me with the resources needed to complete this thesis.

I would like to extend my gratitude to the NMR, MS, microanalytical laboratory, cell culture facility, and the X-ray analysis teams at the University of Vienna for sample analysis. Special thanks to Steven for providing great insight into crystallography and fonts.

Thank you to all colleagues in and beyond the Institute of Inorganic Chemistry for the help and the laughter, creating a great work environment I would never hesitate to come back to.

Thank you to my colleagues in Lab 6. Paul has been of great support and guidance since my Bachelors studies and has taught me the ins and outs related to the practical work of this topic as well as the importance of boxing gloves in an office. Alex has always offered great advice, expertise and bad jokes whenever needed. Thank you to Judith and Joni for the great exchange of thoughts and ideas and the emotional support over the last three years.

Thank you Sarah, my first friend at the University of Vienna, for accompanying me over the last five years through highs and lows. Thank you to all my movie night friends. Pushing each other to work hard and allowing us to lean on each other when needed was essential for completing my studies.

Thank you to my closest friends, whom I consider family. Gea, Hannah, Kathe, Michi, Maxi and Vale. Thank you for always believing in me and picking me back up when I needed it the most, and for always keeping me in check. Thank you Chiara, for being a great roommate, therapist, tennis partner, and friend, and thank you for never keeping me in check.

Thank you to my parents, Sara and Klaus, for your incredible emotional and financial support over the course of my whole life. Thank you for inheriting me and bearing my temper. Thank you to my sister Silvia for reminding me of the vastness of life and never to limit myself.

Abstract

Accounting for nearly one in six deaths worldwide, cancer is of great societal concern, and research for novel therapies is pivotal. The diversity of neoplastic disease makes the search for treatment options particularly difficult. Chemotherapy offers a broad range of anticancer therapeutics with various modes of action. Metal-based chemotherapeutics possess unique properties due to the metal centers' charge variation, structural variety, redox potential, and ligand interaction, and hence offer a great reference point for further research.

This thesis focuses on the development of novel rhodium(III) based organometallic compounds bearing a 4-(4-mesyl)phenylthiazole bidentate ligand. Osmium(II) and ruthenium(II) compounds of the same genre have already shown great promise in anticancer activity.

The precursor chlorido-complex was synthesized and the leaving group exchanged, resulting in five novel charged complexes bearing either a *P*- or *N*-donor monodentate ligand. PTA, triethylphosphine, triphenylphosphine, pyrazole, and isoquinoline were introduced as leaving groups to assess their effect on the solubility, stability, and anticancer activity of the compound, crucial factors for biological application. All complexes were successfully synthesized and obtained in elemental analysis purity. The compounds were characterized *via* NMR spectroscopy, mass spectrometry, and crystals suitable for X-ray diffraction analysis were obtained. The complexes bearing a *P*-donor leaving group (**I**-**III**) were isolated with chloride as counterion, whereas the *N*-donor complexes (**IV** and **V**) with PF_6^-, resulting in lesser solubility for the latter. All complexes were stable in 10% DMSO in PBS 7.4 pH over 24 h and MTT assays were performed to assess the anticancer potential of the synthesized compounds. The obtained results emphasize the importance and impact of the leaving group on the physico-chemical and cytotoxic properties of organometallic complexes.

Zusammenfassung

Krebs ist weltweit für beinahe jeden sechsten Todesfall verantwortlich und die Forschung nach neuartigen Therapien bleibt weiterhin von zentraler gesellschaftlicher Bedeutung. Die biologische Vielfalt neoplastischer Erkrankungen macht die Suche nach Behandlungsmöglichkeiten besonders schwierig. Chemotherapie bietet eine breite Palette an Medikamenten mit unterschiedlichen Wirkmechanismen. Metallbasierte Chemotherapeutika besitzen aufgrund ihrer unterschiedlichen Eigenschaften, wie verschiedene Oxidationsstufen, strukturelle Flexibilität, Redoxpotentiale und ihrer Liganden-Interaktion, einzigartige Möglichkeiten und bieten dadurch einen vielversprechenden Anhaltspunkt für weitere Forschungen.

Diese Arbeit konzentriert sich auf die Entwicklung neuartiger Rhodium(III) basierter metallorganischer Verbindungen, die einen zweizähnigen 4-(4-Mesyl)phenylthiazol-Liganden besitzen. Osmium(II)- und Ruthenium(II)verbindungen derselben Familie haben sich schon als potentielle, vielversprechende krebsbekämpfende Verbindungen erwiesen.

Der Vorläufer-Chloridokomplex wurde erfolgreich synthetisiert und die Abgangsgruppe ausgetauscht, was zu fünf neuen, geladenen Komplexen führte, die entweder einen monodentaten *P*- oder *N*-donor -Liganden tragen. PTA, Triethylphosphin, Triphenylphosphin, Pyrazol und Isochinolin wurden als Abgangsgruppen eingeführt, um ihre Auswirkungen auf die Löslichkeit, Stabilität und Zytotoxizität der Verbindung zu beobachten. Alle Komplexe wurden erfolgreich synthetisiert und mittels Elementaranalyse, NMR-Spektroskopie, Massenspektrometrie und Röntgenbeugungsanalyse charakterisiert. Die Komplexe, die eine *P*-donor-Liganden tragen (**I**-**III**), wurden mit Chlorid-als Gegenion isoliert, während Komplexe die eine *N*-donor-Abgangsgruppe besitzen (**IV** und **V**) als PF_6^- Salze hergestellt wurden, was zu einer geringeren Löslichkeit der letzteren führt. Alle Komplexe wurden in 10 % DMSO in PBS 7,4 pH auf ihre Stabilität untersucht und zeigten keine Zersetzung über 24 Stunden. Zur Bestimmung des krebshemmenden Potenzials der synthetisierten Verbindungen wurden MTT-Tests durchgeführt. Die Ergebnisse unterstreichen die Bedeutung und den Einfluss der Abgangsgruppe auf die physikalisch-chemischen, als auch der cytotoxischen Eigenschaften von metallorganischen Komplexen.

1. Introduction

Cancer is an all-encompassing term to describe a group of genetic diseases caused by the uncontrolled cell proliferation and ultimately invasion of neighboring tissue and formation of metastases.[1] Two types of genes responsible for cancer formation can be differentiated: oncogenes and tumor suppressor genes. Oncogenes mutate to promote uncontrolled cell proliferation, and tumor suppressor genes mutate to the loss of control of the cell growth. At the basis of the progression of cancer are molecular alterations of the genome. This evolutionary process results in a broad genetic diversity of mutations within one tumor. There are over 277 distinct types of cancer with a variety of distinguished features. [1]

1.2 Incidence and mortality

Cancer remains one of the leading causes of death worldwide, alongside cardiovascular diseases, accounting for nearly one in six deaths per year, amounting to almost 10 million deaths in 2020.[1] These numbers are predicted to increase in future.[2] The five most common types of cancer in terms of absolute numbers in 2022 were lung, breast, colorectum, prostate and stomach cancer, with lung cancer accounting for the most deaths overall (Figure 1, left).

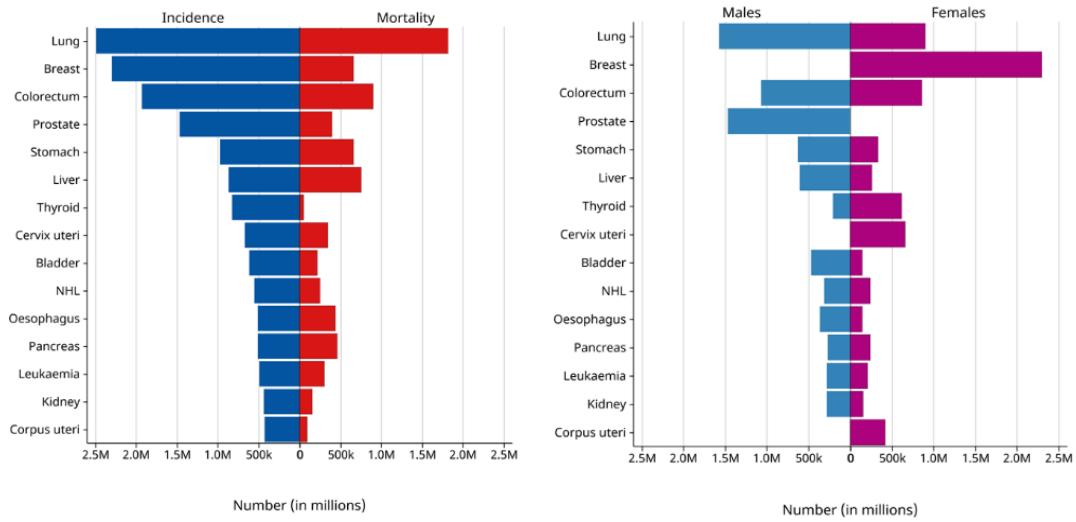

Figure 1: Worldwide cancer incidence and mortality (left) and worldwide cancer incidence by gender (right) in absolute numbers as of 2022.[3]

Tobacco use is considered the main cause of cancers as far as external factors, alongside alcohol consumption and a poor diet and little physical activity resulting in a high body mass index.[1] It is believed these lifestyle factors are more likely to occur in males, therefore increasing the risk of cancer, as reflected in the absolute incidence numbers by gender (Figure 1, right). However, more recent studies have shown external factors to not be the only, nor necessarily the main reason for this cancer incidence gender disparity.[4] With the exception of thyroid and gallbladder cancer, men are more likely to develop cancer at shared anatomic sites.[3] Jackson et al., 2022[4] found this trend remained even after accounting for carcinogenic exposure and the main, above mentioned, risk behaviors. This suggests sex-related biological mechanisms, such as physiological differences in estrogen or testosterone as well as a stronger immune response in women, epigenetic differences and differences in mutation burden, be the main source of the incidence gap.[4]

1.3 Hallmarks of cancer

Neoplastic diseases are incredibly diverse. In an attempt to organize the principles behind cancer Hanahan and Weinberg first established six hallmarks of the disease in 2000.[5] The first proposed hallmarks describe the alterations in cell physiology acquired during tumor development providing a basis for understanding cancer biology.[1-3]

Sustaining proliferative signaling: Cancer cells are independent from regular growth factor signaling. Mutations sustain chronic proliferation.

Evading growth suppressors: Cancer cells do not respond to growth inhibitory signals. Mutations sustain uncontrolled proliferation and hinder homeostasis.

Enabling replicative immortality: Cancer cells avoid senescence and crisis exhibiting unlimited replicative potential, because they maintain the length of their telomers.

Activating invasion and metastasis: Cancer cells can spread throughout the body due to a succession of cell-biologic changes altering cell-to-cell adhesion molecules.

Inducing or accessing vasculature: Cancer cells regulate the growth of new blood vessels to “feed” growing tumors and promote their expansion.

Resisting cell death: Cancer Cells avoid apoptosis by suppressing proapoptotic triggers and stress.

These six hallmarks were revisited by Hanahan and Weinberg in 2011[6] to include two new hallmarks originally proposed as emerging hallmarks and now considered to be part of the core hallmarks of cancer.[7] As well as two enabling characteristics to address the complex mechanisms of cancer pathogenesis and the acquisition of the hallmark capabilities.

Avoiding immune destruction: Cancer cells evade immune surveillance by interfering with the regular immune response to avoid immunological destruction, in particular by T and B lymphocytes, macrophages, and natural killer cells.

Deregulating cellular metabolism: Cancer cells modify the cellular metabolism in order to most effectively support neoplastic proliferation.

Tumor-promoting inflammation (enabling characteristic)**:** Tumors contain innate inflammatory immune cells, which can support angiogenesis, invasion and other hallmarks, resulting in cancer promoting consequences.

Genome instability and mutation (enabling characteristic)**:** Cancer cells occur due to genetic alterations. Genome instability is promoted by faulty DNA repair pathways.

More recently two new emerging hallmarks and two enabling characteristics were added including the importance of the tumor microenvironment.[7]

Unlocking phenotypic plasticity (emerging hallmark)**:** Cancer cells evade or pass regular cellular differentiation, allowing to change their state in support of tumor promotion and progression.

Non-mutational epigenetic reprogramming (enabling characteristic)**:** Epigenetic modifications, such as DNA methylation or histone modifications, which do not affect the underlying DNA sequence, may further the acquisition of other hallmark capabilities in particular the above mentioned phenotypic plasticity.

Polymorphic microbiomes (enabling characteristic)**:** Microbiota found in various tissues may promote the development of hallmark capabilities enhancing and interfering with genome instability and tumor-promoting inflammation.

Senescent cells (emerging hallmark): Senescent cells of various origins release bioactive molecules known as the senescence-associated secretory phenotype (SASP), contributing to the growth and malignant progression of cancer.

1.3 Cancer Therapy

As the concern and social impact of this disease stay persistent, the interest and research in treatment options continue to increase. The type of therapy employed strongly depends on the type and stage of the cancer to be treated. Usually not only one treatment option, but rather a combination of them, is employed as adjuvant or neoadjuvant therapy. We differentiate between two main types of therapy: local treatments, such as surgery and radiotherapy, and systemic treatments, such as chemotherapy, immunotherapy and targeted therapy.[1]

Surgery

The surgical removal of malignant tumors is the oldest form of cancer treatment. Its historical relevance in the treatment of cancers throughout time, such as mastectomies, is undeniable and has had a great impact on society. It can, however, be an invasive procedure and is unprecise at a molecular level. Furthermore it is mostly limited to solid tumors contained in one area and needs to be accompanied by an adjuvant and/or neoadjuvant therapy in most cases.[8] In recent years technology advancements have allowed research in fluorescence imaging-guided precision surgery to emerge showing first promising results.[9]

Radiotherapy

As of 2021 more than 50% of all cancer patients are estimated to receive radiation as part of their therapy process, both as the main form of therapy and as a adjuvant or neoadjuvant therapy.[10,11] Radiation can be delivered to the target in two ways; Brachytherapy, exploits radioactive sources to deliver radiation from inside the body, whereas external beam radiation is delivered from outside the body.[12] High dose radiation can damage tissue directly and indirectly. Directly, radiation interacts with cellular DNA. Indirectly, free radicals, derived from the ionization or excitation of water in the cells, interact mainly with the nucleic bases. Generally the DNA is damaged by oxidizing nucleobases and by causing both single- and double-strand breaks.[12] If they remain unrepaired, these lesions can block proliferation, causing cell death through mitotic catastrophe and apoptosis.[11] Since cancer cells generally operate less efficiently, normal cells repair themselves at a faster pace which results in differential cancer cell killing.[13]

Immunotherapy

Immunotherapy aims to upregulate the hosts innate anticancer immune response.[14] Cancer vaccines[15], adoptive T cell therapy[16] and immune checkpoint inhibitors[17] are some of the treatments developed for this endeavor. They are based on the various mechanisms behind

the last step of cancer immunoediting, immune escape, during which cancer cells evade the antitumor immune response.[18] Depending on what mechanism the treatment is based on, its toxicity profile varies and can be hard to manage, often steroids or immune suppression are used to manage this unique toxicity.[19] Immunotherapy has shown great success in difficult-to-treat cancers, such as leukemia[20] and melanoma.[21]

Targeted Therapy

Targeted therapy deploys cancer-specific characteristics, like specific proteins, to selectively target cancer cells without harming normal cells. Drugs are designed according to these specific characteristics in the hopes of minimizing adverse effects of cancer treatment.[22] Usually small molecule drugs, like nintedanib, a triple angiogenase inhibitor approved for non-small cell lung cancer and in clinical trials for various other types of cancer[23], or monoclonal antibodies, such as bevazizumab, approved for metastatic breast and colorectal cancer as well as non-small cell lung cancer (NSCLC) and others[24], are used.

Chemo Therapy

Chemotherapy is a cornerstone of cancer treatment alongside radiotherapy and surgery. Cytostatic drugs are often administered intravenously, orally or topically to reach systemic levels and induce apoptosis, cell cycle arrest and/or DNA damage[25]. Chemotherapeutics are used both to treat cancer, as neoadjuvant, adjuvant, combined and antimetastatic therapy, and to reduce symptoms (palliative care), albeit often causing severe side effects due to their lack of selectivity as well as often causing immune suppression and stimulating inflammation[26]. The large variety of chemotherapeutic drugs can be classified according to their mode of action.[27]

Alkylating agents, such as nitrogen mustards or nitrosoureas, carry an unstable alkyl group that can react with nucleophilic centers on proteins and nucleic acids. They alkylate the DNA causing single and double strand breaks, inhibiting DNA replication and transcription and ultimately leading to cell death.[27] A prime example for this subclass is cyclophosphamide, an inactive prodrug activated to its nitrogen mustard and used primarily for breast, lymphoid and pediatric cancers, as well as being a strong immunosuppressant.[28]

Antimetabolites can prevent and inhibit DNA and RNA synthesis and replication in several ways. Cytidine analogues, like gemcitabine[29] for instance, inhibit DNA methyltransferase or polymerase by incorporating into the DNA. Purine analogues can act as false metabolites because of their structural similarity to guanine.[27] Clofarabine for example, an adenosine

analogue, is used in pediatric leukemia.[30] Folate antagonists, on the other hand, reduce the, for the synthesis of purine bases essential, folate.[27] Pralatrexate is such a folate antagonist used to treat multiple types of cancer showing great promise in the treatment of peripheral T-cell lymphomas.[31]

Antimicrotubular agents inhibit the formation of microtubules, they are therefore M-phase specific. Taxanes disrupt the microtubule polarization to depolarization equilibrium, whereas vinca alkaloids bind to tubulin. Both ultimately inhibit cell division resulting in cell death.[27] Paclitaxel is a well-known taxane approved for ovarian, breast and lung cancer.[32] Vincristine is a vinca alkaloid mainly used in combination with other chemotherapeutics like doxorubicin and the above mentioned cyclophosphamide.[33]

Antibiotics are secondary metabolites with anticancer potential. They may affect the cell cycle and thus show anti-proliferative activity or inhibit cancer metastasis by regulating the anti-epithelial-mesenchymal-transition (EMT), like salinomycin.[34] Others may target apoptosis related enzymes or tumor suppressor genes to stimulate apoptosis. Moreover, anthracyclines like doxorubicin can intercalate into DNA and thus inhibit its replication. They also interfere with topoisomerase I and II which can lead to single and double strand breaks not being repaired and hence causing cell death.[35]

It is important to note that chemotherapy is mostly applied in combination and is often associated with higher chance of cancer development after treatment as well as cancer relapse.[26] This is associated both to the aforementioned caused inflammation, an enabling characteristic of cancer, and cancer stem cell resistance mainly caused by their high DNA repair, G0 latency and resistance to apoptosis.[26]

Transition metals possess unique characteristics, such as different oxidation states, unique geometries compared to purely organic drugs, redox activity, versatile ligand architecture, metal-ligand interaction and Lewis acid properties. These properties are exploited in the design of potential anticancer metal complexes that selectively bind to the biomolecular target resulting in an alteration in the cellular mechanism of proliferation.[36] Therefore, the potential of metal complexes in cancer therapy has attracted a lot of interest and will be discussed in more detail in the following chapters.

1.3.1 Platinum(II) based drugs

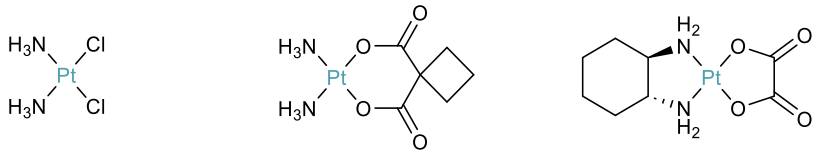

Figure 2: Structure of worldwide approved platinum(II) drugs.

Platinum(II) compounds play a key role in cancer therapy. Three compounds of this class are approved worldwide and will be discussed in this chapter, whereas three more, Nedaplatin, Lobaplatin and Heptaplatin are regionally approved.

Cisplatin is an anticancer drug approved by the FDA in 1978 to treat a variety of different cancer types.[37] The compound is activated through the substitution of the chlorido ligands by water molecules, the so-called activation by aquation. The resulting cationic species can form coordinative bonds with the nitrogen atoms of DNA, which interferes with DNA replication and transcription mechanisms depending on concentration and cell type. It damages tumors by inducing apoptosis through the activation of different signal transduction pathways, such as the activation of mitochondrial pathways, death receptor signaling and calcium signaling.

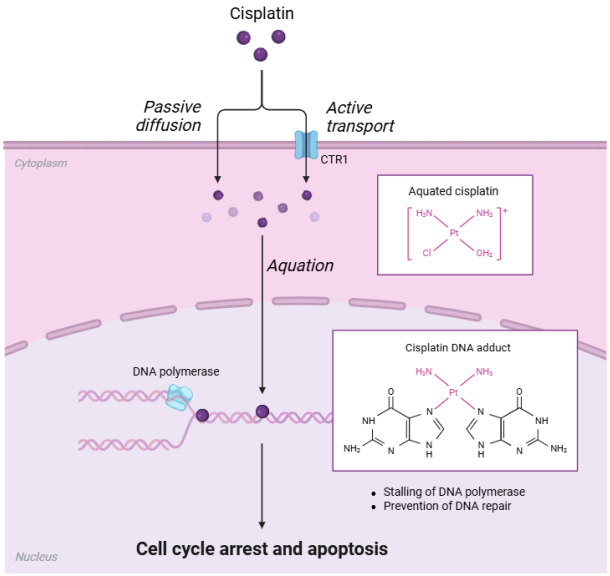

Figure 3: Mechanism of action of cisplatin, created and adapted via biorender.com (BioRender Basic).

Cisplatin lacks selectivity and thus also affects healthy cells, leading to various side-effects such as neurotoxicity, renal toxicity or bone marrow-suppression. Moreover, cancer cells can become cisplatin-resistant. Multiple mechanisms of cisplatin resistance are known, including

changes in cellular uptake, inhibition of apoptosis, increased detoxification, drug efflux and increased DNA repair.[38] With growing understanding of the biochemical mechanisms of cisplatin in tumor cells, more efficient platinum derivates were designed, reducing side effects and providing new therapeutic strategies.[39]

Carboplatin is considered a second generation platinum anticancer drug and was approved in 1986.[40] It is equipped with a bidentate 1,1-cyclobutanedicarboxylate ligand instead of the two cisplatin chloride moieties. Despite cisplatin's higher toxicity and better therapeutic results, carboplatin remains of great importance for its more favorable toxicity profile attributed to the chelating ligand.[41–43] Due to its better tolerability higher doses can be administered and primarily used in the treatment of ovarian[44,45], lung[46], head and neck[47,48] cancers.

Oxaliplatin is a third generation platinum drug that carries a bidentate oxalate and a diamino-cyclohexane (DACH) ligand and was approved in 1996.[40] Its mechanism of action has recently been questioned to differ from the one of cisplatin. PM Bruno et al.[9] showed that oxaliplatin does not kill cells through the DNA-damage response, but by inducing ribosome biogenesis stress, hence the difference in oxaliplatin's clinical application compared to that of cisplatin. Oxaliplatin has shown great success in combination therapy, especially with FOLFOX (folinic acid, fluorouracil and oxaliplatin) as an established regimen in the treatment of colorectal cancer.[49–51]

Many more platinum-based drugs have been screened through clinical trials but failed with regard to clinically applied standard chemotherapeutics.[36]

Platinum-based drugs have undeniably been very successful in chemotherapy over years. Nonetheless, they present multiple limitations such as drug resistance, side effects and limited spectrum of activity. More recently, efforts have been made to develop anticancer metal-based complexes with different metal centers, such as gallium, gold and ruthenium complexes.[36]

1.3.2 Non-Platinum based drugs

Gold

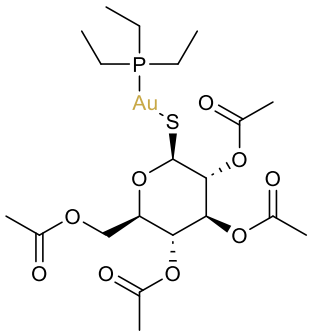

Auranofin

Figure 4: Structure of auranofin.

Gold(I) complexes first gained interest as anticancer drugs thanks to **auranofin**. It was originally used to treat rheumatoid arthritis and has since been studied as an anticancer agent for various cancers.[52] The gold(I) complex carries a phosphine and a thiolate ligand. Auranofin inhibits thioredoxin reductase (TR), hence suppressing ROS reduction and leading to mitochondria related apoptosis.[53] This compound has inspired the development of many gold(I) thiolate analogues and gold(III) compounds.[54]

Gallium(III)

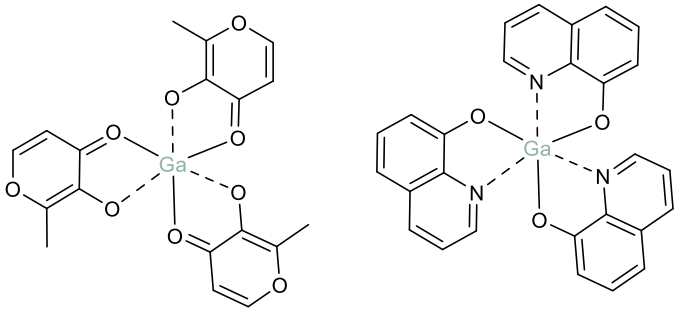

gallium maltolate **KP46**

Figure 5: Structure of gallium maltolate and KP46.

As far as gallium based complexes research is mainly focused on the two gallium(III) complexes [tris(3-hydroxy-2-methyl-4Hpyran-4-onato) gallium(III)], better known as **gallium maltolate**, and [tris(8-chinolinolato)gallium(III)], better known as **KP46**. Gallium(III) specifically is of interest due to its similarity to Fe(III), but lacks redox activity. Gallium maltolate releases free gallium upon degradation, enabling it to bind to transferrin. KP46 is a stable gallium(III) complex that induces apoptosis by inhibiting the ribonucleotide reductase.

It is administered orally and has been tested in phase I/II clinical trials[55] in the treatment of renal cancer, in patients with advanced solid tumors involving bones for its anti-bone resorption potential and has shown to sensitize resistant leukemia cells.[53,56,57]

Ruthenium

Ruthenium(II) and ruthenium(III) compounds, often times carrying bioactive scaffolds, are being developed and investigated as platinum alternatives.[58] Other approaches to ruthenium drug design include directed therapy and a multinuclear approach. In directed therapy organic molecules with known biological targets are attached to ruthenium. Through ruthenium's multinuclear and supramolecular architecture cluster complexes, DNA intercalators and ruthenium–platinum–mixed metal compounds have been designed.[36]

TLD-1433 is being evaluated in a phase 2 clinical trial for treating high-risk non-muscle invasive bladder cancer with PDT (photodynamic therapy) using green light. It contains a ruthenium(II) center that facilitates efficient population of the triplet excited state and an organic α-terthienyl group that affords a triplet intraligand charge transfer excited state with a prolonged lifetime and high sensitivity to oxygen.[59] Recently TLD-1433 iridium analogues have shown great promise as the research for alternative organometallic drugs continues.[60]

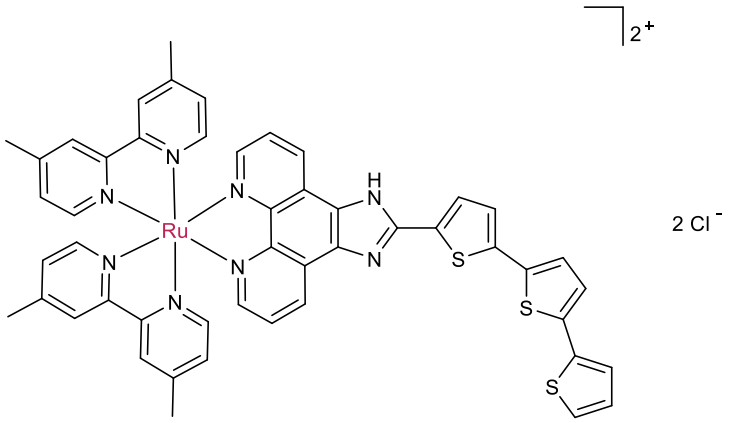

TLD-1433

Figure 6:Structure of TLD-1433.

The ruthenium(III) prodrug **NAMI-A** is the imidazolium salt of its precursor complex NAMI, the sodium salt of a pseudo-octahedral ruthenium(III) center carrying one axial imidazole ligand and one axial S-bound dimethyl sulfoxide (DMSO) ligand, as well as four chlorido ligands in the equatorial plane. The counter ion exchange improved the solid-state stability of the complex, facilitated its preparation process and accounted for an enhanced analytical profile, albeit maintaining a good aqueous solubility. NAMI-A is promptly hydrolyzed to its active form in the

body and may be reduced to its more reactive Ru(II) state.[61,62] These processes are strongly pH dependent.[63] NAMI-A can bind to serum proteins and inhibit cancer proliferation by altering the cell membranes morphology, inhibit angiogenesis and halt the cell cycle.[63,64] It also reduces invasion and is known to selectively target lung metastases, sparing the primary tumor unlike other drugs.[58,64] However, clinical trials were terminated due to the insufficient efficacy and high toxicity of the compound while trying to reach the maximum tolerated dose, despite its capacity to inhibit metastasis being dose-independent in preclinical studies.[65]

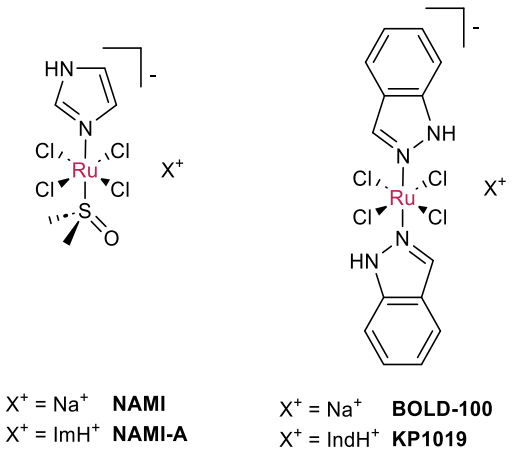

Figure 7: Structure of clinically evaluated ruthenium(III) based anticancer agents.

KP1019 is a ruthenium(III) complex carrying two axial indazole ligands and for equatorial chlorido ligands developed to improve the therapeutic effect of its predecessor KP418. The compound is thought to be taken up by the cell mainly via albumin binding.[66] In a phase I clinical trial for solid tumors the compound was well tolerated and disease stabilization was observed for 5 out of 6 patients for up to ten weeks. However, due to solubility issues further clinical trials were interrupted.[58,67]

BOLD-100, formerly known as KP1339, NKP-1339 or IT-139, was developed by exchanging the indazolium counterion of KP1019 by sodium to increase the aqueous solubility.[68] It is the most clinically advanced ruthenium-based therapeutic being investigated. Promising phase II clinical trials for gastrointestinal cancers using BOLD-100 in combination with FOLFOX are ongoing.[69] BOLD-100 received Orphan Drug Designations in gastric and pancreatic cancer by the FDA in 2021.[70]

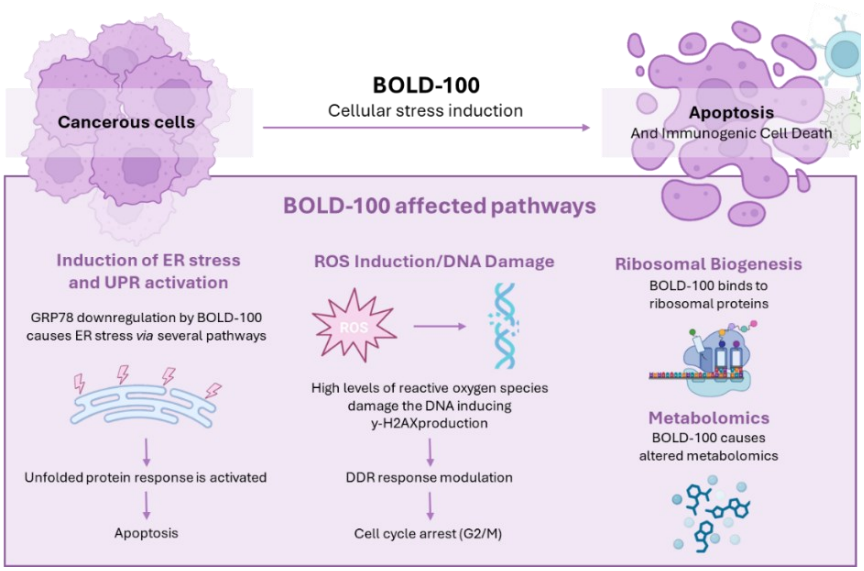

Figure 8: Mechanism of action of BOLD-100. Created via biorender.com (BioRender Basic) and adapted from BOLD Therapeutics[71].

BOLD-100 is known for its multimodal mode of action (Figure 8) e.g. by inducing cellular stress and apoptosis through several pathways. It downregulates GRP78, leading to endoplasmic reticulum (ER) stress.[72] Furthermore it produces reactive oxygen species (ROS), damaging the DNA and stopping the cell cycle.[73] It is also known to bind to ribosomal proteins and alter metabolomics. BOLD-100 has been discovered to induce immunogenic cell death[74] as well as to act as an anti-Warburg drug, meaning glycolysis is disrupted by lactate and pyruvate depletion. The lipid metabolism and epigenetic regulation caused by these metabolic changes are linked to the development of BOLD-100 resistence.[75] In addition it restores chemosensitivity in cancer cells which have already developed resistances.[76]

Rhodium

More recently rhodium has been subject of anti-cancer drug research. However, there is significantly less research available compared to the other, here discussed, transition metals platinum and ruthenium. Nonetheless the metal has been attracting attention over the past years. Berton et al.[77], Different potential anti-cancer rhodium complexes have been developed and analyzed with one of the most promising being $[Rh(HDPA)_2chrysi]^{3+}$, a metalloinsertor developed to target DNA mismatches.[77]

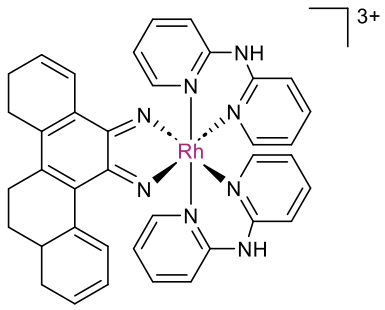

[Rh(HDPA)$_2$-chrysi]$^{3+}$

Figure 9: Structure of a rhodium(III) based DNA intercalator.

Mismatches occur naturally in DNA, however they are promptly corrected by MMR-proteins (MisMatchRepair) before further replication. Various types of cancer-cells, such as in secondary leukemia, are known to be MMR deficient. This deficiency is increased by resistance to commonly used anticancer agents like cisplatin and increases mutation rates of the cell. DNA mismatches are thermodynamically destabilized compared to well-matched DNA, allowing to target the mismatches. The chrysi (5,6-chrysenequinonediimine) ligand can be preferentially accommodated by mismatched DNA sites due to its planar and sterically expansive aromatic system. Rhodium metalloinsertors are preferentially cytotoxic to MMR-deficient cells inducing necrosis rather than apoptosis.[77,78]

Novel cytotoxic organorhodium(III) complexes able to alter cell migration, DNA condensation and DNA replication, like rhodium RAPTA-C analogues, are also being explored as potential anti-cancer drugs.[79]

1.3.3 Organometallic therapeutics

Continuous efforts in the research of potential transition metal based anticancer therapeutics led to the development of organometallic therapeutics. This compound class is defined by featuring at least one stable direct metal-carbon bond and is traditionally encountered in catalysis. The five main classes are metallocenes, metal-arenes, metal-carbonyls, metal-carbenes and metallacycles.[80,81] Organometallics are hence very structurally versatile and present many opportunities for further research.[80]

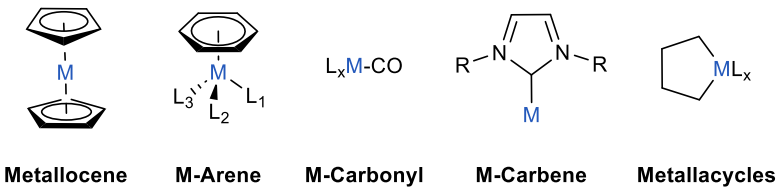

Figure 10: General structures of organometallic motifs used in drug development.

Some of the most promising organometallic anticancer complexes are ruthenium(II) metal-arenes, forming so called piano stool.[82,83] While the arene forms the seat of the piano stool, the ligands form its legs. The name half sandwich, on the other hand, derives from the metallocene class in which complexes are also known as sandwich complexes because of the two arenes constituting the bread containing a metal center. Two extensively studied ruthenium(II) compound families of this class are the RAED and RAPTA compounds.[84]

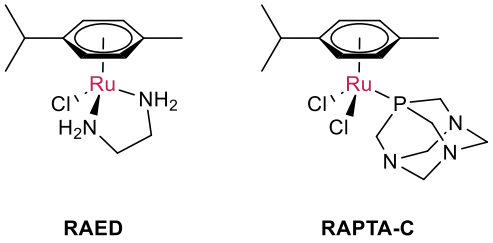

Figure 11: Structures of Ru(II) based piano-stool metal-arene complexes.

RAED complexes are ruthenium(II) arene compounds bearing a bidentate 1,2-ethylenediamine ligand. They are known to bind to the DNA by forming guanine adducts and have shown promising cytotoxicity in in vitro neoplastic cells.[83,84] RAED-C targets the DNA of chromatin cells and is highly cytotoxic. Its activity against primary tumors is comparable to the one of cisplatin.[85] Despite their great structural similarity, RAPTA complexes have a remarkably different toxicity profile.[85]

RAPTA complexes are ruthenium(II) arene compounds bearing a monodentate amphiphilic PTA (1,3,5-triaza-7-phosphaadamantane) ligand enhancing its aqueous solubility. They display a very low toxicity *in vivo* and limited cytotoxic potential *in vitro*.[38] RAPTA-C is known to inhibit angiogenesis, metastasis and tumoral activities. Its mode of action mainly involves forming protein adducts and altering histone-deoxyribonucleic acid as well as some DNA binding.[86] Chromatin, and more recently thioredoxin reductase and cathepsin B, have been suggested as its primary protein targets inducing G2/M-phase arrest.[85,87] Its activation, hydrolysis, occurs fast and is highly pH dependent making it of high interest as a prodrug activated in the lower pH cancer environment.[88] Inspired by the great success of RAPTA-C several analogues have been investigated. Amongst these the RAPTA-C rhodium(III) analogue

has shown promising results in the T47D cell line and superior activity in the A549 cell line compared to the ruthenium compound.[79]

1.3.4 Bioactive Ligands

The coordination of bioactive ligands to transition metal complexes for the development of anticancer agents has been revealing itself as a very promising approach over the past years. A large variety of ligands with different bioactivity, like anticancer activity, antifungal properties or mucosal protection, continue to be investigated.[89] Design strategies can be categorized in direct coordination to the metal center, coordination after derivatization, structural resemblance of a bioactive molecule after coordination, prodrugs releasing the bioactive ligand, and ligand improved selectivity and cell uptake.[90]

Ruthenium(II) arene compounds featuring bidentate *N,O*-, *O,O*-, or *S,O*- chelating ligand were intensively investigated over the last decades; however, the stability of the attached chelate was found to be a major issue. *C,N*-coordinating ligand systems show high stability in physiological media as well as promising anticancer activity.[89] Two prime examples of utilized classes in recent years were triazole,[91] as well as 2-phenylbenzothiazole scaffolds[92] (Figure 12). 1,2,3-Triazoles provide high variability by introduction of different substituents. While these ligands barely show any cytotoxic effect, the respective organometallic ruthenium(II) and osmium(II) complexes exhibit promising cytotoxicity *in vitro*. [91,92]

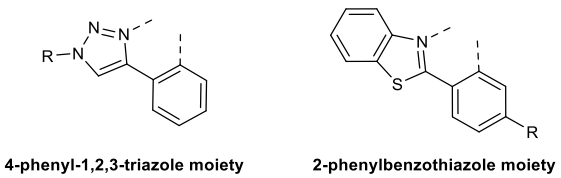

4-phenyl-1,2,3-triazole moiety 2-phenylbenzothiazole moiety

Figure 12: Representative C,N-chelating ligands.

4-Phenylthiazoles can be synthesized in a straight-forward manner and therefore constitute a very versatile group of bidentate *C,N* ligands. Recently very promising results of such half sandwich ruthenium(II) and osmium(II) complexes have been reported.[93] The respective complexes had cytotoxic effects with IC_{50} values in the low micromolar range for the cancer cell lines A549, SW480 and CH1/PA-1.[93]

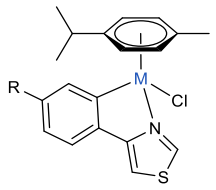

M = Ru, Os
R = H, F, Me, OMe, SO_2Me

Figure 13: Structure of half sandwich 4-phenylthiazole based complexes.[93]

Lipophilicity has often been linked with higher cellular uptake and hence improved cytotoxic activity of organometallic complexes. However, with higher lipophilicity comes lower solubility in aqueous solution, which is needed for drug administration. Furthermore, premature aquation of the chlorido complex can lead to severe side effects and anticancer lack of activity. In an effort to find the right balance between these characteristics monodentate ligands can be exploited as leaving groups to compounds already bearing a bidentate ligand. Most often a halide constitutes this co-ligand, nevertheless *N*-, *S*-, and *P*-donor monodentate ligands have shown to improve the properties of interest as well as the compounds stability compared to the respective halido-complex.[94]

Within this work, variation *P*- and *N*- donors such as PTA, triethylphosphine, triphenylphosphine, pyrazole and isoquinoline were explored in this work as leaving groups to investigate their impact on the stability and solubility in aqueous solution and their effect on the cytotoxicity of a 4-phenylthiazole bearing rhodium(III)-Cp* piano-stool complex.

2. Results and Discussion

Aim

The main goal of this thesis was the synthesis of novel complexes **I–V** *via* the general synthetic pathway shown in Scheme 1**.** The introduced monodentate leaving groups either feature a *P*-(**LG$_{1–3}$**) or a *N*-donor atom (**LG$_{4–5}$**). The lipophilicity and steric volume of these moieties may alter the stability and solubility of the complex as well as their anticancer activity. These characteristics may also vary depending on the employed counter ion.

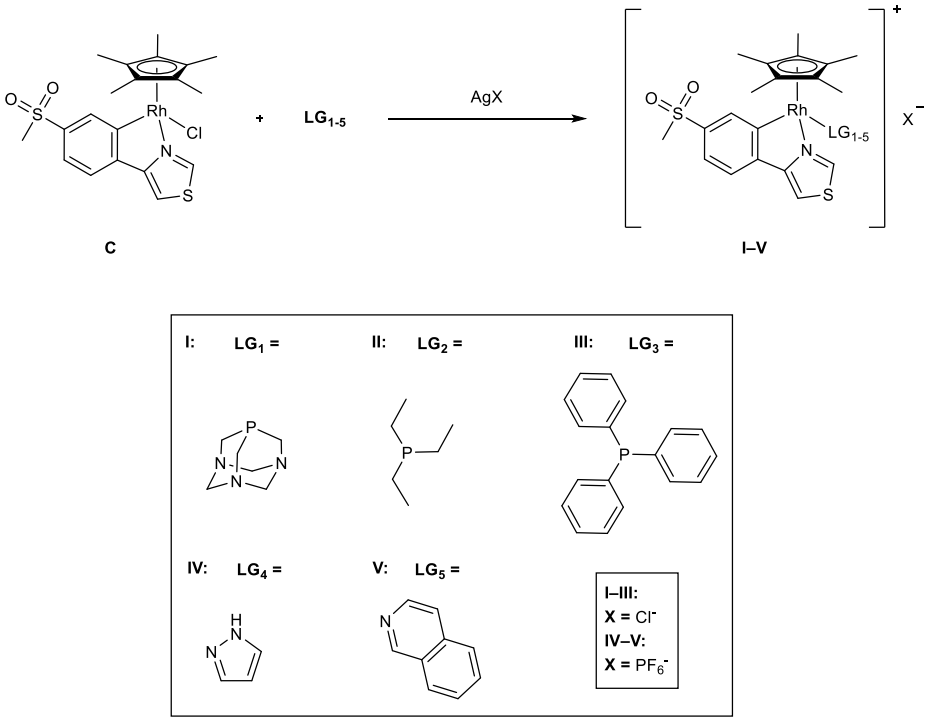

Scheme 1: Different applied leaving groups leading to complexes I-V.

2.1 Syntheses

2.1.1 4-Phenylthiazole ligand

The Suzuki-Miyaura (SM) coupling is a widely used transition-metal-catalyzed C-C bond-forming reaction.[95] The coupling proceeds through a three-stage sequence as shown in Scheme 2. The active palladium species forms an organopalladium complex with the halide *via* oxidative addition (stage one). The complex is then activated by base for the transmetalation with the boronate-complex resulting in a different organopalladium species (stage two). The desired product is ultimately obtained *via* reductive elimination and the palladium catalyst is restored (stage three).

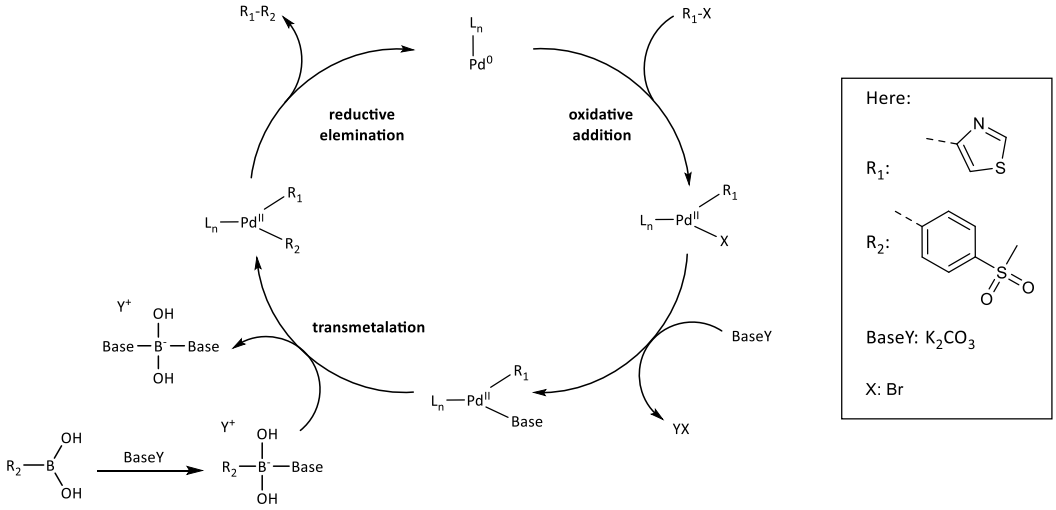

Scheme 2: Ligand synthesis mechanism via the Suzuki-Miyuara cross-coupling.

The 4-phenylthiazole ligand **L** was synthesized (yield: 84%) according the above-mentioned cross coupling following the method established by Lee et al., 2019[96]. The reaction follows the synthetic pathway of Scheme 3.

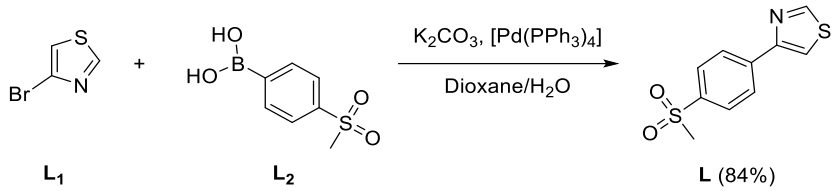

Scheme 3: Synthetic pathway towards the 4-phenylthiazole ligand.

*2.1.2 Synthesis of the Rhodium precursor complex **C***

The proposed mechanism for the synthesis of metal arene chlorido-complexes is based on Jones et al. (2009)[25] and Flegeau et al. (2011)[26] and is shown on the example of the here synthesized rhodium chlorido-complex **C** in Scheme 4.

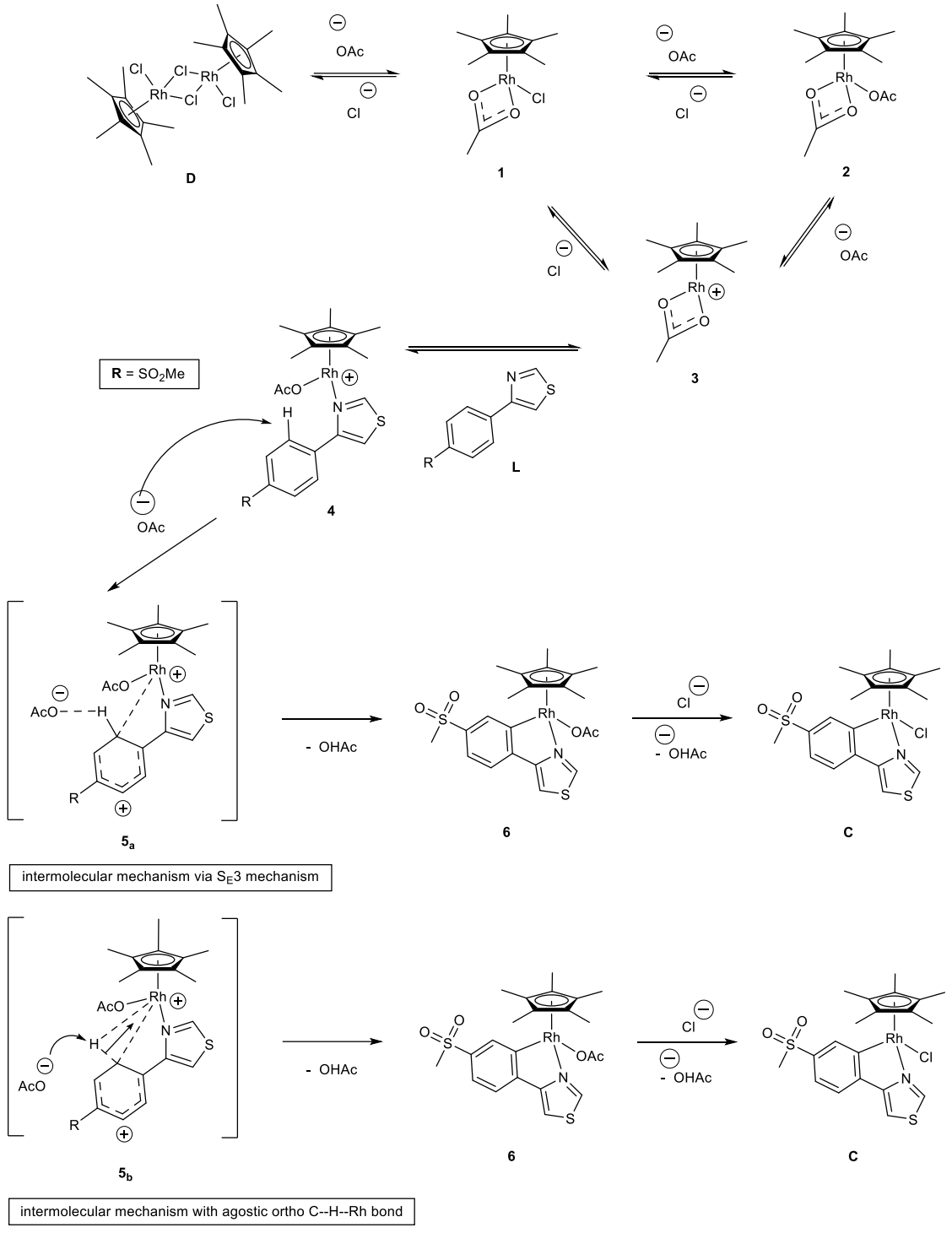

Scheme 4: Mechanism of the chlorido-complex synthesis on the example of the synthesized rhodium chlorido-complex proposed via two C-H activation steps.

As proposed by Jones et al.[97] the compounds **D**, **1** and **2** are in equilibrium and rapidly formed. Cl^- and AcO^- respectively dissociate to form the intermediate cation **3**, able to coordinate the phenylthiazole-ligand *via* the N atom to form the monodentately bound compound **4**. Flegeau et al.[98] suggest that the free acetate plays a key role in the mechanism of the C-H activation process. An intermolecular S_E3 (trimolecular electrophilic substitution) like deprotonation is proposed. The free AcO^- as an external base deprotonates the arene at the same time as the M-C bond is formed (**5$_a$**), resulting in the compound **6**. However, an alternative intermolecular mechanism based on an agnostic M(C-H) bond (**5$_b$**) could not be fully excluded.[98,99] Therefore both suggested mechanisms are illustrated in Scheme 4. Since chloride coordinates more tightly than the acetate, the product **6** is rapidly converted to its chlorido-form (**C**).[25]

The chlorido-complex **C** was synthesized with a 61% yield according to Scheme 5*Scheme 5* following a previously established method.

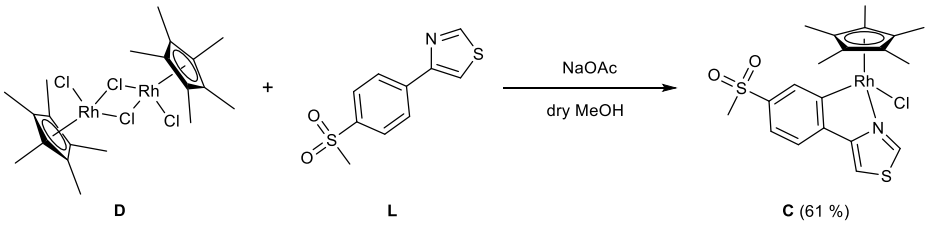

Scheme 5: Synthesis of the rhodium chlorido-complex.

2.1.3 Leaving group exchange

***P*-donor leaving groups**

PTA

Chlorido complex **C** (1.0 eq) was activated by $AgNO_3$ (2.0 eq). and treated with the *P*-donor ligand PTA (1.0 eq). These reaction conditions aimed to prepare the complex as the respective nitrate salt. However, the synthesis was unsuccessful as revealed *via* ^{1}H-NMR.

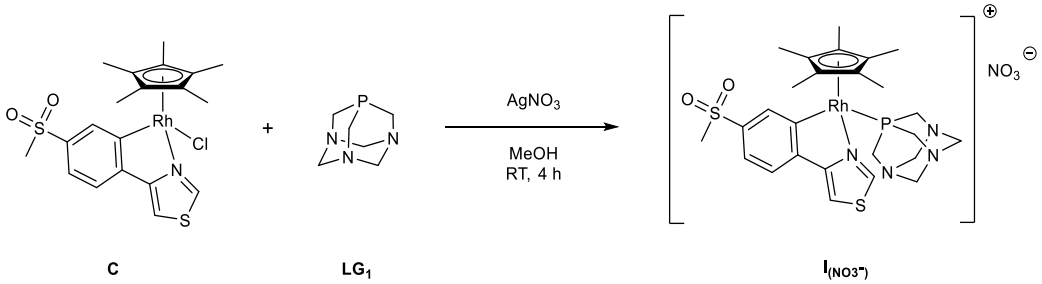

*Scheme 6: Synthetic pathway towards the nitrate salt of complex **I**.*

Hence a new approach was needed and the LG exchange was attempted without the usage of silver salt. Under these reaction conditions complex **I** was successfully synthesized (yield: 64%) with chloride as counterion using PTA **LG_1** (1.0 eq) and the chlorido complex **C** (1.0 eq).

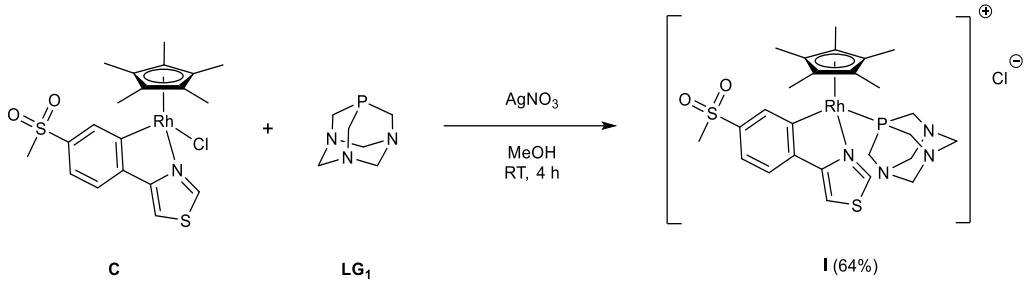

*Scheme 7: Synthetic pathway towards complex **I**.*

The work up procedure presented a challenge as column chromatography was not suitable as established *via* 2D NMR. Further purification was; however, not needed as the product was obtained in EA purity after simple filtration and drying in vacuo at 50 °C for 48 h in moderate yield (64%). The complex was characterized *via* ^{1}H- and ^{13}C-NMR as well as 2D NMR, ESI-MS and X-ray diffraction analysis.

Triethylphosphine & Triphenylphosphine

For the synthesis of the respective *P*-ligand complexes either triethylphosphine **LG_2** or triphenylphosphine **LG_3** (1.0 eq) were reacted with the chlorido complex **C** (1.0 eq) in methanol.

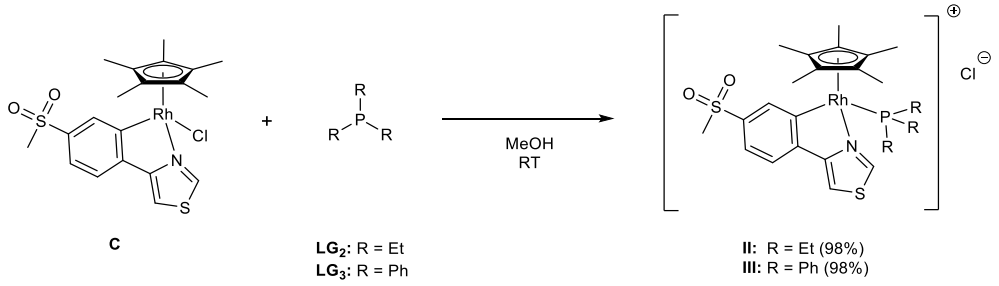

*Scheme 8: Synthetic pathway towards complexes **II** and **III**.*

They were purified by column chromatography over silica (50 g; 10% MeOH in DCM and 50 g; 5–10% MeOH in DCM, respectively). Drying *in vacuo* at 50 °C for 48 h resulted in elemental analysis pure products in excellent yields (>95%). The complexes were characterized *via* ^{1}H- and ^{13}C-NMR as well as 2D NMR, ESI-MS and X-ray diffraction analysis.

N-donor leaving groups

Pyrazole & Isoquinoline

As a first approach the synthesis of the pyrazole and isoquinoline complexes were attempted employing $AgNO_3$ under light exclusion to incite the leaving group exchange by producing AgCl and the respective nitrate salts. Under these reaction conditions, the complexes, **IV**$_{(NO3-)}$ and **V**$_{(NO3-)}$ were successfully synthesized and characterized *via* ^{1}H-NMR.

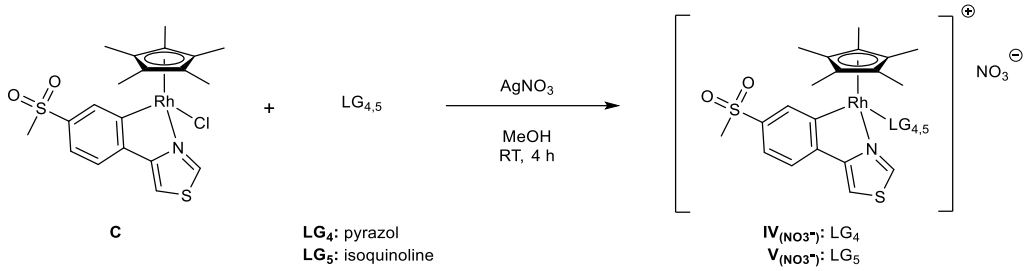

*Scheme 9: Synthetic pathway towards the nitrate salt of complexes **IV** and **V**.*

However, complications were faced during the work up. Chromatography over silica was not possible as established *via* 2D TLC, and no efficient precipitation system could be found. Hence a new approach was needed and the LG exchange was tried without the silver salt, leaving chloride as the counter ion to the complexes. However the same problems were met and even though the chloride complexes were characterized via ^{1}H-NMR the purification process remained unsuccessful.

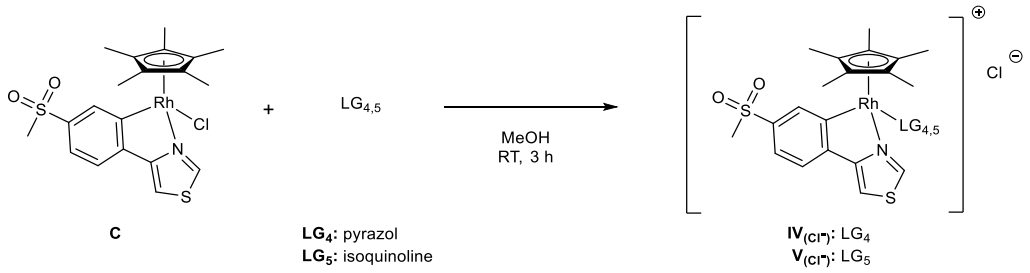

*Scheme 10: Synthetic pathway towards the chloride salt of complexes **IV** and **V**.*

To facilitate the purification process the counter ion of the complex was exchanged again. The chlorido complex **C** was treated with the respective **LG$_4$** or **LG$_5$** in the presence of $AgPF_6$ as seen in Scheme 11.

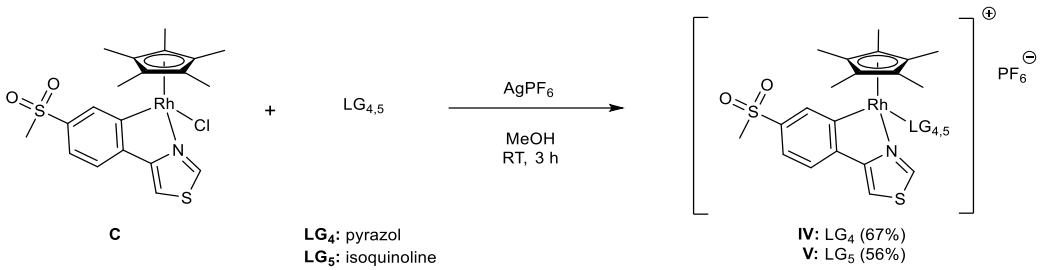

*Scheme 11: Synthetic pathway towards complexes **IV** and **V**.*

The purified products **IV** and **V** were collected via filtration and drying *in vacuo* at 50 °C for 48 h resulted in elemental analysis purity. The complexes were characterized *via* ^{1}H- and ^{13}C-NMR as well as 2D NMR, ESI-MS and X-ray diffraction analysis.

The formation of the complexes was unambiguously confirmed by NMR spectroscopy and the purity of the isolated compounds was proven by elemental analyses. As expected, the organometallics showed hygroscopic behavior, which was shown by determination of the O-values *via* elemental analysis. In the case of complex **III**, additional CH_2Cl_2 was detected in the ^{1}H-NMR spectrum, which could not be removed even at increased temperature and prolonged drying *in vacuo*.

2.2 NMR Characterization

The synthesized complexes **I**–**V** were characterized by standard 1D-NMR (^{1}H-NMR, ^{13}C-NMR) and 2D-NMR (COESY, HSQC, HMBC).

^{1}H NMR

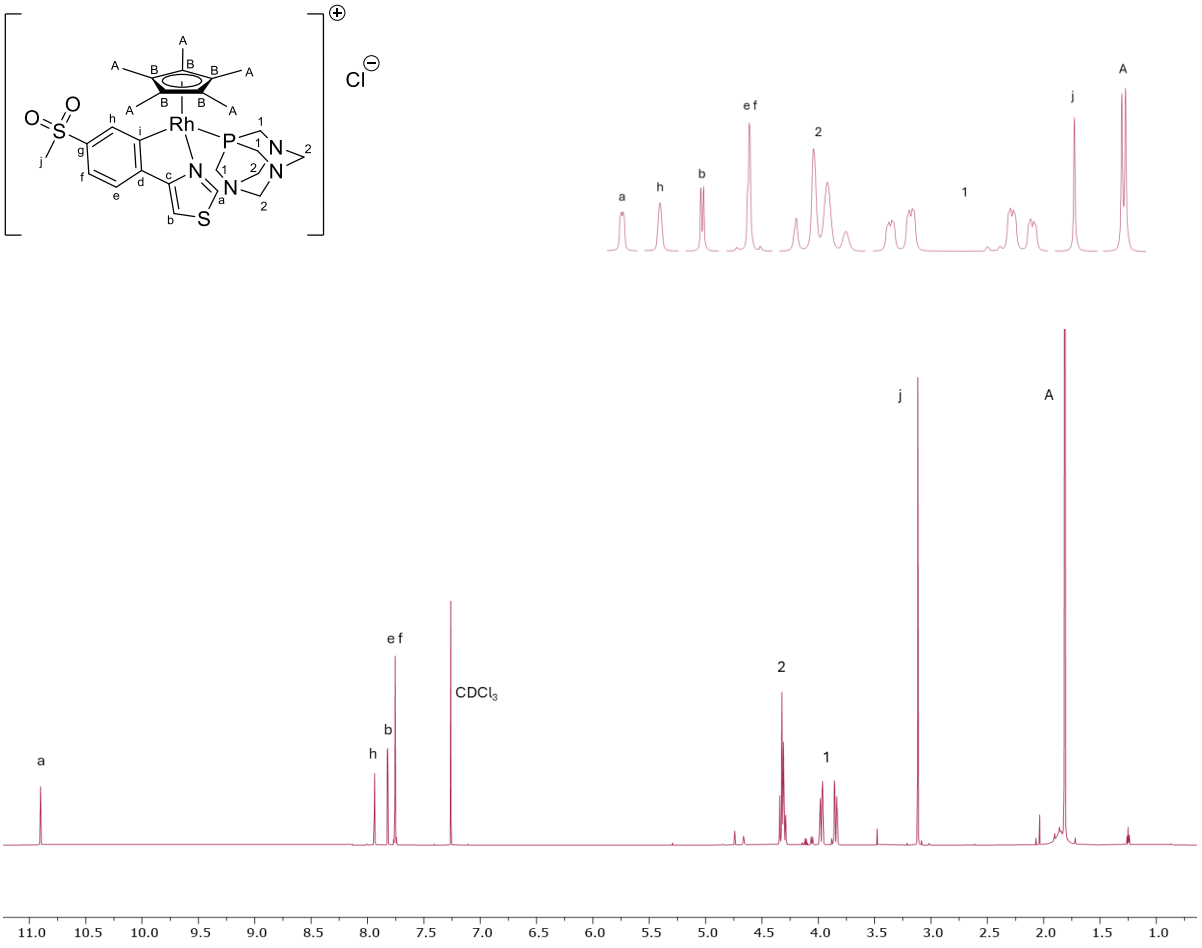

*Figure 14: ^{1}H-NMR of complex **I** in $CDCl_3$.*

The ^{1}H-NMRs of complex **I** and **II** were measured in deuterated chloroform, complex **III** was measured in deuterated methanol and the ones of complex **IV** and **V** in deuterated DMSO-d^{6}. The signals of the ligand and Cp* protons will be discussed on the example of the ^{1}H-NMR spectrum of complex **I** (Figure 14).

The two protons of the thiazole ligand at 10.90 ppm (a) and 7.82 ppm (b) both appear as doublets due coupling over the heteroatom. The phenyl signals at 7.94 ppm (h) and 7.76 ppm (e and f) of the ligand appear as a singlet and a doublet, respectively. The Cp* signal (A) at 1.81 ppm appears as a doublet for all *P*-donor leaving group complexes likely due to coupling with phosphorous over the rhodium metal center;.

The PTA methylene signals appear at 4.32 ppm (2) and the P-CH_2-N protons (1) at 3.91 ppm with characteristic additional ^2J and ^3J phosphor couplings. These signals confirm the PTA binding to the metal center as they differ from the free PTA signals due to less rotational freedom of the ligand. The phenyl signals of the triphenylphosphine leaving group of complex **III** at 7.50 ppm (3), 7.39 ppm (2) and 7.03 ppm (1) appear as rather large singlets with the protons 1 at 7.03 ppm resulting in the broadest signal. Furthermore, relevant amounts of DCM are visible at 5.63 ppm.

The aromatic signals of the *N*-donor ligands of complex **IV** and **V** showed small shifts compared to free heterocycles, confirming the formation of the desired products..

^{13}C NMR

The ^{13}C-NMR spectrum of complex **I** (Figure 15) measured in $CDCl_3$ was chosen to be discussed representatively.

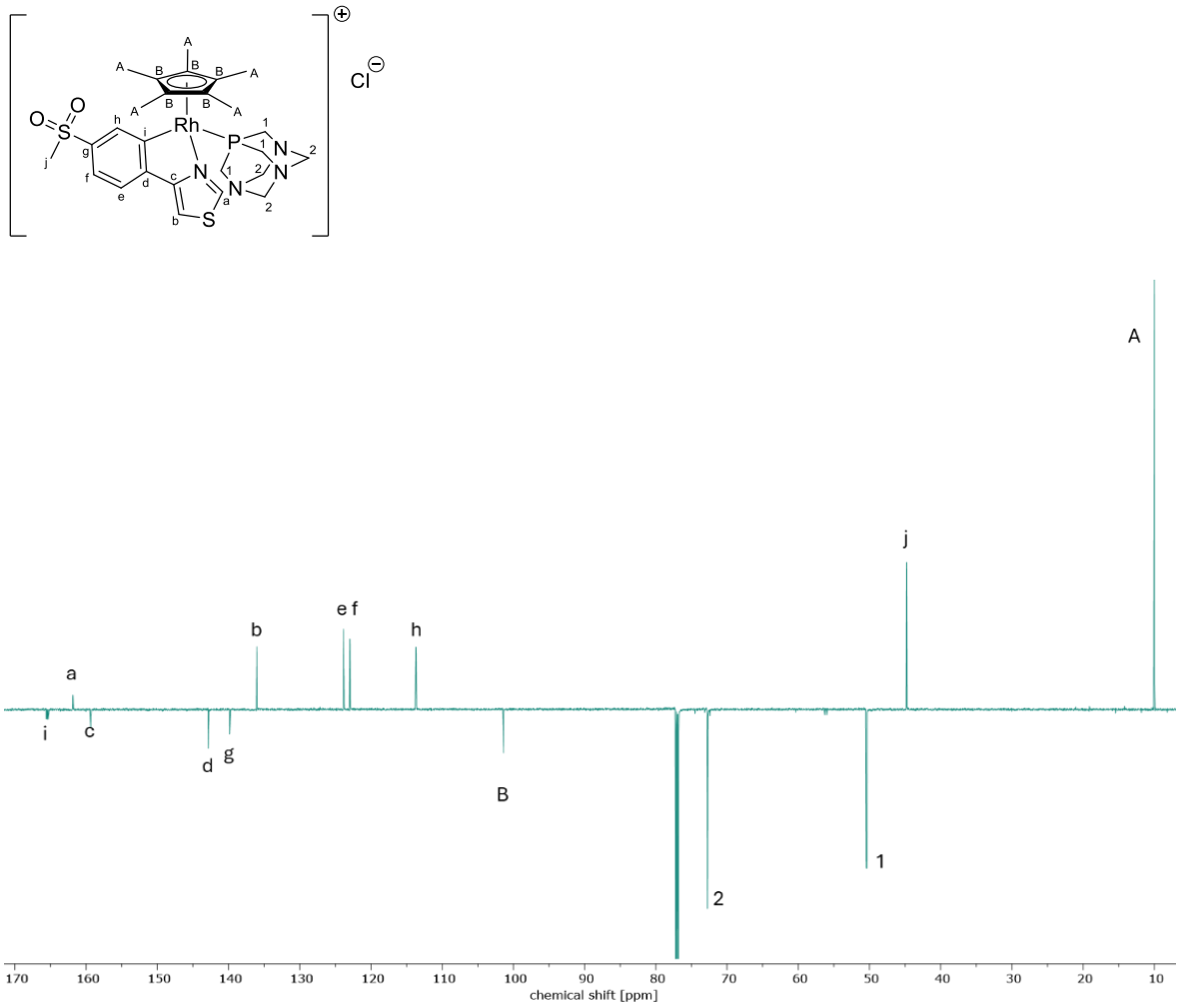

*Figure 15: ^{13}C-NMR spectrum of complex **I** in $CDCl_3$.*

The Cp* methyl carbons and the mesyl CH_3 carbon are observed at 10.0 (A) ppm at 44.8 (j) ppm respectively which corresponds to typical methyl upfield shifts with the mesyl group resonating more downfield due to the proximity to sulfur. The quaternary Cp* carbons resonate at 101.4 (B) ppm and the coordinated phenyl carbon resonates at 165.4 (i) ppm. For complex **I**, **II** and **III**, the coordinated carbons (Cp* and phenyl) are observed as doublets of doublets due to couplings with both, rhodium and phosphorous atoms in close proximity. The respective rhodium-carbon coupling unambiguously confirms the coordination of the Cp* and the thiazole to the metal center. For complexes **IV** and **V** these signals appear as doublets (**IV**:

166.4 (d, *J* = 32.1 Hz, i), 101.7 (d, *J* = 5.4 Hz, B) ppm; **V**: 166.4 (d, *J* = 32.4 Hz, i), 101.7 (d, *J* = 5.7 Hz, B)). The signals of the thiazole carbons at 161.8 (d, *J* = 4.5 Hz, a) ppm and 136.03 (d, *J* = 3.8 Hz, b) ppm are observed as doublets for complex **I–III** and further experiments are necessary to explain the observed splitting of the signal..

The two methylene signals of the PTA carbons in complex **I** at 72.7 (d, *J* = 7.0 Hz, 2) and 50.4 (d, *J* = 14.6 Hz, 1) ppm are observed as doublets due to coupling with phosphorous. The CH_2 signal of the triethylphosphine ligand of complex **II** at 16.2 ppm appears as a doublet due to phosphorous coupling , whereas the CH_3 signal at 8.0 (2) ppm appears as a singlet. The CH signals of the triphenylphosphine in complex **III** at 132.5 (3) and 130.0 (2) ppm both appear as singlets. The CH signal at 134.6 ppm appears as a weak signal and can thus not be identified as a doublet although phosphorous coupling would be expected.

The pyrazole carbons of complex **IV** at 138.1 (1) and 128.1 (3) ppm appear as very small peaks due to their nitrogen bond. The CH signal at 104.2 (2) ppm belonging to the carbon between the two nitrogen bound carbon is clearly visible as a singlet. All signals of the isoquinoline moiety of complex **V** appear as singlets in the aromatic range between 152.3 and 120.3 ppm, with the two quaternary carbons at 135.2 (8) and 128.2 (3) ppm resulting in smaller peaks.

2.3 X-Ray diffraction analysis

Single crystals suitable for diffraction analysis of all compounds **I–V** were obtained via slow diffusion of *n*-hexane into DCM. The respective CCDC-codes as well as the data collection parameters and structure refinement details can be found in the appendix. These findings confirm the pseudo octahedral piano-stool configuration, in which the metal center (Rh) is surrounded by a stabilizing arene moiety (Cp*) constituting the seat, as well as a bidentate 4-phenylthiazole ligand and a monodentate leaving group (PTA, Et_3P, Ph_3P, pyrazole or isoquinoline) forming its legs. Selected bond lengths and angles are listed in Table 1 and their structures are shown in Figures 16–18.

Complex **I** crystallized in the triclinic space group $P\overline{1}$, complex **II** crystalized in the monomeric space group $P2_1/n$, complex **III** and **V** in the orthorhombic space group P b c a and complex **IV** in the monoclinic space group $P2_1/c$.

The Rh – N and Rh – C bond lengths corresponding to the 4-phenylthiazole ligand as well as the Rh – Cp* bond stay in a consistent range for all compounds, suggesting the leaving group variation having no major influence on the compounds remaining structure. The Rh – L (leaving group) bond strongly differs according to the leaving group donor atom. The Rh-Cl bond of the chlorido complex is the longest due to the chlorides large atom radius. As expected the *P*-donor leaving groups (**I**–**III**) show a longer bond length compared to the *N*-donor leaving groups (**IV** and **V**) due to phosphorus's larger atom radius and lower electronegativity. The Rh – PTA bond length corresponds to the bond length of the Rh RAPTA-C analogue (2.285(7) Å) found in literature[79].

Table 1: Selected bond lengths of all synthesized complexes.

	Bond length [Å]					
Compound	**c**	**I**	**II**	**III**	**IV**	**V**
Rh – N	2.083(8)	2.090(5)	2.081(4)	2.086(3)	2.116(3)	2.095(2)
Rh – C	2.033(7)	2.066(6)	2.046(4)	2.054(3)	2.069(4)	2.075(3)
Rh – L	2.392(1)	2.277(2)	2.305(1)	2.308(1)	2.107(3)	2.135(5)
Rh – Cp*	2.137(1)	2.173(5)	2.180(5)	2.204(3)	2.155(4)	2.153(3)
	2.258(4)	2.265(5)	2.269(4)	2.257(3)	2.242(5)	2.227(3)

The dark green atoms represent rhodium (Rh), the light green atoms chloride (Cl), the grey atoms carbon (C), the white atoms hydrogen (H), the lavender atoms nitrogen (N), the yellow atoms sulfur (S), the orange atoms phosphorous (P), and the red atoms represent oxygen (O). The PF_6^- counter ion to complexes **IV** and **V** was omitted for clarity.

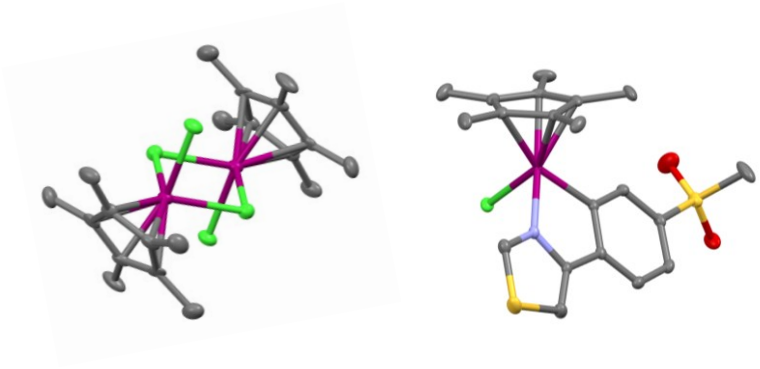

Figure 16: Crystal structure of the rhodium-Cp-dimer **D** (left) and the chlorido complex **C** (right).*

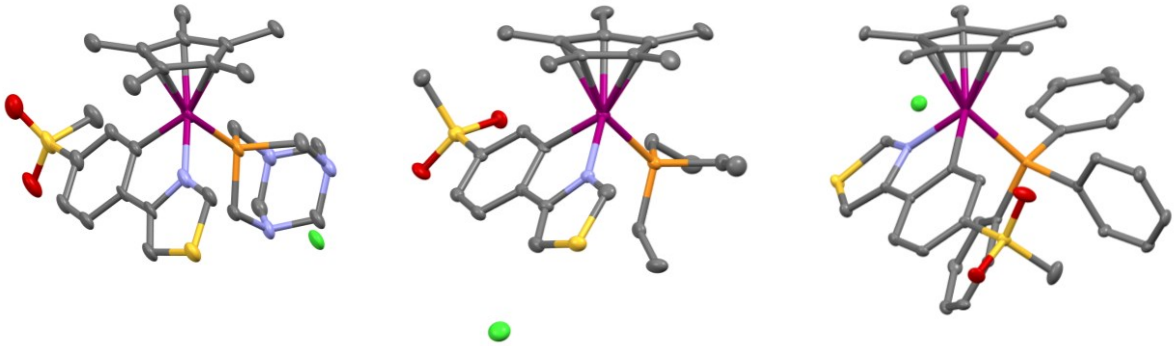

*Figure 17: Crystal structure of the complex **I** (left), complex **II** (center) and complex **III** (right).*

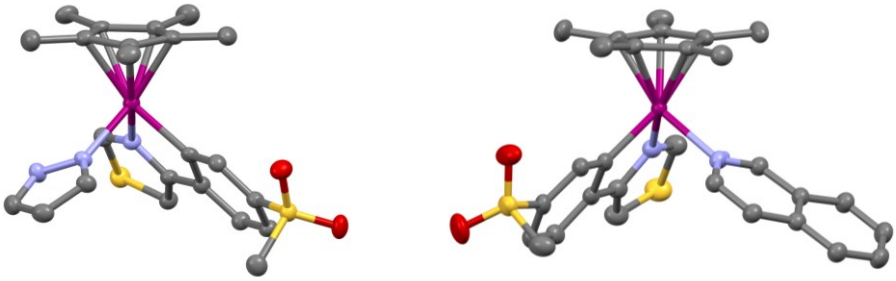

*Figure 18: Crystal structure of the complex **IV** (left) and complex **V** (right).*

2.4 Stability in aqueous solution

The aqueous stability of the complexes was determined *via* UV-Vis spectroscopy over 24 h at 20 °C under pseudo-physiological conditions in PBS (40 µM compound concentration, pH 7.4) using 1% DMSO as solubilizer. Based on the obtained spectra, the tested compounds **I–III** remained intact (Figure 19) whereas compounds **IV** and **V** undergo microprecipitation (Figure 20), visible as a slight decrease of absorption over time. This can be attributed to PF_6^- being the counter ion to the latter complexes, lowering their solubility in PBS. No isosbestic points, new peaks, or shifts of peak maxima were observed over 24 h for any of the compounds.

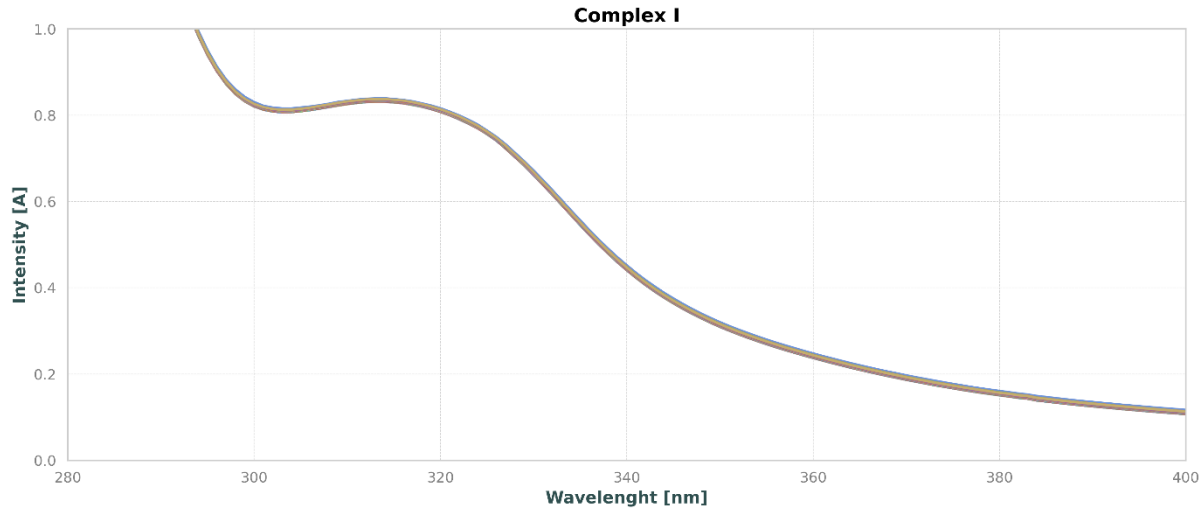

*Figure 19: UV/Vis absorption spectrum of complex **I** measured every half hour over 24 h.*

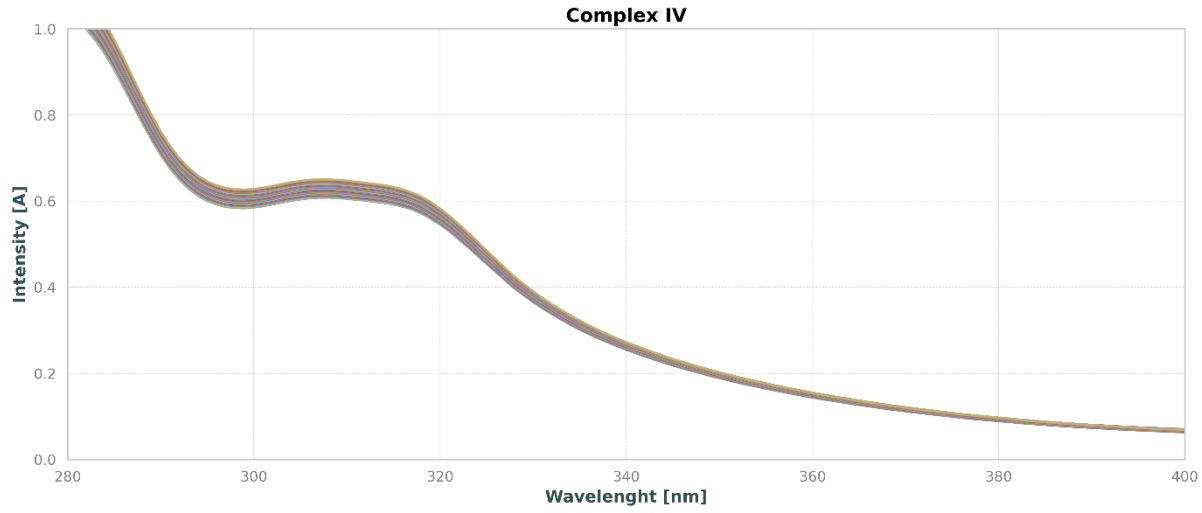

*Figure 20: UV/Vis absorption spectrum of complex **IV** measured every half hour over 24 h.*

2.5 Cytotoxicity

3-(3,5-Dimethylthiazol-2-yl)-2,5-diphenyltetrazolium bromide (MTT) assays were performed at the cell culture facility of the Institute of Inorganic Chemistry, University of Vienna. To establish cell viability in MTT assays the quantitative reduction of a tetrazolium salt to formazan is visually determined. These tests were carried out in 3 different human cancer cell lines to assess the anticancer potential of the synthesized compounds (Table 2). The utilized cell lines were A549, a multi-drug resistant non-small lung cancer cell line, SW480, a partially chemo-resistant colorectal cancer cell line, and CH1/PA-1, a rather chemo-sensitive ovarian carcinoma cell line.

Table 2: 50% cancer cell growth inhibition concentration determined by MTT assays in three different cancer cell lines over 96 h exposure time (means ± standard deviation).

	IC_{50} [µM]		
Compound	**A549**	**SW480**	**CH1/PA-1**
C	133 ± 11	9.8 ± 0.5	30 ± 2
I	>200	>200	>200
II	5.82 ± 0.86	2.09 ± 0.04	1.08 ± 0.04
III	> 200	88.09 ± 11.25	17.86 ± 0.56
IV	98.15 ± 6.73	10.17 ± 0.45	15.06 ± 1.62
V	111.51 ± 11.10	10.53 ± 1.59	18.40 ± 1.82
Cisplatin[100]	3.8 ± 1.0	2.3 ± 0.2	0.073 ± 0.001
BOLD-100[101]	67 ± 12	50 ± 5	36 ± 3

The chlorido complex **C** shows less anticancer potential than its ruthenium and osmium analogues reported in literature[93] in all three cancer cell lines,. Overall, the leaving group exchange had a strong impact on the determined cytotoxicities. The IC_{50} values of the *P*-donor complexes **I**–**III** strongly vary. The PTA bearing complex **I** shows IC_{50} values above 200 µM in the tested cell lines. This might indicate a particularly high stability of complex **I** preventing its activation at the biological target. Previously, rhodium(III) complexes bearing an *S,O*-donor chelating ligand and PTA as a leaving group have shown greater antiproliferative activity down to the low micromolar range than the parental chlorido complex. This highlights the importance of the coordinated chelate and that leaving groups might have opposite effects when coordinated to different organometallic scaffolds[94].

Complex **II**, bearing triethylphosphine, showed the best results of the complex series with IC_{50} values in the lower micromolar range, comparable to the values of cisplatin. In contrast, complex **III** bearing triphenylphosphine showed no relevant cell growth inhibition in the A459 cell line and moderate activity in the other two cell lines. Higher lipophilicity is often correlated to lower values in MTT assays, nevertheless this is not reflected in this case when comparing complex **II** and **III**. However, cellular accumulation studies are necessary to clarify the observed differences in cytotoxicity. The *N*-donor compounds **IV** and **V** showed very similar IC_{50} values in all tested cell lines; however, the difference in lipophilicity of the attached *N*-donors, does not seem to impact cell growth inhibition significantly. In comparison to *N*,*C*-triazole-based ruthena(II)cycles, the pyrazole derivative (A549: 4.5 ± 0.5 µM, SW480: 3.7 ± 0.5 µM, CH1: 2.1 ± 0.1 µM)[102] was found to be slightly less active than the corresponding isoquinoline derivative (A549: 1.10 ± 0.03 µM, SW480: 0.65 ± 0.01 µM, CH1: 0.70 ± 0.05 µM)[102].

Overall, complex **II**, bearing the triethylphosphine leaving group, showed the most promising result *in vitro*, followed by the two *N*-donor leaving group compounds **IV** and **V** and the chlorido complex **C**.

3. Experimental Part

3.1 Equipment

Chromatography on silica was performed with the Biotage® Isolera system and silica gel.

Routine NMR spectra were measured on a Bruker AV NEO 500 spectrometer at 500.10 (^{1}H) MHz. Service NMR spectra were measured on a Bruker AV III 60 spectrometer at 600.18 (^{1}H) and 150.92 (^{13}C) MHz or a Bruker AV III HD 700 spectrometer at 700.40 (^{1}H) and 176.12 (^{13}C) MHz. DMSO d-^{6}, MeOD-d^{4} and $CDCl_3$ were used as solvents and used as internal reference for chemical shifts: ^{1}H (DMSO-d^{6}: 2.50 ppm; MeOD-d^{4}: 3.10 ppm; $CDCl_3$: 7.26 ppm) and ^{13}C (DMSO-d^{6}: 39.53 ppm; MeOD-d^{4}: 49.03 ppm; $CDCl_3$: 77.26 ppm).

The ESI-MS spectra were measured in the positive mode with a Bruker maXis ESI-QqTOF (electrospray ionization quadrupole–quadrupole time-of-flight) spectrometer in ACN/MeOH/H_2O (49.5:49.5:1) as solvent.

Elemental analyses were performed by the microanalytical laboratory of the University of Vienna with a PerkinElmer 2400 Series II CHNS/O Elemental Analyzer or Eurovector EA3000 Elemental Analyzer.

UV/vis measurements were performed on a Perkin Elmer Lambda 35 photometer with PTP (Peltier Temperature Programmer) and Julabo AWC 100 recirculating cooler.

An ELx808 Absorbance Microplate Reader (Bio Tek, Winooski, VT, USA) was utilized to measure optical densities for the cell viability assays in 96-well microculture plates (Starlab, UK).

3.2 Materials

All solvents were obtained from commercial sources and used without further purification. 1,3,5-triaza-7-phosphaadamantane (Alfa Aesar, 97+%), triphenylphosphine (Sigma, 99%), triethylphosphine (Sigma, 99.9%), isoquinoline (Fluka, >97%), pyrazole (ACROS, 98%), $AgPF_6$ (TCI, 99%), $AgNO_3$ (Sigma Aldrich, puriss.) were used without further purification.

3-(3,5-Dimethylthiazol-2-yl)-2,5-diphenyltetrazolium bromide (MTT, Acros Organics, Geel, Belgium) was used for cell viability assays.

3.3 Solubility in Aqueous Medium

The solubility of the complexes **I–V** was determined in PBS with 1% DMSO (pH 7.4). Approximately 1 mg of compound was weighed in and dissolved in DMSO in 10 µL steps creating a stock solution which was then added to 990 µL of PBS buffer.

3.4 Cell viability assays

MTT assays performed at the cell culture facility of the Institute of Inorganic Chemistry, University of Vienna, were used to assess the cytotoxicity of the isolated compounds following 96 h incubation. The cells were dissociated from culture flasks with trypsin and seeded into 96-well microculture plates in 100 µL portions with different densities (1 ×103 (CH1/PA-1), 2 × 103 (SW480) and 3 × 103 (A549)). Before being exposed to the complexes, the cells were incubated for 24 h. 100 µL of serial dilutions of previously prepared stock solutions (diluted in MEM for a maximum organic solvent concentration of 0.5% v/v per well) of the compounds in DMF were added to each well. After 96 h of exposure to the drugs, the solutions were removed and the cells were exposed to 100 µL of a 6:1 medium:MTT mixture consisting of RPMI 1640 medium with 10% heat-inactivated fetal bovine serum and 2 mM L-glutamine, and 5 mg/mL MTT solution in PBS for 4 h. The solutions were then removed and, per well, the formazan crystals were dissolved in 150 µL DMSO. Optical densities at 550 nm were quantified with a microplate reader and unspecific absorption was corrected with a reference wavelength (690 nm). Dose-response curves were generated from at least three independent experiments with triplicates for each concentration level and the 50% inhibitory concentrations (IC_{50} values) were interpolated.

3.5 Ligand synthesis

4-(4-(Methylsulfonyl)phenyl)thiazole **L**

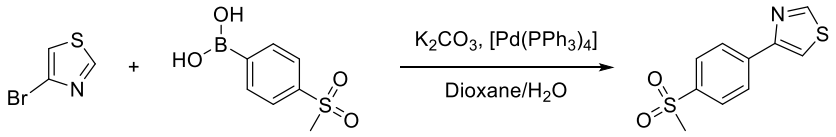

L_1
C_3H_2BrNS
164.02 g/mol

L_2
$C_7H_9BO_4S$
200.02 g/mol

L
$C_{10}H_9NO_2S_2$
239.31 g/mol

4-Bromothiazole **L_1** (1.000 g, 6 mmol, 1.0 eq.), 4-methylsulfonylphenylboronic acid **L_2** (2.440 g, 12 mmol, 2.0 eq.) and potassium carbonate (1.690 g, 12 mmol, 2.0 eq.) were dissolved in 8 mL of a (3 : 1) dioxane : water mixture and purged with argon for 20 minutes. Tetrakis (tetrakis-(triphenylphosphine)palladium(0)) (0.141 g, 122 µmol, 0.02 eq.) was added under inert conditions and the reaction mixture was stirred at 100 °C overnight. Subsequently, the cooled off mixture was transferred to a separating funnel and 40 mL of distilled water were added. The aqueous layer was extracted 3 times with 40 mL EtOAc and the combined organic layers were first washed with 40 mL of brine and subsequently dried over anhydrous sodium sulfate. The solvent was removed in vacuo and the crude product was purified *via* chromatography on silica (40% EtOAc in *n*-hexane). The final product **L** a was obtained as a pure white solid.

Yield: 1.22 g (84%)

^{1}H NMR (500.10 MHz, $CDCl_3$): δ = 8.86 (d, *J* = 1.9 Hz, 1H, Ha), 8.09 – 8.06 (m, 2H, Hf; Hh), 7.96 – 7.93 (m, 2H, He; Hi), 7.67 (d, *J* = 1.9 Hz, 1H, Hb), 3.03 (s, 3H, Hj) ppm.

*3.6 Rhodium-dimer synthesis **D***

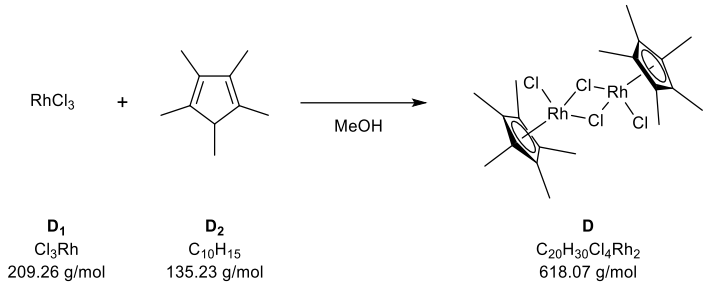

D₁
Cl_3Rh
209.26 g/mol

D₂
$C_{10}H_{15}$
135.23 g/mol

D
$C_{20}H_{30}Cl_4Rh_2$
618.07 g/mol

$RhCl_3$ **D_1** (1.500 g, 7.17 mmol, 1.0 eq.) and 1,2,3,4,5-pentamethylcyclopentadiene **D_2** (1.940 g, 14.34 mmol, 2.0 eq.) were dissolved in 50 mL MeOH and refluxed for 24 h. After cooling the product was filtered and washed with Et_2O and dried *in vacuo*. The filtrate was concentrated to half its volume and stored at 4 °C for 2 days. Both batches were united and dried *in vacuo* at 50 °C for two days. The rhodium-dimer **D** product was obtained as a dark red solid.

Yield: 1.787 g (81%)

^1H NMR (500.10 MHz, $CDCl_3$): δ = 1.62 (s, 15H, HA) ppm.

*3.7 Chlorido complex synthesis **C***

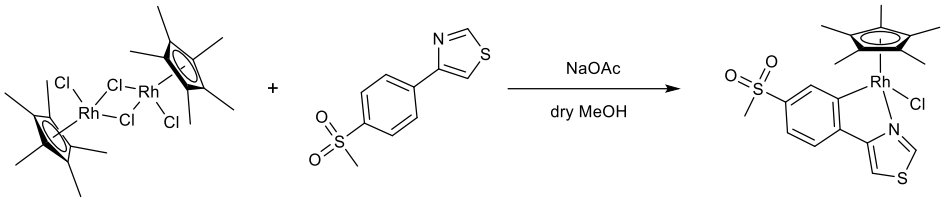

D
$C_{20}H_{30}Cl_4Rh_2$
618.07 g/mol

L
$C_{10}H_9NO_2S_2$
239.31 g/mol

C
$C_{20}H_{23}ClNO_2RhS_2$
511.88 g/mol

Dichlorido-(Cp*)-rhodium(III) dimer **D** (500 mg, 809 µmol, 1.0 eq.), 4(4-(methylsulfonyl)phenyl)thiazole **L** (387 mg, 1.6 mmol, 2.0 eq.) and anhydrous sodium acetate (266 mg, 3.2 mmol, 4.0 eq.) were dissolved in 20 mL dry MeOH under argon atmosphere and stirred at RT for 18 h. The pure product precipitated out of the reaction mixture and was collected *via* filtration. The filtrate was then concentrated to half its volume and cooled to 4 °C for 24 h before another product batch was collected after filtration. The crude product was dissolved in DCM and filtered again. Finally the solvent was removed *in vacuo*. This process was repeated 3 times. Drying the obtained product **C** *in vacuo* at 50 °C for two days delivered the desired elemental analysis purity.

Yield: 632 mg (76%)

^{1}H NMR (700.40 MHz, $CDCl_3$): δ = 8.99 (d, *J* = 2.0 Hz, 1H, Ha), 8.30 (d, *J* = 1.7 Hz, 1H, Hb), 7.60 – 7.56 (m, 3H,He; Hf; Hh), 3.09 (s, 3H, Hj), 1.67 (s, 15H, HA) ppm.

EA found (calculated) for $C_{20}H_{23}ClNO_2RhS_2$: C 46.42 (46.68), H 4.36 (4.56), N 2.77 (2.72), S 12.46 (12.46) w-%.

Solubility (PBS 1% DMF, pH 7.4): 0.33 mg/mL (0.64 mM)

3.8 Leaving group exchange

All complexes were synthesized according to the following general procedure (*GP)*.

General procedure (GP)

Rhodium(III)-chlorido-complex **C** (1.0 eq.) and the respective *N*- or *P*- donor leaving group (1.0 eq.) were dissolved in MeOH. The reaction mixture was stirred at room temperature (RT) for 2.5 to up to 4 hours according to the respective leaving group. The solvent of the crude product was then removed *in vacuo*. After the respective work up procedure, the solvent was removed under reduced pressure where necessary, and the product was obtained in elemental analysis purity after drying *in vacuo* at 50 °C for 48 h in fair to excellent yields.

[(1,3,5-Triaza-7-phosphaadamantane-κP)(4(4-(methylsulfonyl)phenyl)-thiazolato-κN,κC2´)(1,2,3,4,5-pentamethylcyclopentadienyl)rhodium(III)] chloride ***I***

C
$C_{20}H_{23}NO_2RhS_2Cl$
511.88 g/mol

LG_1
$C_6H_{12}N_3P$
157.16 g/mol

I
$C_{26}H_{35}N_4O_2PRhS_2Cl$
669.04 g/mol

The chlorido-complex **C** (100 mg, 195 µmol, 1.0 eq.), 1,3,5-triaza-7-phosphaadamantane **LG_1** (31 mg, 195 µmol, 1.0 eq.) and 15 mL MeOH were stirred for 4 h. The crude product was dissolved in DCM , filtered and the solvent removed under reduced pressure. Product **I** was obtained as a bright yellow solid.

Yield: 84 mg (64%)

^{1}H NMR (700.40 MHz, $CDCl_3$): δ = 10.90 (dd, *J* = 2.1, 0.9 Hz, 1H, Ha), 7.94 (d, *J* = 1.3 Hz, 1H, Hh), 7.82 (d, *J* = 2.1 Hz, 1H, Hb), 7.76 (d, *J* = 1.5 Hz, 2H, He; Hf), 4.32 (m, 6H, H2), 3.91 (ddd, *J* = 89.3, 14.9, 2.2 Hz, 6H, H1), 3.12 (s, 3H, Hj), 1.81 (d, *J* = 2.8 Hz, 15H, HA) ppm.

^{13}C-NMR (176.12 MHz, $CDCl_3$): δ = 165.4 (Cq, Ci), 161.8 (CH, Ca), 159.3 (Cq, Cc), 142.8 (Cq, Cd), 139.8 (Cq, Cg), 136.0 (CH, Cb), 123.8 (CH, Ce), 122.9 (CH, Cf), 113.7 (CH, Ch), 101.4 (Cq, CB), 72.7 (CH_2, C2), 50.4 (CH_2, C1), 44.8 (Cq, Cj), 10.0 (CH_3, CA) ppm.

EA found (calculated) for $C_{26}H_{35}N_4O_2PRhS_2Cl \cdot 1.6\ H_2O$: C 45.13 (44.75), H 5.38 (5.52), N 8.38 (8.03), O 8.62 (8.25), S 8.86 (9.19) w-%.

HR-MS: calcd. 633.0994, found 633.0976 g/mol [M^+].

Solubility (PBS 1% DMSO, pH 7.4): 1.26 mg/mL (1.78 mM)

[(Triethylephosphine-κP)(4(4-(methylsulfonyl)phenyl)thiazolato-κN,κC2´)(1,2,3,4,5 pentamethylcyclopentadienyl)rhodium(III)] chloride ***II***

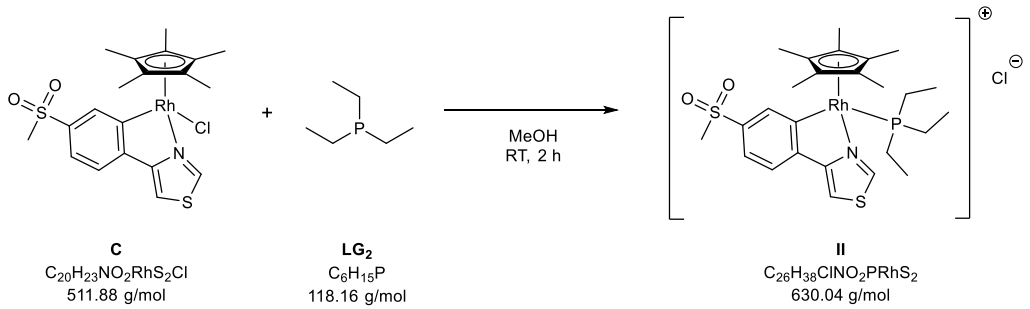

C
$C_{20}H_{23}NO_2RhS_2Cl$
511.88 g/mol

LG_2
$C_6H_{15}P$
118.16 g/mol

II
$C_{26}H_{38}ClNO_2PRhS_2$
630.04 g/mol

Chlorido-complex **C** (120 mg, 235 µmol, 1.0 eq.), triethylphosphine **LG_2** (28 mg, 235 µmol, 1.0 eq.) and 12 mL MeOH were stirred for 2 h. The crude product was purified *via* chromatography on silica (50 g; 10% MeOH in DCM). Product **II** was obtained as a yellow solid.

Yield: 96 mg (98%)

^{1}H NMR (700.40 MHz, $CDCl_3$): δ = 10.39 (s, 1H, Ha), 8.16 (d, *J* = 1.8 Hz, 1H, Hb), 8.05 (s, 1H, Hh), 7.84 (d, *J* = 8.1 Hz, 1H, He), 7.72 (dd, *J* = 8.0, 2.5 Hz, 1H, Hf), 3.09 (s, 3H, Hj), 1.70 (d, *J* = 2.5 Hz, 15H, HA), 1.48 – 1.37 (m, 6H, H1), 0.89 (dt, *J* = 15.5, 7.6 Hz, 9H, H2) ppm.

^{13}C-NMR (150.92 MHz, $CDCl_3$): δ = 167.0 – 166.5 (Cq, Ci), 162.1 (CH, Ca), 159.6 (Cq, Cc), 143.5 (Cq, Cd), 139.3 (Cq, Cg), 135.2 (CH,Ch), 123.6 (2 CH, Ce, Cf), 116.0 (CH, Cb), 100.8 (Cq, CB), 44.8 (CH, Cj), 16.2 (CH_2, C1), 9.7 (CH_3, CA), 8.0 (CH_3, C2) ppm.

EA found (calculated) for $C_{26}H_{38}NO_2PRhS_2Cl \cdot 1.25\ H_2O$: C 48.02 (47.85), H 6.08 (6.26), N 2.36 (2.15), O 7.98 (7.97), S 9.50 (9.83) w-%.

HR-MS: calcd. 594.1137, found 594.1123 g/mol [M^+].

Solubility (PBS 1% DMSO, pH 7.4): 1.36 mg/mL (2.08 mM)

*[(Triephenylphosphine-κP)(4(4-(methylsulfonyl)phenyl)thiazolato-κN,κC2´)(1,2,3,4,5 pentamethylcyclopentadienyl)rhodium(III)] chloride **III***

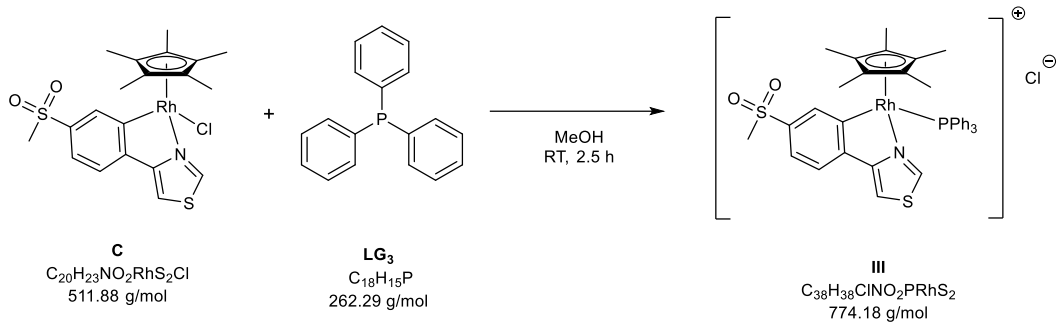

C
$C_{20}H_{23}NO_2RhS_2Cl$
511.88 g/mol

LG_3
$C_{18}H_{15}P$
262.29 g/mol

III
$C_{38}H_{38}ClNO_2PRhS_2$
774.18 g/mol

Chlorido-complex **C** (200 mg, 391 µmol, 1.0 eq.), triphenylphosphine **LG_3** (103 mg, 391 µmol, 1.0 eq.) and 20 mL MeOH were stirred for 2.5 h. The crude product was purified *via* chromatography on silica (50 g; 5–10% MeOH in DCM). Product **III** was obtained as a dark yellow solid.

Yield: 222 mg (98%)

^{1}H NMR (600.18 MHz, MeOD-d^4): δ = 9.61 (s, 1H, Ha), 8.12 (s, 1H, Hh), 7.89 (d, *J* = 2.0 Hz, 1H, Hb), 7.60 (d, *J* = 9.7 Hz, 1H, He), 7.53 (d, *J* = 7.9 Hz, 1H, Hf), 7.50 (s, 3H, H3), 7.39 (s, 6H, H2), 7.03 (s, 6H, H1), 2.96 (s, 3H, Hj), 1.52 (d, *J* = 2.9 Hz, 15H, HA) ppm.

^{13}C-NMR (150.92 MHz, MeOD-d^4): δ = 168.3 – 168.0 (Cq, Ci), 161.9 (Cq, Cc), 158.8 (CH, Ca), 145.2 (Cq, Cd), 140.7 (Cq, Cg), 136.5 (CH,Ch), 134.6 (CH, C1), 132.5 (CH, C3), 130.0 (CH, C2), 125.0 (CH, Ce), 124.4 (CH, Cf),116.6 (CH, Cb), 103.2-103.3 (Cq, CB), 44.7 (CH, Cj), 9.4 (CH_3, CA), ppm.

EA found (calculated) for $C_{38}H_{38}NO_2PRhS_2Cl \cdot 0.66\ CH_2Cl_2$*0.25 H_2O: C 54.92 (55.03), H 7.51 (4.88), N 1.99 (1.66), S 7.46 (7.60) w-%.

HR-MS: calcd. 738.1137, found 738.1119 g/mol [M$^+$].

Solubility (PBS 1% DMSO, pH 7.4): 0.82 mg/mL (0.97 mM)

*[(Pyrazole-κN)(4(4-(methylsulfonyl)phenyl)thiazolato-κN,κC2´)(1,2,3,4,5 pentamethylcyclopentadienyl)rhodium(III)] hexafluorophosphate **IV***

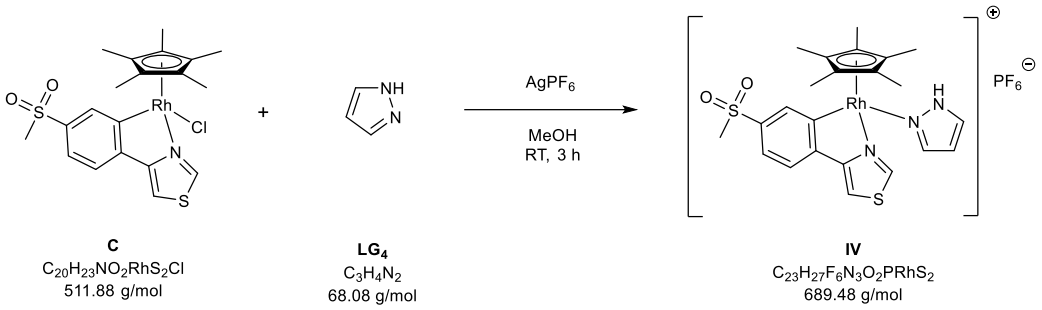

C
$C_{20}H_{23}NO_2RhS_2Cl$
511.88 g/mol

LG$_4$
$C_3H_4N_2$
68.08 g/mol

IV
$C_{23}H_{27}F_6N_3O_2PRhS_2$
689.48 g/mol

Pyrazole salt **IV** was synthesized according to *GP1* with the addition of silver hexafluorophosphate ($AgPF_6$) (108 mg, 430 µmol, 1.1 eq.) to the chlorido-complex **C** (200 mg, 390 µmol, 1.0 eq.) and pyrazole **LG$_4$** (26 mg, 390 µmol, 1.0 eq.) reaction mixture in 20 mL MeOH and stirring at RT for 3 h. The crude product was redissolved in DCM and filtered. After removing the solvent under reduced pressure, the product was dissolved in a minimum quantity of DCM and precipitated with diethyl ether. Product **IV** was collected *via* filtration and obtained as a bright orange solid.

Yield: 122 mg (67%)

^{1}H NMR (700.40 MHz, DMSO): δ = 12.80 (s, 1H, NH) 9.70 (d, *J* = 2.0 Hz, 1H, Ha), 8.64 (d, *J* = 2.0 Hz, 1H, Hb), 8.08 (d, *J* = 8.0 Hz, 1H, Hf), 8.07 (d, *J* = 1.8 Hz, 1H, Hh), 7.78 (dd, *J* = 8.0, 1.8 Hz, 1H, He), 7.72 (s, 1H, H1), 7.48 (s, 1H, H3), 6.25 (dd, *J* = 2.0, 2.0 Hz, 1H, H2), 3.29 (s, 3H, Hj), 1.66 (s, 13H, HA) ppm.

^{13}C-NMR (176.12 MHz, DMSO d-6): δ = 166.4 (Cq, Ci), 159.7 (CH, Ca), 159.1 (Cq, Cc), 143.1 (Cq, Cd), 140.5 (Cq, Cg), 138.1 (CH, C1), 133.9 (CH, Ch), 128.1 (CH, C3), 124.0 (CH, Ce), 123.6 (CH, Cf), 117.1 (CH, Cb), 104.2 (CH, C2), 101.7 (Cq, CB), 43.73 (CH_3, Cj), 30.3, 8.6 (CH_3, CA) ppm.

EA found (calculated) for $C_{23}H_{27}N_3O_2RhS_2PF_6 \cdot 0.25\ H_2O$: C 39.91 (39.81), H 3.64 (3.99), N 5.83 (6.05), S 8.91 (9.24) w-%.

HR-MS: calcd. 476.0225, found 476.0208 g/mol [M^+ - $C_3H_4N_2$].

Solubility (PBS 1% DMSO, pH 7.4): 0.35 mg/mL (0.5 mM)

*[(Isoquinoline-κN)(4(4-(methylsulfonyl)phenyl)thiazolato-κN,κC2´)(1,2,3,4,5 pentamethylcyclopentadienyl)rhodium(III)] hexafluorophosphate **V***

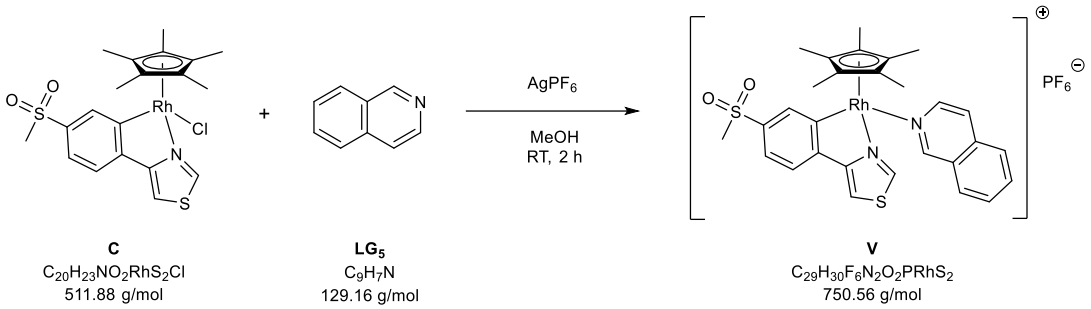

C
$C_{20}H_{23}NO_2RhS_2Cl$
511.88 g/mol

LG_5
C_9H_7N
129.16 g/mol

V
$C_{29}H_{30}F_6N_2O_2PRhS_2$
750.56 g/mol

Isoquinoline salt **V** was synthesized according to *GP1* with the addition of silver hexafluorophosphate ($AgPF_6$) (108 mg, 430 µmol, 1.1 eq.) stirring with the rhodium(III)-chlorido-complex **C** (200 mg, 391 µmol, 1.0 eq.) and isoquinoline **LG_5** (50 mg, 391 µmol, 1.0 eq.) in 20 mL of MeOH for 2 hours. The crude product was redissolved in DCM and filtered and the solvent removed under reduced pressure. the product was precipitated with diethyl ether upon dissolving in DCM. The product **V** was collected *via* filtration and obtained as a bright yellow solid.

Yield: 164 mg (56%)

^{1}H NMR (700.40 MHz, DMSO-d^6): δ = 9.70 (d, J = 2.0 Hz, 1H, Ha), 9.32 (s, 1H, H9), 8.64 (d, J = 2.0 Hz, 1H, Hb), 8.50 (d, J = 5.7 Hz, 1H, H1), 8.13 (dd, J = 8.2, 1.0 Hz, 1H, H7), 8.08 (d, J = 8.0 Hz, 1H, Hf), 8.07 (d, J = 1.8 Hz, 1H, Hh), 7.97 (dd, J= 8.2, 1.1 Hz, 1H, H4), 7.83 (d, J = 5.7 Hz, 1H, H2), 7.81 – 7.77 (m, 2H, H5, He), 7.70 (ddd, J = 8.1, 6.8, 1.2 Hz, 1H, H6), 3.29 (s, 3H, Hj), 1.66 (s, 15H, HA) ppm.

^{13}C-NMR (176.12 MHz, DMSO-d^6): δ = 166.4 (Cq, Ci), 159.7 (CH, Ca), 159.1 (Cq, Cc), 152.3 (CH, C9), 143.1 (Cq, Cd), 142.9 (CH, C1), 140.5 (Cq, Cg), 135.2 (Cq, C8), 133.9 (CH, Ch), 130.6 (Ch, C5), 128.2 (Cq, C3), 127.5 (CH, C7), 126.4 (CH, C4), 124.0 (CH, Ce), 123.6 (CH, Cf), 120.3 (CH, C2), 117.1 (CH, Cb), 101.7 (Cq, CB), 64.9, 43.7 (CH_3, Cj), 8.6 (CH_3, CA) ppm.

EA found (calculated) for $C_{29}H_{30}N_2O_2RhS_2PF_6$: C 46.39 (46.41), H 3.85 (4.03), N 3.93 (3.73), S 8.40 (8.54) w-%.

HR-MS: calcd. 605.0804, found 605.0798 g/mol [M^+].

Solubility (PBS 1% DMSO, pH 7.4): 0.15 mg/mL (0.2 mM)

4. Conclusion

The attempted syntheses of five novel rhodium complexes bearing different *P*- or *N*-donor atom leaving groups were overall successful. The compounds were based on the previously synthesized 4-(4-mesyl)phenylthiazole-rhodium-chlorido complex and any difficulties encountered during the synthesis and work up processes could be resolved. All obtained organometallics were isolated in elemental analysis purity, sufficient for biological studies. The formation of the complexes was proven *via* ^{1}H- and ^{13}C-NMR as well as ESI-MS. In addition, crystals suitable for X-ray diffraction analysis were obtained for all compounds **I**–**V**.

The solubility of the precursor chlorido complex **C** was significantly improved by introducing different leaving groups with the exception of complex **IV** and **V**. Their poorer solubility is attributed to their counter ion PF_6^-, but was still found in the same range as the precursor complex. The stability of the complexes under pseudo-physiological conditions was investigated via *UV/Vis* measurements. The complexes **I**–**III** were stable over 24 h in 10% DMSO/PBS, whereas complex **IV** and **V** showed micro precipitation over time.

In regards to their anticancer potential complex **II** showed the most potent antiproliferative activity in the lower micromolar range with the best results in ovarian carcinoma cell line CH1/PA-1. In contrast, complex **I** showed no relevant antiproliferative activity with IC_{50} values > 200 µM in all tested cell lines, highlighting the impact of the leaving group on the anticancer potential of the compound.

Overall the novel compounds **I**–**V** presented in this work constitute a promising approach to the design and synthesis of new rhodium-based anticancer therapeutics. The results obtained in this work provide valuable information for the further understanding of rhodium-metallocene chemistry.

5. References

(1) *Cancer*. https://www.who.int/news-room/fact-sheets/detail/cancer (accessed 2025-05-15).

(2) NCD Countdown 2030: Pathways to Achieving Sustainable Development Goal Target 3.4. *Lancet Lond. Engl.* **2020**, *396* (10255), 918–934. https://doi.org/10.1016/S0140-6736(20)31761-X.

(3) *Cancer Today*. https://gco.iarc.who.int/today/ (accessed 2025-05-15).

(4) Jackson, S. S.; Marks, M. A.; Katki, H. A.; Cook, M. B.; Hyun, N.; Freedman, N. D.; Kahle, L. L.; Castle, P. E.; Graubard, B. I.; Chaturvedi, A. K. Sex Disparities in the Incidence of 21 Cancer Types: Quantification of the Contribution of Risk Factors. *Cancer* **2022**, *128* (19), 3531–3540. https://doi.org/10.1002/cncr.34390.

(5) Hanahan, D.; Weinberg, R. A. The Hallmarks of Cancer. *Cell* **2000**, *100* (1), 57–70. https://doi.org/10.1016/S0092-8674(00)81683-9.

(6) Hanahan, D.; Weinberg, R. A. Hallmarks of Cancer: The next Generation. *Cell* **2011**, *144* (5), 646–674. https://doi.org/10.1016/j.cell.2011.02.013.

(7) Hanahan, D. Hallmarks of Cancer: New Dimensions. *Cancer Discov.* **2022**, *12* (1), 31–46. https://doi.org/10.1158/2159-8290.CD-21-1059.

(8) Wyld, L.; Audisio, R. A.; Poston, G. J. The Evolution of Cancer Surgery and Future Perspectives. *Nat. Rev. Clin. Oncol.* **2015**, *12* (2), 115–124. https://doi.org/10.1038/nrclinonc.2014.191.

(9) Cheng, H.; Xu, H.; Peng, B.; Huang, X.; Hu, Y.; Zheng, C.; Zhang, Z. Illuminating the Future of Precision Cancer Surgery with Fluorescence Imaging and Artificial Intelligence Convergence. *Npj Precis. Oncol.* **2024**, *8* (1), 1–14. https://doi.org/10.1038/s41698-024-00699-3.

(10) *New WHO/IAEA publication provides guidance on radiotherapy equipment to fight cancer*. https://www.who.int/news/item/05-03-2021-new-who-iaea-publication-provides-guidance-on-radiotherapy-equipment-to-fight-cancer (accessed 2025-05-19).

(11) *Strategies to improve radiotherapy with targeted drugs | Nature Reviews Cancer*. https://www.nature.com/articles/nrc3007 (accessed 2025-05-19).

(12) Baskar, R.; Lee, K. A.; Yeo, R.; Yeoh, K.-W. Cancer and Radiation Therapy: Current Advances and Future Directions. *Int. J. Med. Sci.* **2012**, *9* (3), 193–199. https://doi.org/10.7150/ijms.3635.

(13) *Radiation oncology: a century of achievements | Nature Reviews Cancer*. https://www.nature.com/articles/nrc1451 (accessed 2025-05-19).

(14) Waldman, A. D.; Fritz, J. M.; Lenardo, M. J. A Guide to Cancer Immunotherapy: From T Cell Basic Science to Clinical Practice. *Nat. Rev. Immunol.* **2020**, *20* (11), 651–668. https://doi.org/10.1038/s41577-020-0306-5.

(15) Guo, C.; Manjili, M. H.; Subjeck, J. R.; Sarkar, D.; Fisher, P. B.; Wang, X.-Y. Chapter Seven - Therapeutic Cancer Vaccines: Past, Present, and Future. In *Advances in Cancer Research*; Tew, K. D., Fisher, P. B., Eds.; Academic Press, 2013; Vol. 119, pp 421–475. https://doi.org/10.1016/B978-0-12-407190-2.00007-1.

(16) Southam, C. M.; Brunschwig, A.; Levin, A. G.; Dizon, Q. S. Effect of Leukocytes on Transplantability of Human Cancer. *Cancer* **1966**, *19* (11), 1743–1753. https://doi.org/10.1002/1097-0142(196611)19:11<1743::AID-CNCR2820191143>3.0.CO;2-U.

(17) *Control of peripheral T-cell tolerance and autoimmunity via the CTLA-4 and PD-1 pathways - Fife - 2008 - Immunological Reviews - Wiley Online Library*. https://onlinelibrary.wiley.com/doi/full/10.1111/j.1600-065X.2008.00662.x?casa_token=1SOq2IaW7J0AAAAA%3ADdTz3zcFr7dS4sbzCmpq5M0_vllyGcgxp2TAFizv1p21qfYHG2pVyAuTZVvwxDtsdU1HzIlS8AydJvs (accessed 2025-05-20).

(18) Bhatia, A.; and Kumar, Y. Cellular and Molecular Mechanisms in Cancer Immune Escape: A Comprehensive Review. *Expert Rev. Clin. Immunol.* **2014**, *10* (1), 41–62. https://doi.org/10.1586/1744666X.2014.865519.

(19) Kennedy, L. B.; Salama, A. K. S. A Review of Cancer Immunotherapy Toxicity. *CA. Cancer J. Clin.* **2020**, *70* (2), 86–104. https://doi.org/10.3322/caac.21596.

(20) Weiden, P. L.; Flournoy, N.; Thomas, E. D.; Prentice, R.; Fefer, A.; Buckner, C. D.; Storb, R. Antileukemic Effect of Graft-versus-Host Disease in Human Recipients of Allogeneic-Marrow Grafts. *N. Engl. J. Med.* **1979**, *300* (19), 1068–1073. https://doi.org/10.1056/NEJM197905103001902.

(21) Rosenberg, S. A.; Yannelli, J. R.; Yang, J. C.; Topalian, S. L.; Schwartzentruber, D. J.; Weber, J. S.; Parkinson, D. R.; Seipp, C. A.; Einhorn, J. H.; White, D. E. Treatment of Patients With Metastatic Melanoma With Autologous Tumor-Infiltrating Lymphocytes and Interleukin 2. *JNCI J. Natl. Cancer Inst.* **1994**, *86* (15), 1159–1166. https://doi.org/10.1093/jnci/86.15.1159.

(22) *Monoclonal Antibodies - NCI*. https://www.cancer.gov/about-cancer/treatment/types/immunotherapy/monoclonal-antibodies (accessed 2025-05-20).

(23) Caglevic, C.; Grassi, M.; Raez, L.; Listi, A.; Giallombardo, M.; Bustamante, E.; Gil-Bazo, I.; Rolfo, C. Nintedanib in Non-Small Cell Lung Cancer: From Preclinical to Approval. *Ther. Adv. Respir. Dis.* **2015**, *9* (4), 164–172. https://doi.org/10.1177/1753465815579608.

(24) Garcia, J.; Hurwitz, H. I.; Sandler, A. B.; Miles, D.; Coleman, R. L.; Deurloo, R.; Chinot, O. L. Bevacizumab (Avastin®) in Cancer Treatment: A Review of 15 Years of Clinical Experience and Future Outlook. *Cancer Treat. Rev.* **2020**, *86*. https://doi.org/10.1016/j.ctrv.2020.102017.

(25) Sharma, A.; Jasrotia, S.; Kumar, A. Effects of Chemotherapy on the Immune System: Implications for Cancer Treatment and Patient Outcomes. *Naunyn. Schmiedebergs Arch. Pharmacol.* **2024**, *397* (5), 2551–2566. https://doi.org/10.1007/s00210-023-02781-2.

(26) Behranvand, N.; Nasri, F.; Zolfaghari Emameh, R.; Khani, P.; Hosseini, A.; Garssen, J.; Falak, R. Chemotherapy: A Double-Edged Sword in Cancer Treatment. *Cancer Immunol. Immunother.* **2022**, *71* (3), 507–526. https://doi.org/10.1007/s00262-021-03013-3.

(27) Bardal, S. K.; Waechter, J. E.; Martin, D. S. Chapter 20 - Neoplasia. In *Applied Pharmacology*; Bardal, S. K., Waechter, J. E., Martin, D. S., Eds.; W.B. Saunders: Philadelphia, 2011; pp 305–324. https://doi.org/10.1016/B978-1-4377-0310-8.00020-8.

(28) Emadi, A.; Jones, R. J.; Brodsky, R. A. Cyclophosphamide and Cancer: Golden Anniversary. *Nat. Rev. Clin. Oncol.* **2009**, *6* (11), 638–647. https://doi.org/10.1038/nrclinonc.2009.146.

(29) Toschi, L.; Finocchiaro, G.; Bartolini, S.; Gioia, V.; Cappuzzo, F. Role of Gemcitabine in Cancer Therapy. *Future Oncol. Lond. Engl.* **2005**, *1* (1), 7–17. https://doi.org/10.1517/14796694.1.1.7.

(30) Pession, A.; Masetti, R.; Kleinschmidt, K.; Martoni, A. Use of Clofarabine for Acute Childhood Leukemia. *Biol. Targets Ther.* **2010**, *4*, 111–118. https://doi.org/10.2147/btt.s10123.

(31) Elgemeie, G. H.; Mohamed-Ezzat, R. A. Chapter 2 - Antifolate-Based Anticancer Drugs. In *New Strategies Targeting Cancer Metabolism*; Elgemeie, G. H., Mohamed-Ezzat, R. A., Eds.; Elsevier, 2022; pp 35–67. https://doi.org/10.1016/B978-0-12-821783-2.00007-8.

(32) Weaver, B. A. How Taxol/Paclitaxel Kills Cancer Cells. *Mol. Biol. Cell* **2014**, *25* (18), 2677–2681. https://doi.org/10.1091/mbc.E14-04-0916.

(33) Škubník, J.; Pavlíčková, V. S.; Ruml, T.; Rimpelová, S. Vincristine in Combination Therapy of Cancer: Emerging Trends in Clinics. *Biology* **2021**, *10* (9), 849. https://doi.org/10.3390/biology10090849.

(34) Farouk, F.; Elmaaty ,Ayman Abo; Elkamhawy ,Ahmed; Tawfik ,Haytham O.; Alnajjar ,Radwan; Abourehab ,Mohammed A. S.; Saleh ,Mohamed A.; Eldehna ,Wagdy M.; and Al-Karmalawy, A. A. Investigating the Potential Anticancer Activities of Antibiotics as Topoisomerase II Inhibitors and DNA Intercalators: In Vitro, Molecular Docking, Molecular Dynamics, and SAR Studies. *J. Enzyme Inhib. Med. Chem.* **2023**, *38* (1), 2171029. https://doi.org/10.1080/14756366.2023.2171029.

(35) Gao, Y.; Shang, Q.; Li, W.; Guo, W.; Stojadinovic, A.; Mannion, C.; Man, Y.; Chen, T. Antibiotics for Cancer Treatment: A Double-Edged Sword. *J. Cancer* **2020**, *11* (17), 5135–5149. https://doi.org/10.7150/jca.47470.

(36) Ndagi, U.; Mhlongo, N.; Soliman, M. E. Metal Complexes in Cancer Therapy – an Update from Drug Design Perspective. *Drug Des. Devel. Ther.* **2017**, *11*, 599–616. https://doi.org/10.2147/DDDT.S119488.

(37) *Drugs@FDA: FDA-Approved Drugs*. https://www.accessdata.fda.gov/scripts/cder/daf/index.cfm?event=overview.process&ApplNo=018057 (accessed 2025-05-25).

(38) Allardyce, C. S.; Dyson, P. J. Metal-Based Drugs That Break the Rules. *Dalton Trans.* **2016**, *45* (8), 3201–3209. https://doi.org/10.1039/C5DT03919C.

(39) Florea, A.-M.; Büsselberg, D. Cisplatin as an Anti-Tumor Drug: Cellular Mechanisms of Activity, Drug Resistance and Induced Side Effects. *Cancers* **2011**, *3* (1), 1351–1371. https://doi.org/10.3390/cancers3011351.

(40) IUPAC; Fischer, J.; Ganellin, C. R. *Analogue-Based Drug Discovery*; John Wiley & Sons, 2006.

(41) Canetta, R.; Rozencweig, M.; Carter, S. K. Carboplatin: The Clinical Spectrum to Date. *Cancer Treat. Rev.* **1985**, *12*, 125–136. https://doi.org/10.1016/0305-7372(85)90027-1.

(42) Stewart, D. J. Mechanisms of Resistance to Cisplatin and Carboplatin. *Crit. Rev. Oncol. Hematol.* **2007**, *63* (1), 12–31. https://doi.org/10.1016/j.critrevonc.2007.02.001.

(43) van der Vijgh, W. J. F. Clinical Pharmacokinetics of Carboplatin. *Clin. Pharmacokinet.* **1991**, *21* (4), 242–261. https://doi.org/10.2165/00003088-199121040-00002.

(44) du Bois, A.; Lück, H.-J.; Meier, W.; Adams, H.-P.; Möbus, V.; Costa, S.; Bauknecht, T.; Richter, B.; Warm, M.; Schröder, W.; Olbricht, S.; Nitz, U.; Jackisch, C.; Emons, G.; Wagner, U.; Kuhn, W.; Pfisterer, J.; For the Arbeitsgemeinschaft Gynäkologische Onkologie (AGO) Ovarian Cancer Study Group. A Randomized Clinical Trial of Cisplatin/Paclitaxel Versus Carboplatin/Paclitaxel as First-Line Treatment of Ovarian Cancer. *JNCI J. Natl. Cancer Inst.* **2003**, *95* (17), 1320–1329. https://doi.org/10.1093/jnci/djg036.

(45) Jodrell, D. I.; Egorin, M. J.; Canetta, R. M.; Langenberg, P.; Goldbloom, E. P.; Burroughs, J. N.; Goodlow, J. L.; Tan, S.; Wiltshaw, E. Relationships between Carboplatin Exposure and Tumor Response and Toxicity in Patients with Ovarian Cancer. *J. Clin. Oncol.* **1992**, *10* (4), 520–528. https://doi.org/10.1200/JCO.1992.10.4.520.

(46) Rossi, A.; Di Maio, M.; Chiodini, P.; Rudd, R. M.; Okamoto, H.; Skarlos, D. V.; Früh, M.; Qian, W.; Tamura, T.; Samantas, E.; Shibata, T.; Perrone, F.; Gallo, C.; Gridelli, C.; Martelli, O.; Lee, S.-M. Carboplatin- or Cisplatin-Based Chemotherapy in First-Line Treatment of Small-Cell Lung Cancer: The COCIS Meta-Analysis of Individual Patient Data. *J. Clin. Oncol.* **2012**, *30* (14), 1692–1698. https://doi.org/10.1200/JCO.2011.40.4905.

(47) Sun, L.; Candelieri-Surette, D.; Anglin-Foote, T.; Lynch, J. A.; Maxwell, K. N.; D'Avella, C.; Singh, A.; Aakhus, E.; Cohen, R. B.; Brody, R. M. Cetuximab-Based vs Carboplatin-Based Chemoradiotherapy for Patients With Head and Neck Cancer. *JAMA Otolaryngol. Neck Surg.* **2022**, *148* (11), 1022–1028. https://doi.org/10.1001/jamaoto.2022.2791.

(48) Xiang, M.; Colevas, A. D.; Holsinger, F. C.; Le, Q.-T. X.; Beadle, B. M. Survival After Definitive Chemoradiotherapy With Concurrent Cisplatin or Carboplatin for Head and Neck Cancer. *J. Natl. Compr. Canc. Netw.* **2019**, *17* (9), 1065–1073. https://doi.org/10.6004/jnccn.2019.7297.

(49) Tournigand, C.; André, T.; Achille, E.; Lledo, G.; Flesh, M.; Mery-Mignard, D.; Quinaux, E.; Couteau, C.; Buyse, M.; Ganem, G.; Landi, B.; Colin, P.; Louvet, C.; de Gramont, A. FOLFIRI Followed by FOLFOX6 or the Reverse Sequence in Advanced Colorectal Cancer: A Randomized GERCOR Study. *J. Clin. Oncol.* **2004**, *22* (2), 229–237. https://doi.org/10.1200/JCO.2004.05.113.

(50) Sanoff, H. K.; Sargent, D. J.; Campbell, M. E.; Morton, R. F.; Fuchs, C. S.; Ramanathan, R. K.; Williamson, S. K.; Findlay, B. P.; Pitot, H. C.; Goldberg, R. M. Five-Year Data and Prognostic Factor Analysis of Oxaliplatin and Irinotecan Combinations for Advanced Colorectal Cancer: N9741. *J. Clin. Oncol. Off. J. Am. Soc. Clin. Oncol.* **2008**, *26* (35), 5721–5727. https://doi.org/10.1200/JCO.2008.17.7147.

(51) Ruzzo, A.; Graziano, F.; Loupakis, F.; Rulli, E.; Canestrari, E.; Santini, D.; Catalano, V.; Ficarelli, R.; Maltese, P.; Bisonni, R.; Masi, G.; Schiavon, G.; Giordani, P.; Giustini, L.; Falcone, A.; Tonini, G.; Silva, R.; Mattioli, R.; Floriani, I.; Magnani, M. Pharmacogenetic Profiling in Patients With Advanced Colorectal Cancer Treated With First-Line FOLFOX-4 Chemotherapy. *J. Clin. Oncol.* **2007**, *25* (10), 1247–1254. https://doi.org/10.1200/JCO.2006.08.1844.

(52) Fries, J. F.; Bloch, D.; Spitz, P.; Mitchell, D. M. Cancer in Rheumatoid Arthritis: A Prospective Long-Term Study of Mortality. *Am. J. Med.* **1985**, *78* (1), 56–59. https://doi.org/10.1016/0002-9343(85)90247-5.

(53) Omer, P. K.; Aziz, N. M.; Omer, R. A. Comprehensive Review of Metal-Based Coordination Compounds in Cancer Therapy: From Design to Biochemical Reactivity. *Rev. Inorg. Chem.* **2024**, *44* (4), 699–710. https://doi.org/10.1515/revic-2024-0030.

(54) Tiekink, E. R. T. Gold Derivatives for the Treatment of Cancer. *Crit. Rev. Oncol. Hematol.* **2002**, *42* (3), 225–248. https://doi.org/10.1016/S1040-8428(01)00216-5.

(55) *Clinical Trial: NCT04143789 - My Cancer Genome*. https://www.mycancergenome.org/content/clinical_trials/NCT04143789/ (accessed 2025-06-10).

(56) Wilke, N. L.; Abodo, L. O.; Frias, C.; Frias, J.; Baas, J.; Jakupec, M. A.; Keppler, B. K.; Prokop, A. The Gallium Complex KP46 Sensitizes Resistant Leukemia Cells and Overcomes Bcl-2-Induced Multidrug Resistance in Lymphoma Cells via Upregulation of Harakiri and Downregulation of XIAP in Vitro. *Biomed. Pharmacother.* **2022**, *156*, 113974. https://doi.org/10.1016/j.biopha.2022.113974.

(57) Valiahdi, S. M.; Heffeter, P.; Jakupec, M. A.; Marculescu, R.; Berger, W.; Rappersberger, K.; Keppler, B. K. The Gallium Complex KP46 Exerts Strong Activity against Primary Explanted Melanoma Cells and Induces Apoptosis in Melanoma Cell Lines. *Melanoma Res.* **2009**, *19* (5), 283–293. https://doi.org/10.1097/CMR.0b013e32832b272d.

(58) Alessio, E.; Messori, L. NAMI-A and KP1019/1339, Two Iconic Ruthenium Anticancer Drug Candidates Face-to-Face: A Case Story in Medicinal Inorganic Chemistry. *Mol. Basel Switz.* **2019**, *24* (10), 1995. https://doi.org/10.3390/molecules24101995.

(59) Karges, J. Clinical Development of Metal Complexes as Photosensitizers for Photodynamic Therapy of Cancer. *Angew. Chem. Int. Ed.* **2022**, *61* (5), e202112236. https://doi.org/10.1002/anie.202112236.

(60) Wang, W.; Wang, L.; Zhang, Y.; Shi, Y.; Zhang, R.; Chen, L.; Shi, Z.; Yuan, S.; Li, X.; He, C.; Li, X. Chiral Iridium-Based TLD-1433 Analogues: Exploration of Enantiomer-Dependent Behavior in Photodynamic Cancer Therapy. *Inorg. Chem.* **2024**, *63* (17), 7792–7798. https://doi.org/10.1021/acs.inorgchem.4c00215.

(61) Mestroni, G.; Alessio, E.; Sava, G.; Pacor, S.; Coluccia, M.; Boccarelli, A. Water-Soluble Ruthenium(III)-Dimethyl Sulfoxide Complexes: Chemical Behaviour and Pharmaceutical Properties. *Met.-Based Drugs* **1994**, *1* (1), 748960. https://doi.org/10.1155/MBD.1994.41.

(62) Sava, G.; Bergamo, A.; Zorzet, S.; Gava, B.; Casarsa, C.; Cocchietto, M.; Furlani, A.; Scarcia, V.; Serli, B.; Iengo, E.; Alessio, E.; Mestroni, G. Influence of Chemical Stability on the Activity of the Antimetastasis Ruthenium Compound NAMI-A. *Eur. J. Cancer* **2002**, *38* (3), 427–435. https://doi.org/10.1016/S0959-8049(01)00389-6.

(63) Bacac, M.; Hotze, A. C. G.; Schilden, K. van der; Haasnoot, J. G.; Pacor, S.; Alessio, E.; Sava, G.; Reedijk, J. The Hydrolysis of the Anti-Cancer Ruthenium Complex NAMI-A Affects Its DNA Binding and Antimetastatic Activity: An NMR Evaluation. *J. Inorg. Biochem.* **2004**, *98* (2), 402–412. https://doi.org/10.1016/j.jinorgbio.2003.12.003.

(64) Liu, M.; Lim, Z. J.; Gwee, Y. Y.; Levina, A.; Lay, P. A. Characterization of a Ruthenium(III)/NAMI-A Adduct with Bovine Serum Albumin That Exhibits a High Anti-Metastatic Activity. *Angew. Chem. Int. Ed.* **2010**, *49* (9), 1661–1664. https://doi.org/10.1002/anie.200906079.

(65) Alessio, E. Thirty Years of the Drug Candidate NAMI-A and the Myths in the Field of Ruthenium Anticancer Compounds: A Personal Perspective. *Eur. J. Inorg. Chem.* **2017**, *2017* (12), 1549–1560. https://doi.org/10.1002/ejic.201600986.

(66) Dömötör, O.; Hartinger, C. G.; Bytzek, A. K.; Kiss, T.; Keppler, B. K.; Enyedy, E. A. Characterization of the Binding Sites of the Anticancer Ruthenium(III) Complexes KP1019 and KP1339 on Human Serum Albumin via Competition Studies. *J. Biol. Inorg. Chem. JBIC Publ. Soc. Biol. Inorg. Chem.* **2013**, *18* (1), 9–17. https://doi.org/10.1007/s00775-012-0944-6.

(67) Hartinger, C. G.; Jakupec, M. A.; Zorbas-Seifried, S.; Groessl, M.; Egger, A.; Berger, W.; Zorbas, H.; Dyson, P. J.; Keppler, B. K. KP1019, A New Redox-Active Anticancer Agent – Preclinical Development and Results of a Clinical Phase I Study in Tumor Patients. *Chem. Biodivers.* **2008**, *5* (10), 2140–2155. https://doi.org/10.1002/cbdv.200890195.

(68) Trondl, R.; Heffeter, P.; Kowol, C. R.; Jakupec, M. A.; Berger, W.; Keppler, B. K. NKP-1339, the First Ruthenium-Based Anticancer Drug on the Edge to Clinical Application. *Chem. Sci.* **2014**, *5* (8), 2925–2932. https://doi.org/10.1039/C3SC53243G.

(69) Spratlin, J. L.; O´Kane, G.; Goodwin, R. A.; McWhirter, E.; Thompson, D.; Halani, K.; Jones, M.; Snow, M.; McAllister, E. R.; Machado, A.; Lemmerick, Y.; Pankovich, J. BOLD-100-001 (TRIO039): A Phase 1b Dose-Escalation Study of BOLD-100 in Combination with FOLFOX Chemotherapy in Patients with Advanced Gastrointestinal Solid Cancers: Interim Safety, Tolerability, and Efficacy. *J. Clin. Oncol.* **2022**, *40* (16_suppl), 3031–3031. https://doi.org/10.1200/JCO.2022.40.16_suppl.3031.

(70) *Bold Therapeutics | FDA Grants Bold Therapeutics BOLD-100 an Orphan Drug Designation (ODD) in the Treatment of Gastric Cancer*. https://www.bold-therapeutics.com/news-post?FDA+Grants+Bold+Therapeutics+BOLD-100+an+Orphan+Drug+Designation+%28ODD%29+in+the+Treatment+of+Gastric+Cancer (accessed 2025-05-22).

(71) *Bold Therapeutics*. Bold-100: Mechanism of Action. https://www.bold-therapeutics.com/technology#Publication (accessed 2025-06-11).

(72) Neuditschko, B.; Legin, A. A.; Baier, D.; Schintlmeister, A.; Reipert, S.; Wagner, M.; Keppler, B. K.; Berger, W.; Meier-Menches, S. M.; Gerner, C. Interaction with Ribosomal Proteins Accompanies Stress Induction of the Anticancer Metallodrug BOLD-100/KP1339 in the Endoplasmic Reticulum. *Angew. Chem. Int. Ed Engl.* **2021**, *60* (10), 5063–5068. https://doi.org/10.1002/anie.202015962.

(73) Griffin, D.; Carson, R.; Moss, D.; Sessler, T.; Lavin, D.; Tiwari, V. K.; Karelia, S.; Kennedy, R.; Savage, K. I.; McDade, S.; Carie, A.; Pankovich, J.; Bazett, M.; Van Schaeybroeck, S. Ruthenium Drug BOLD-100 Regulates BRAFMT Colorectal Cancer Cell Apoptosis through AhR/ROS/ATR Signaling Axis Modulation. *Mol. Cancer Res.* **2024**, *22* (12), 1088–1101. https://doi.org/10.1158/1541-7786.MCR-24-0151.

(74) Wernitznig, D.; Kiakos, K.; Del Favero, G.; Harrer, N.; Machat, H.; Osswald, A.; Jakupec, M. A.; Wernitznig, A.; Sommergruber, W.; Keppler, B. K. First-in-Class Ruthenium Anticancer Drug (KP1339/IT-139) Induces an Immunogenic Cell Death Signature in Colorectal Spheroids in Vitro†. *Metallomics* **2019**, *11* (6), 1044–1048. https://doi.org/10.1039/c9mt00051h.

(75) Baier, D.; Schoenhacker-Alte, B.; Rusz, M.; Pirker, C.; Mohr, T.; Mendrina, T.; Kirchhofer, D.; Meier-Menches, S. M.; Hohenwallner, K.; Schaier, M.; Rampler, E.; Koellensperger, G.; Heffeter, P.; Keppler, B.; Berger, W. The Anticancer Ruthenium Compound BOLD-100 Targets Glycolysis and Generates a Metabolic Vulnerability towards Glucose Deprivation. *Pharmaceutics* **2022**, *14* (2), 238. https://doi.org/10.3390/pharmaceutics14020238.

(76) Baier, D.; Mendrina, T.; Schoenhacker-Alte, B.; Pirker, C.; Mohr, T.; Rusz, M.; Regner, B.; Schaier, M.; Sgarioto, N.; Raynal, N. J.-M.; Nowikovsky, K.; Schmidt, W. M.; Heffeter, P.; Meier-Menches, S. M.; Koellensperger, G.; Keppler, B. K.; Berger, W. The Lipid Metabolism as Target and Modulator of BOLD-100 Anticancer Activity: Crosstalk with Histone Acetylation. *Adv. Sci.* **2023**, *10* (32), 2301939. https://doi.org/10.1002/advs.202301939.

(77) Ernst, R. J.; Komor, A. C.; Barton, J. K. Selective Cytotoxicity of Rhodium Metalloinsertors in Mismatch Repair-Deficient Cells. *Biochemistry* **2011**, *50* (50), 10919–10928. https://doi.org/10.1021/bi2015822.

(78) Threatt, S. D.; Synold, T. W.; Wu, J.; Barton, J. K. In Vivo Anticancer Activity of a Rhodium Metalloinsertor in the HCT116 Xenograft Tumor Model. *Proc. Natl. Acad. Sci. U. S. A.* **2020**, *117* (30), 17535–17542. https://doi.org/10.1073/pnas.2006569117.

(79) Dorcier, A.; Ang, W. H.; Bolaño, S.; Gonsalvi, L.; Juillerat-Jeannerat, L.; Laurenczy, G.; Peruzzini, M.; Phillips, A. D.; Zanobini, F.; Dyson, P. J. In Vitro Evaluation of Rhodium and Osmium RAPTA Analogues: The Case for Organometallic Anticancer Drugs Not Based on Ruthenium. *Organometallics* **2006**, *25* (17), 4090–4096. https://doi.org/10.1021/om060394o.

(80) Gasser, G.; Ott, I.; Metzler-Nolte, N. Organometallic Anticancer Compounds. *J. Med. Chem.* **2011**, *54* (1), 3–25. https://doi.org/10.1021/jm100020w.

(81) Rosenthal, U.; Burlakov, V. V.; Bach, M. A.; Beweries, T. Five-Membered Metallacycles of Titanium and Zirconium – Attractive Compounds for Organometallic Chemistry and Catalysis. *Chem. Soc. Rev.* **2007**, *36* (5), 719–728. https://doi.org/10.1039/B605734A.

(82) Morris, R. E.; Aird, R. E.; del Socorro Murdoch, P.; Chen, H.; Cummings, J.; Hughes, N. D.; Parsons, S.; Parkin, A.; Boyd, G.; Jodrell, D. I.; Sadler, P. J. Inhibition of Cancer Cell Growth by Ruthenium(II) Arene Complexes. *J. Med. Chem.* **2001**, *44* (22), 3616–3621. https://doi.org/10.1021/jm010051m.

(83) Yadav, S. Potential of Metal Complexes for the Treatment of Cancer: Current Update and Future Prospective. In *Chemistry of Biologically Potent Natural Products and Synthetic Compounds*; John Wiley & Sons, Ltd, 2021; pp 183–204. https://doi.org/10.1002/9781119640929.ch7.

(84) Thota, S.; Rodrigues, D. A.; Crans, D. C.; Barreiro, E. J. Ru(II) Compounds: Next-Generation Anticancer Metallotherapeutics? *J. Med. Chem.* **2018**, *61* (14), 5805–5821. https://doi.org/10.1021/acs.jmedchem.7b01689.

(85) Adhireksan, Z.; Davey, G. E.; Campomanes, P.; Groessl, M.; Clavel, C. M.; Yu, H.; Nazarov, A. A.; Yeo, C. H. F.; Ang, W. H.; Dröge, P.; Rothlisberger, U.; Dyson, P. J.; Davey, C. A. Ligand Substitutions between Ruthenium–Cymene Compounds Can Control Protein versus DNA Targeting and Anticancer Activity. *Nat. Commun.* **2014**, *5* (1), 3462. https://doi.org/10.1038/ncomms4462.

(86) Rausch, M.; Dyson, P. J.; Nowak-Sliwinska, P. Recent Considerations in the Application of RAPTA-C for Cancer Treatment and Perspectives for Its Combination with Immunotherapies. *Adv. Ther.* **2019**, *2* (9), 1900042. https://doi.org/10.1002/adtp.201900042.

(87) Casini, A.; Gabbiani, C.; Sorrentino, F.; Rigobello, M. P.; Bindoli, A.; Geldbach, T. J.; Marrone, A.; Re, N.; Hartinger, C. G.; Dyson, P. J.; Messori, L. Emerging Protein Targets for Anticancer Metallodrugs: Inhibition of Thioredoxin Reductase and Cathepsin B by Antitumor Ruthenium(II)−Arene Compounds. *J. Med. Chem.* **2008**, *51* (21), 6773–6781. https://doi.org/10.1021/jm8006678.

(88) Swaminathan, S.; Karvembu, R. Dichloro Ru(II)-p-Cymene-1,3,5-Triaza-7-Phosphaadamantane (RAPTA-C): A Case Study. *ACS Pharmacol. Transl. Sci.* **2023**, *6* (7), 982–996. https://doi.org/10.1021/acsptsci.3c00085.

(89) Tremlett, W. D. J.; Goodman, D. M.; Steel, T. R.; Kumar, S.; Wieczorek-Błauż, A.; Walsh, F. P.; Sullivan, M. P.; Hanif, M.; Hartinger, C. G. Design Concepts of Half-Sandwich Organoruthenium Anticancer Agents Based on Bidentate Bioactive Ligands. *Coord. Chem. Rev.* **2021**, *445*, 213950. https://doi.org/10.1016/j.ccr.2021.213950.

(90) Steel, T. R.; Walsh, F.; Wieczorek-Błauż, A.; Hanif, M.; Hartinger, C. G. Monodentately-Coordinated Bioactive Moieties in Multimodal Half-Sandwich Organoruthenium Anticancer Agents. *Coord. Chem. Rev.* **2021**, *439*, 213890. https://doi.org/10.1016/j.ccr.2021.213890.

(91) Mokesch, S.; Cseh, K.; Geisler, H.; Hejl, M.; Klose, M. H. M.; Roller, A.; Meier-Menches, S. M.; Jakupec, M. A.; Kandioller, W.; Keppler, B. K. Investigations on the Anticancer Potential of Benzothiazole-Based Metallacycles. *Front. Chem.* **2020**, *8*.

(92) Riedl, C. A.; Flocke, L. S.; Hejl, M.; Roller, A.; Klose, M. H. M.; Jakupec, M. A.; Kandioller, W.; Keppler, B. K. Introducing the 4-Phenyl-1,2,3-Triazole Moiety as a Versatile Scaffold for the Development of Cytotoxic Ruthenium(II) and Osmium(II) Arene Cyclometalates. *Inorg. Chem.* **2017**, *56* (1), 528–541. https://doi.org/10.1021/acs.inorgchem.6b02430.

(93) Getreuer, P.; Marretta, L.; Toyoglu, E.; Dömötör, O.; Hejl, M.; Prado-Roller, A.; Cseh, K.; A. Legin, A.; A. Jakupec, M.; Barone, G.; Terenzi, A.; K. Keppler, B.; Kandioller, W. Investigating the Anticancer Potential of 4-Phenylthiazole Derived Ru(Ii) and Os(Ii) Metalacycles. *Dalton Trans.* **2024**, *53* (12), 5567–5579. https://doi.org/10.1039/D4DT00245H.

(94) Harringer, S.; Wernitznig, D.; Gajic, N.; Diridl, A.; Wenisch, D.; Hejl, M.; Jakupec, M. A.; Theiner, S.; Koellensperger, G.; Kandioller, W.; Keppler, B. K. Introducing N-, P-, and S-Donor Leaving Groups: An Investigation of the Chemical and Biological Properties of Ruthenium, Rhodium and Iridium Thiopyridone Piano Stool Complexes. *Dalton Trans.* **2020**, *49* (44), 15693–15711. https://doi.org/10.1039/D0DT03165H.

(95) Lennox, A. J. J.; Lloyd-Jones, G. C. Transmetalation in the Suzuki–Miyaura Coupling: The Fork in the Trail. *Angew. Chem. Int. Ed.* **2013**, *52* (29), 7362–7370. https://doi.org/10.1002/anie.201301737.

(96) Lee, W.; Shin, C.; Park, S. E.; Joo, J. M. Regio- and Stereoselective Synthesis of Thiazole-Containing Triarylethylenes by Hydroarylation of Alkynes. *J. Org. Chem.* **2019**, *84* (20), 12913–12924. https://doi.org/10.1021/acs.joc.9b01619.

(97) Li, L.; Brennessel, W. W.; Jones, W. D. C–H Activation of Phenyl Imines and 2-Phenylpyridines with [Cp*MCl2]2 (M = Ir, Rh): Regioselectivity, Kinetics, and Mechanism. *Organometallics* **2009**, *28* (12), 3492–3500. https://doi.org/10.1021/om9000742.

(98) Ferrer Flegeau, E.; Bruneau, C.; Dixneuf, P. H.; Jutand, A. Autocatalysis for C–H Bond Activation by Ruthenium(II) Complexes in Catalytic Arylation of Functional Arenes. *J. Am. Chem. Soc.* **2011**, *133* (26), 10161–10170. https://doi.org/10.1021/ja201462n.

(99) *Aryl–Aryl Bond Formation by Transition-Metal-Catalyzed Direct Arylation | Chemical Reviews*. https://pubs-acs-org.uaccess.univie.ac.at/doi/10.1021/cr0509760 (accessed 2025-05-25).

(100) Cseh, K.; Geisler, H.; Stanojkovska, K.; Westermayr, J.; Brunmayr, P.; Wenisch, D.; Gajic, N.; Hejl, M.; Schaier, M.; Koellensperger, G.; Jakupec, M. A.; Marquetand, P.; Kandioller, W. Arene Variation of Highly Cytotoxic Tridentate Naphthoquinone-Based Ruthenium(II) Complexes and In-Depth In Vitro Studies. *Pharmaceutics* **2022**, *14* (11), 2466. https://doi.org/10.3390/pharmaceutics14112466.

(101) Kuhn, P.-S.; Pichler, V.; Roller, A.; Hejl, M.; Jakupec, M. A.; Kandioller, W.; Keppler, B. K. Improved Reaction Conditions for the Synthesis of New NKP-1339 Derivatives and Preliminary Investigations on Their Anticancer Potential. *Dalton Trans.* **2014**, *44* (2), 659–668. https://doi.org/10.1039/C4DT01645A.

(102) Riedl, C. A.; Hejl, M.; Klose, M. H. M.; Roller, A.; Jakupec, M. A.; Kandioller, W.; Keppler, B. K. N- and S-Donor Leaving Groups in Triazole-Based Ruthena(II)Cycles: Potent Anticancer Activity, Selective Activation, and Mode of Action Studies. *Dalton Trans.* **2018**, *47* (13), 4625–4638. https://doi.org/10.1039/C8DT00449H.

6. Appendix

Abbreviations

COSY correlated spectroscopy

calcd. calculated

$CDCl_3$ deuterated chloroform

DACH (1R,2R)-Cyclohexane-1,2-diamine, (trans-1,2-diaminocyclohexane)

DCM dichloromethane

d doublet

dd doublet of doublets

DMSO dimethylsulfoxide

DMSO-d^6 deuterated dimethyl sulfoxide

DNA deoxyribonucleic acid

EA elemental analysis

ESI electrospray ionization

Et_3P triethylphosphine

eq. equivalents

FDA Food and Drug Administration

FOLFOX folinic acid, fluorouracil and oxaliplatin

GRP78 78 kDa glucose-regulated protein

hept heptet

HMBC heteronuclear multiple bonds coherence

HSQC heteronuclear single quantum coherence

m multiplet

MEM Minimum Essential Medium

MeOH methanol

MeOD-d^4 deuterated methanol

MTT 3-(4,5-dimethylthiazol-2-yl)-2,5-diphenyltetrazolium bromide

MPLC medium-pressure liquid chromatography

NMR nuclear magnetic resonance

NSCLC non-small cell lung cancer

PBS phosphate-buffered saline

pH potential of hydrogen

Ph_3P triphenylphosphine

PTA 1,3,5-Triaza-7-phosphaadamantane

q quartet

RAED ruthenium arene ethylendiamine

RAPTA ruthenium arene PTA

RNA ribonucleic acid

ROS reactive oxygen species

s singulet

UV/vis ultraviolet/visible

Figures, schemes and tables

NMR Spectra

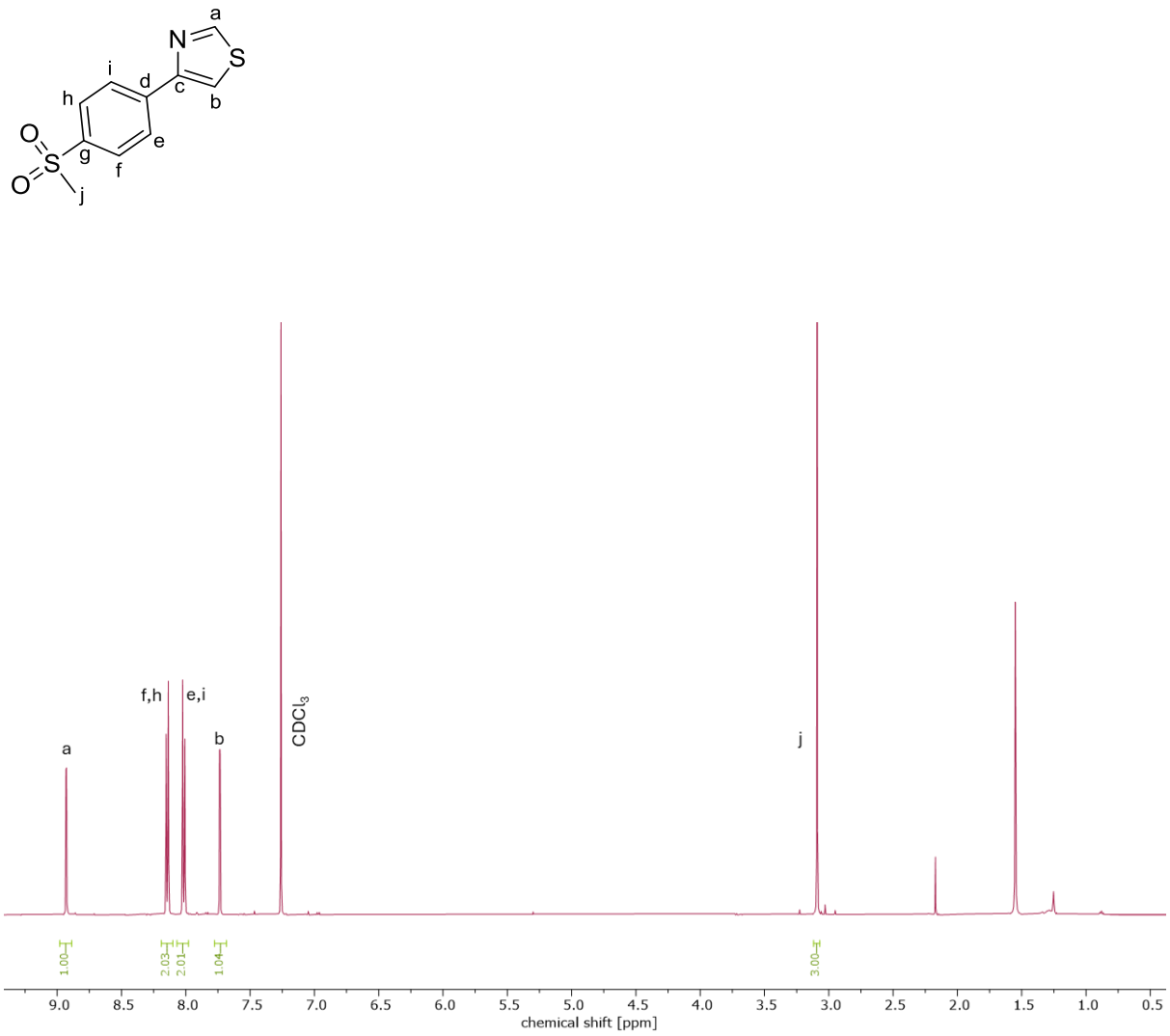

*Figure 21: ^{1}H-NMR spectrum of ligand **L** in $CDCl_3$.*

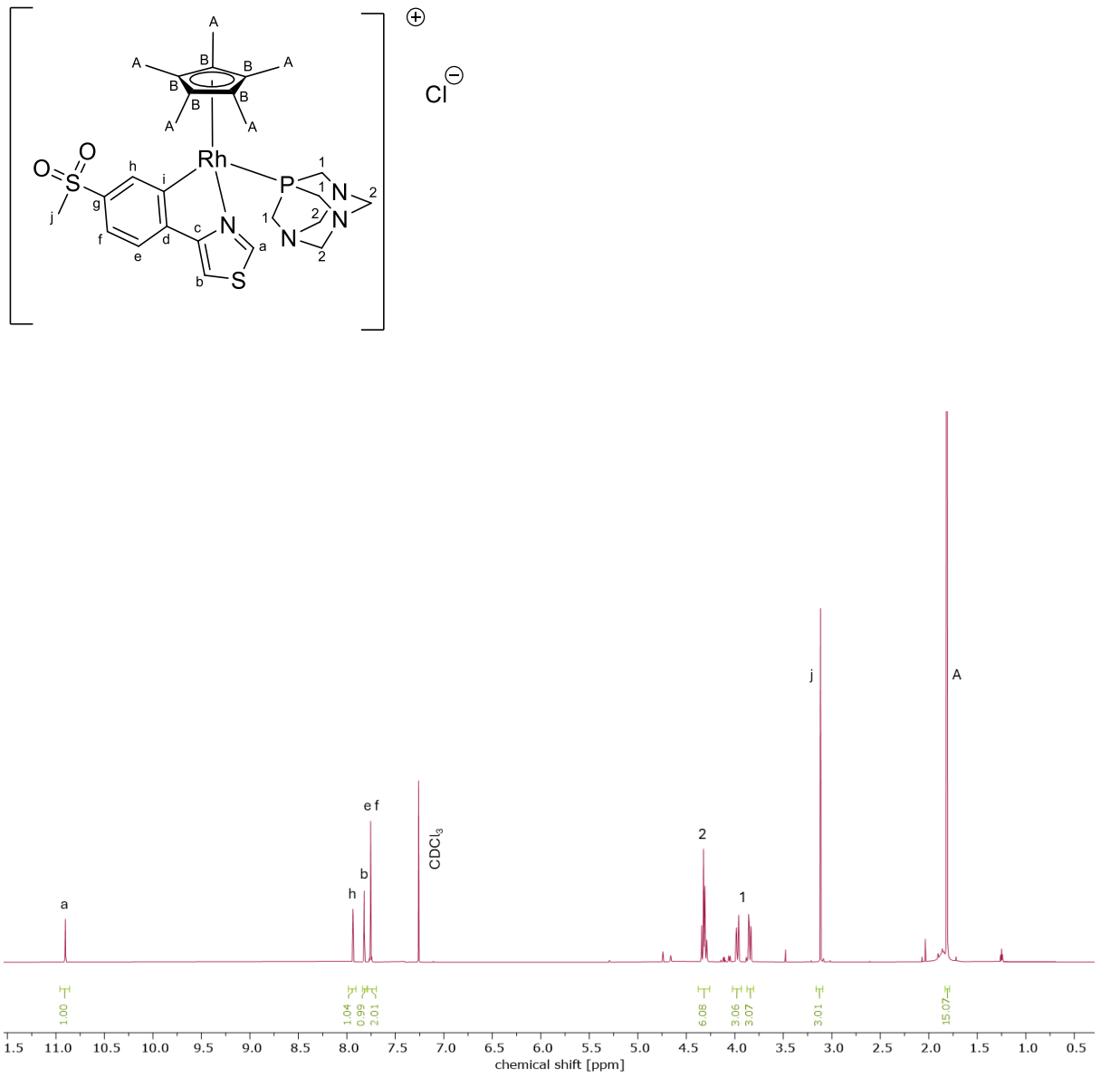

*Figure 22: ^{1}H-NMR spectrum of complex **I** in $CDCl_3$.*

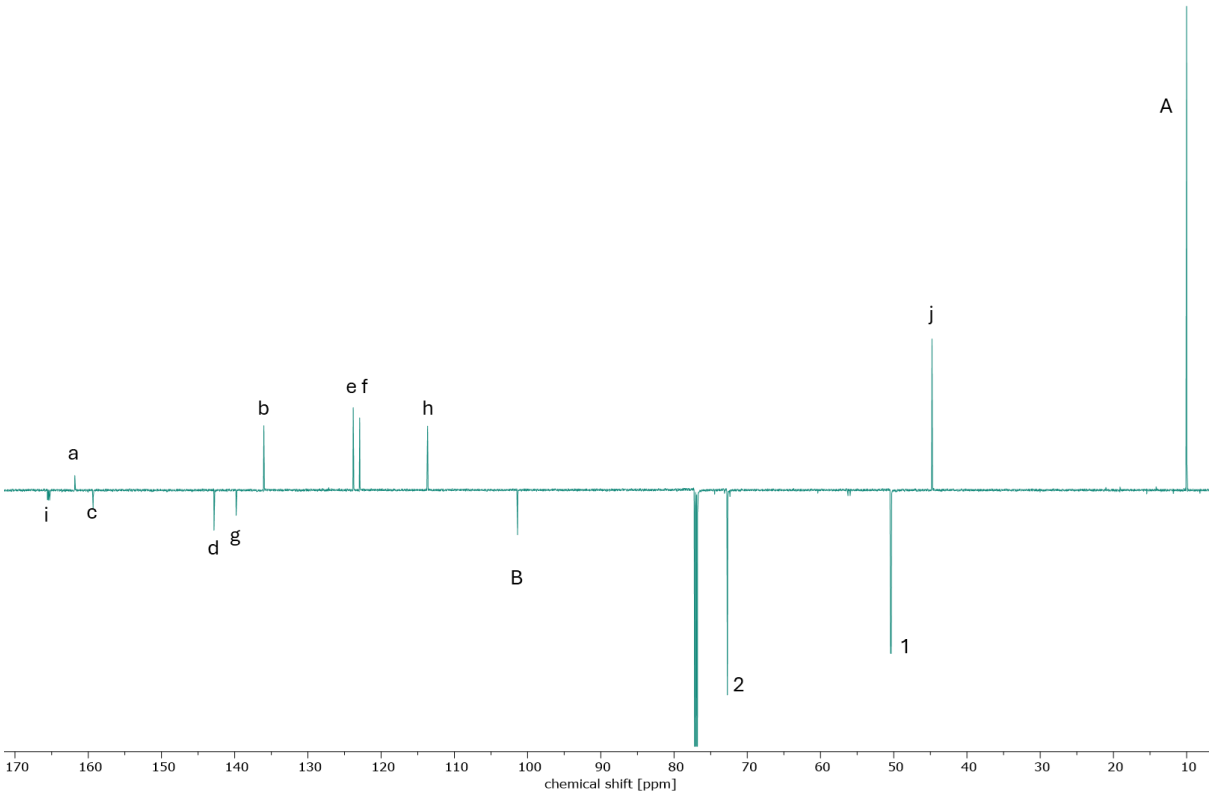

*Figure 23: ^{13}C-NMR spectrum of complex **I** in $CDCl_3$.*

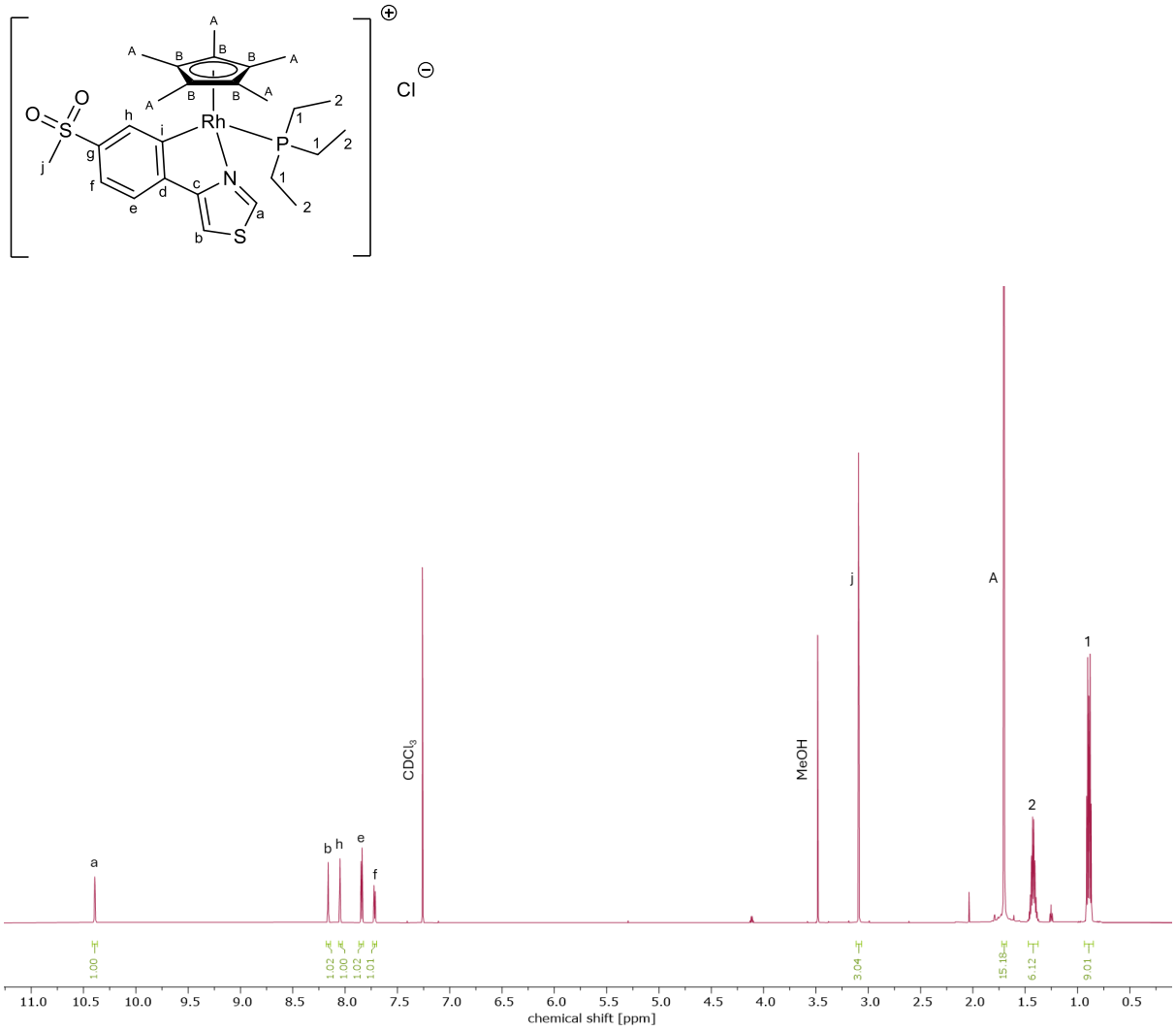

*Figure 24: ^{1}H-NMR spectrum of complex **II** in $CDCl_3$.*

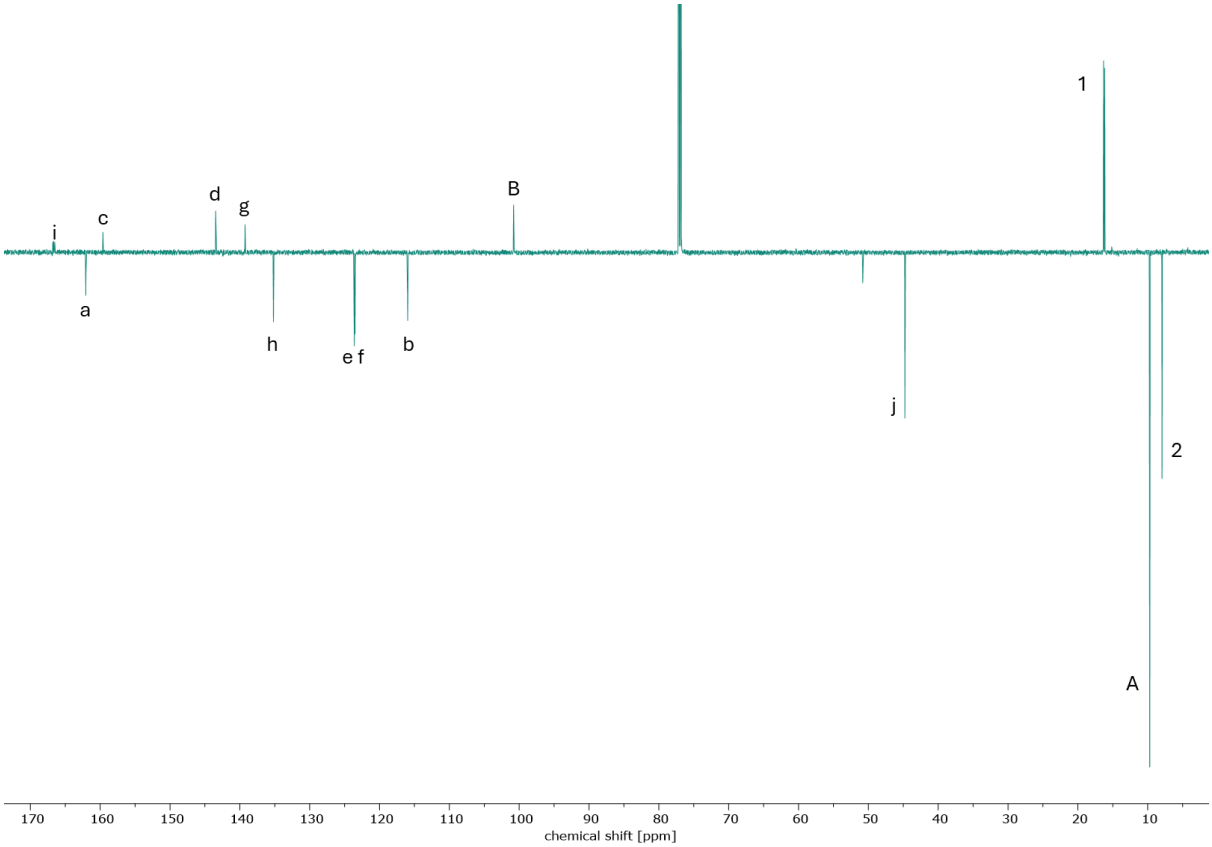

*Figure 25: ^{13}C-NMR spectrum of complex **II** in $CDCl_3$.*

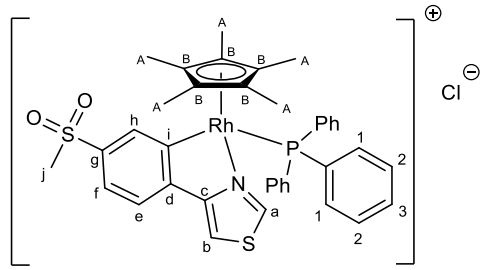

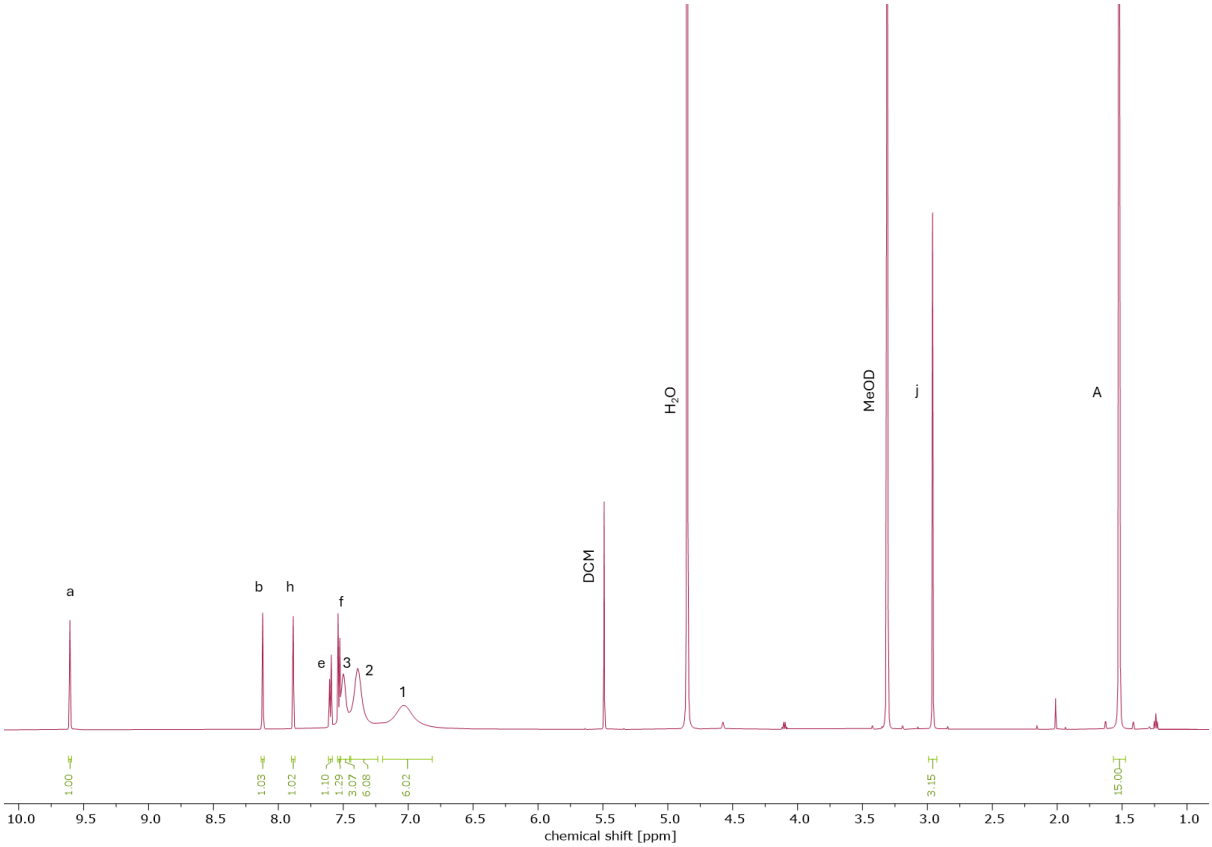

*Figure 26: [1]H-NMr of complex **III** in MeOD-d[4].*

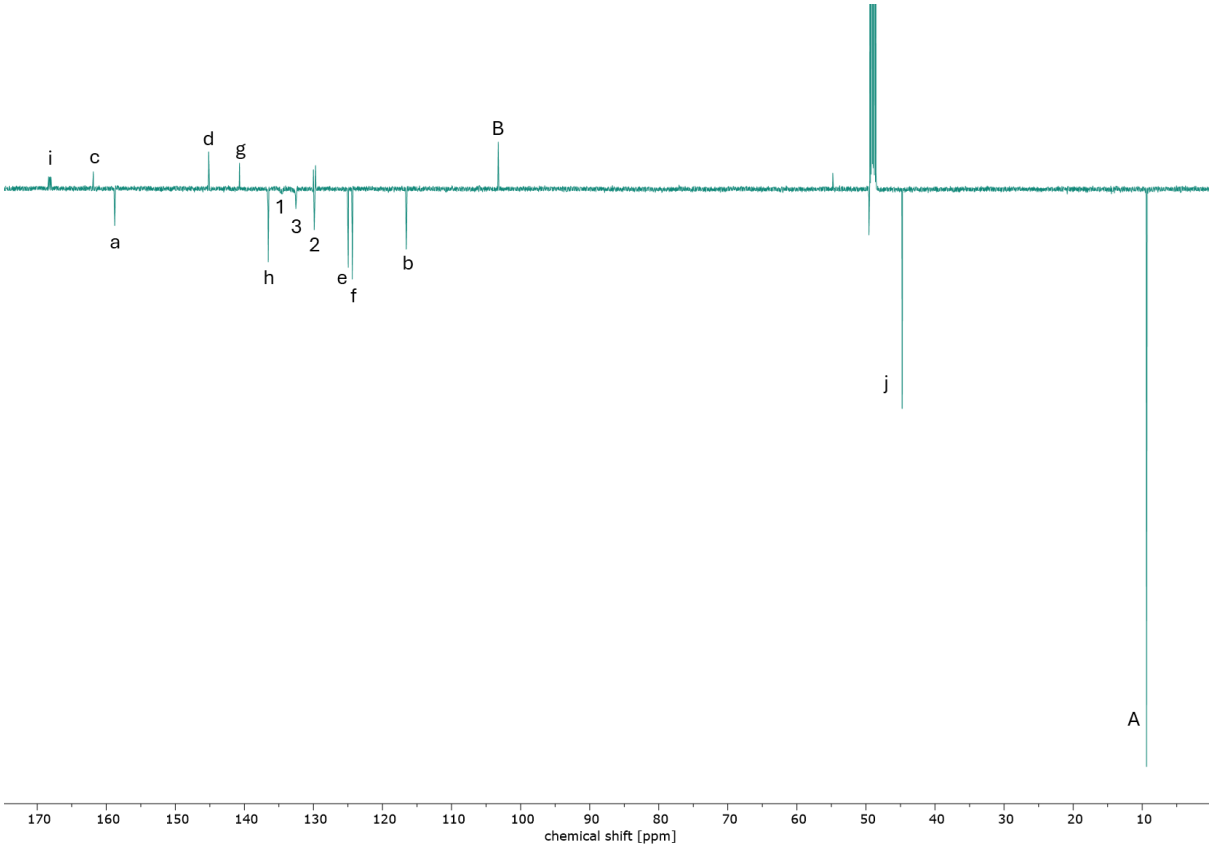

*Figure 27: ^{13}C-NMR of complex **III** in MeOD-d^4.*

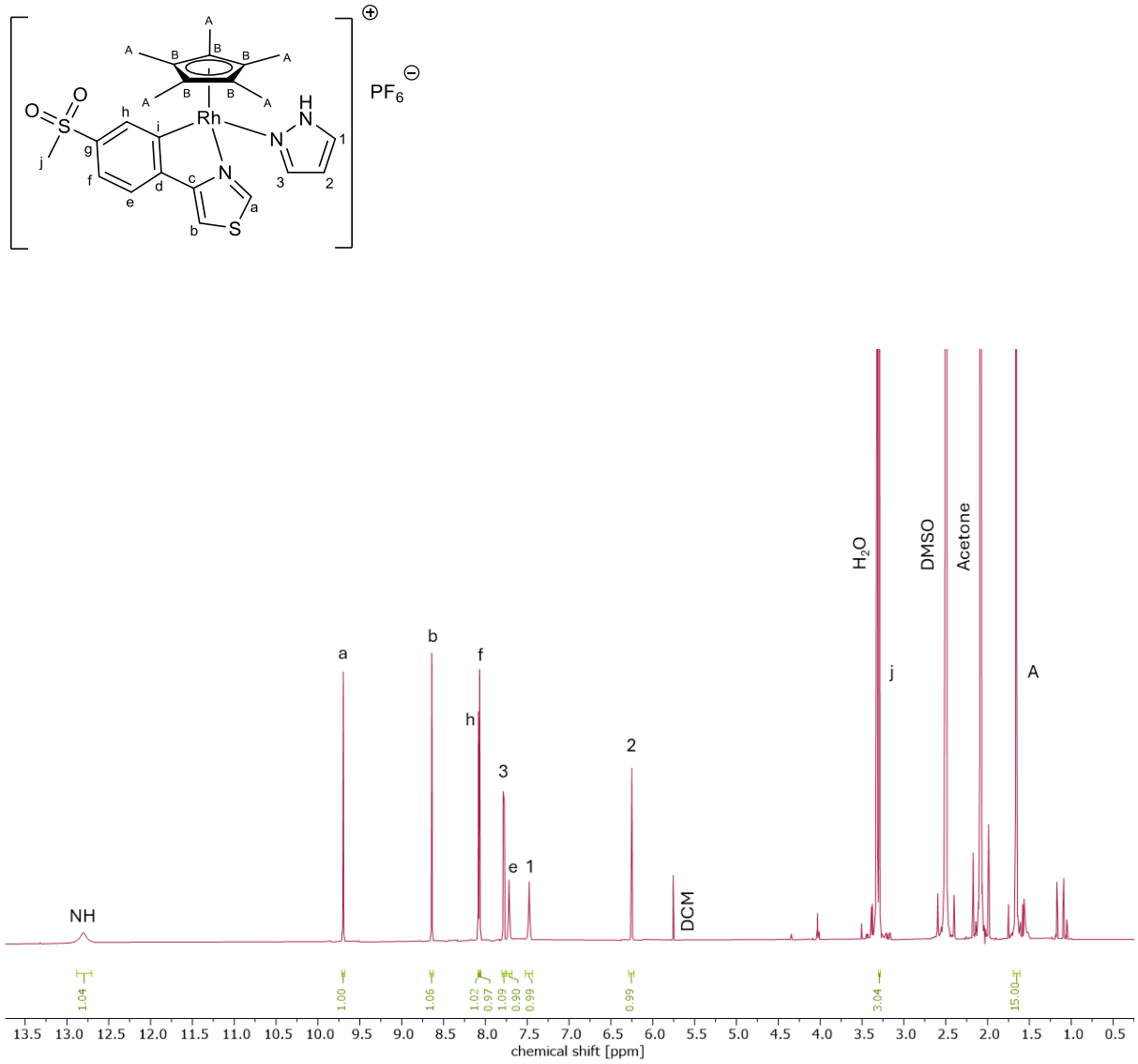

*Figure 28: [1]H-NMR spectrum of complex **IV** in DMSO-d[6].*

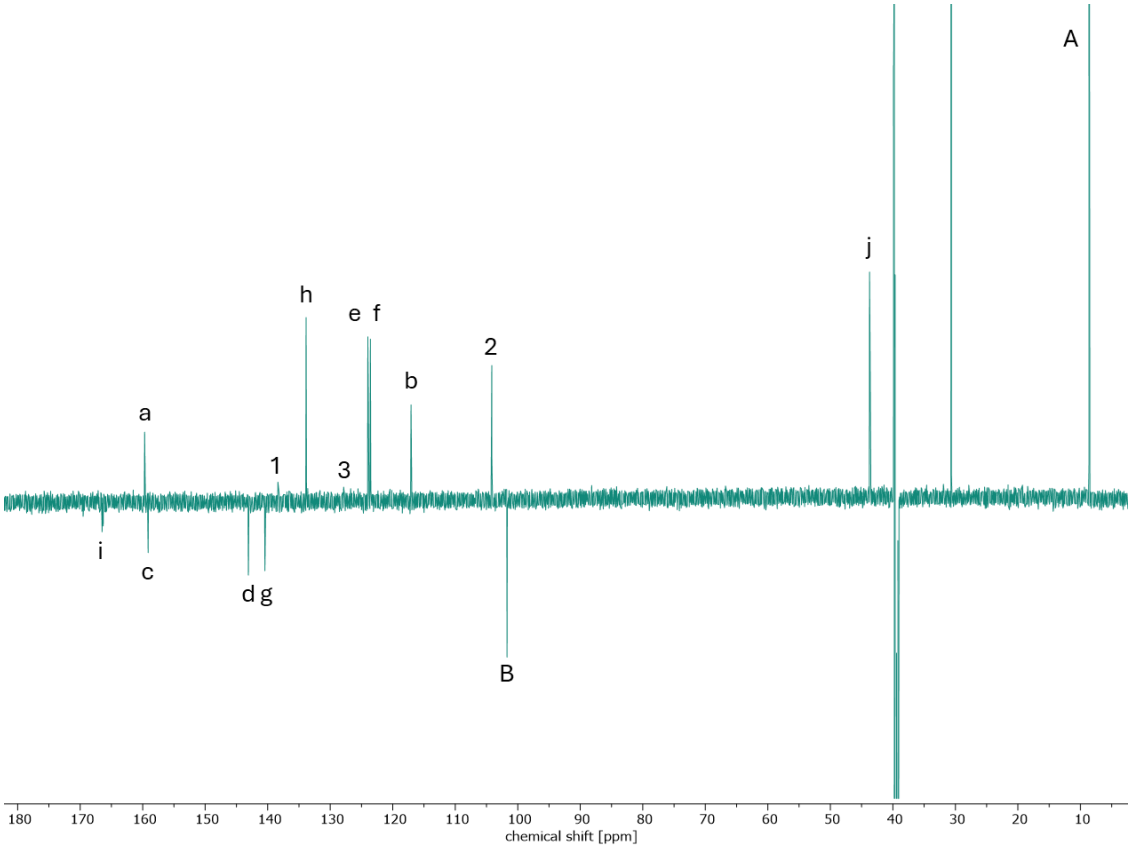

*Figure 29: ^{13}C-NMR spectrum of complex **IV** in DMSO-d^6.*

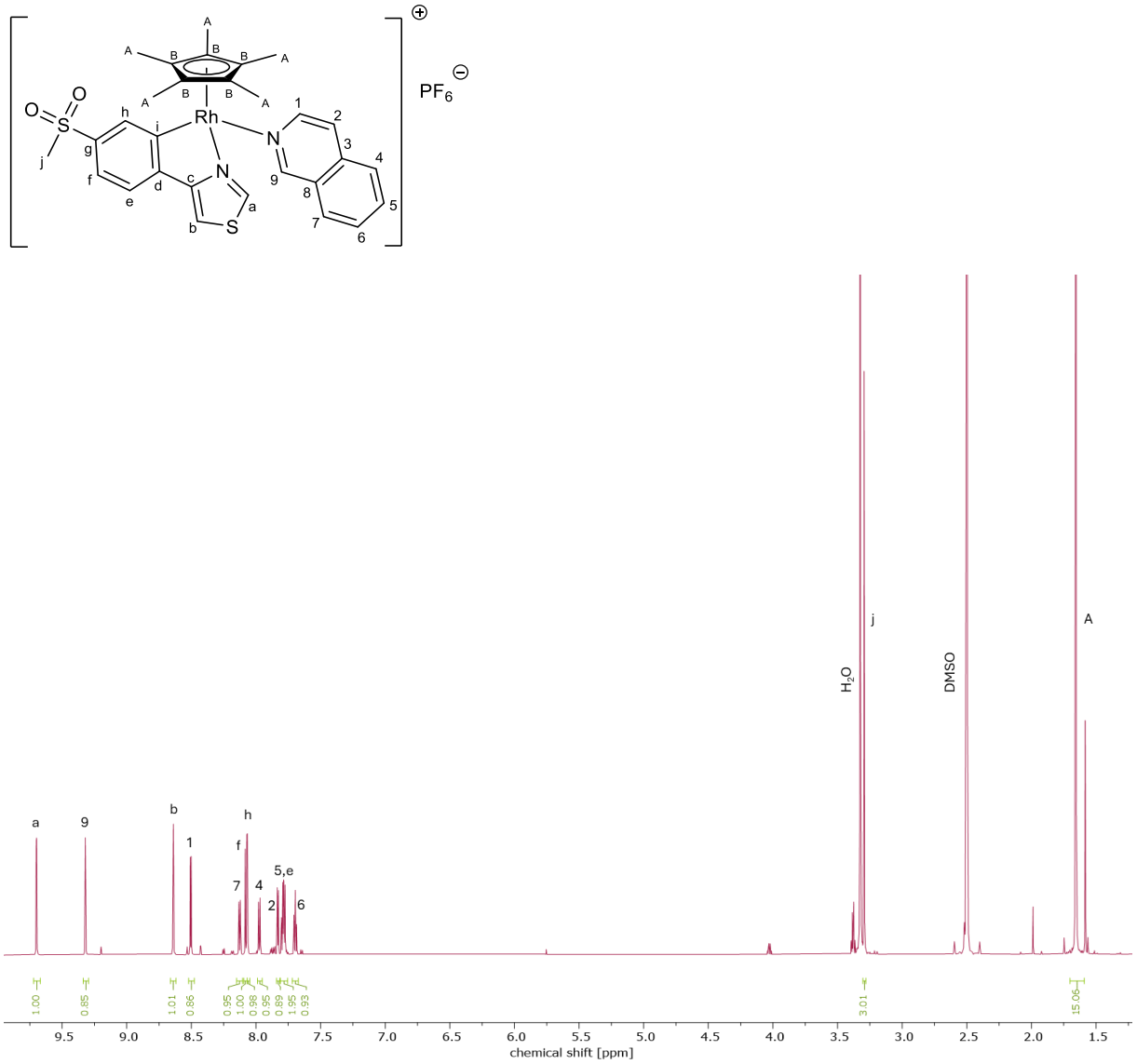

*Figure 30: ^{1}H-NMR spectrum of complex **V** in DMSO-d^{6}.*

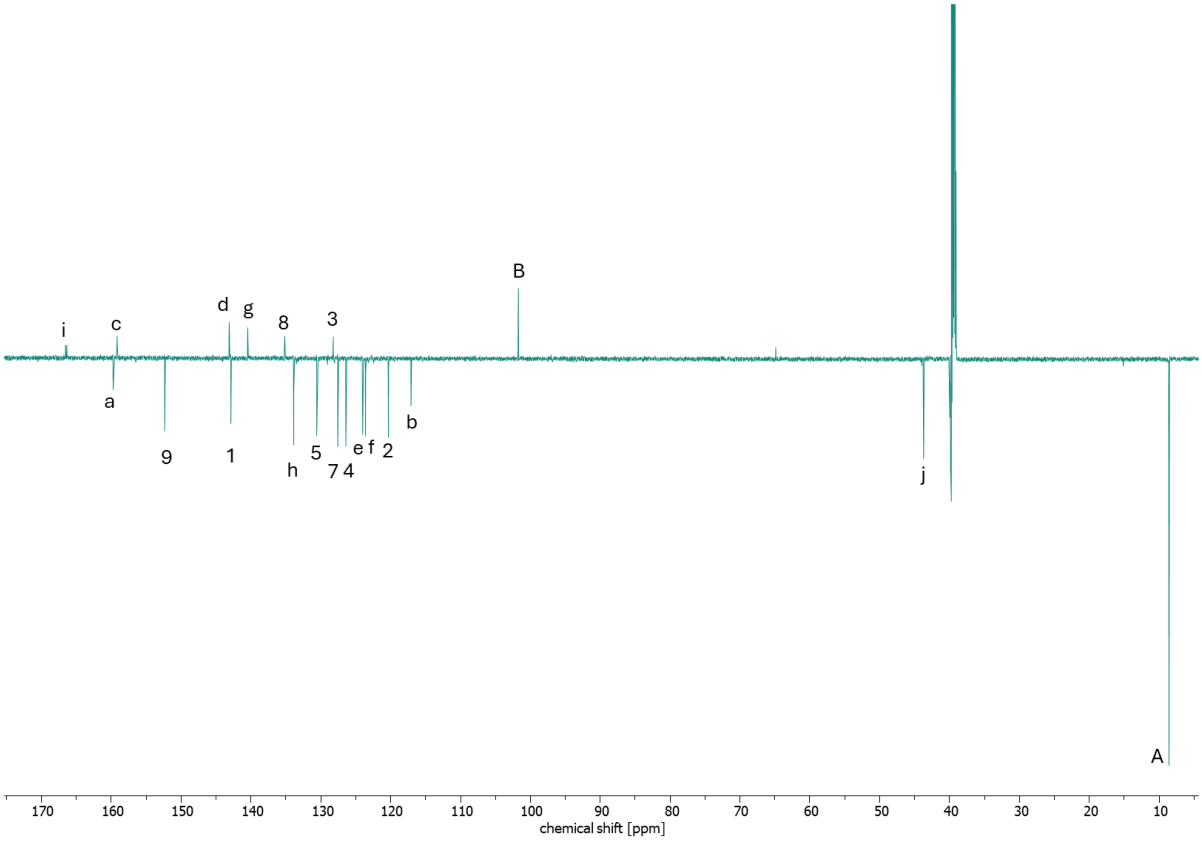

*Figure 31: ^{13}C-NMR spectrum of complex **V** in DMSO-d6.*

Mass Spectra

Complex I

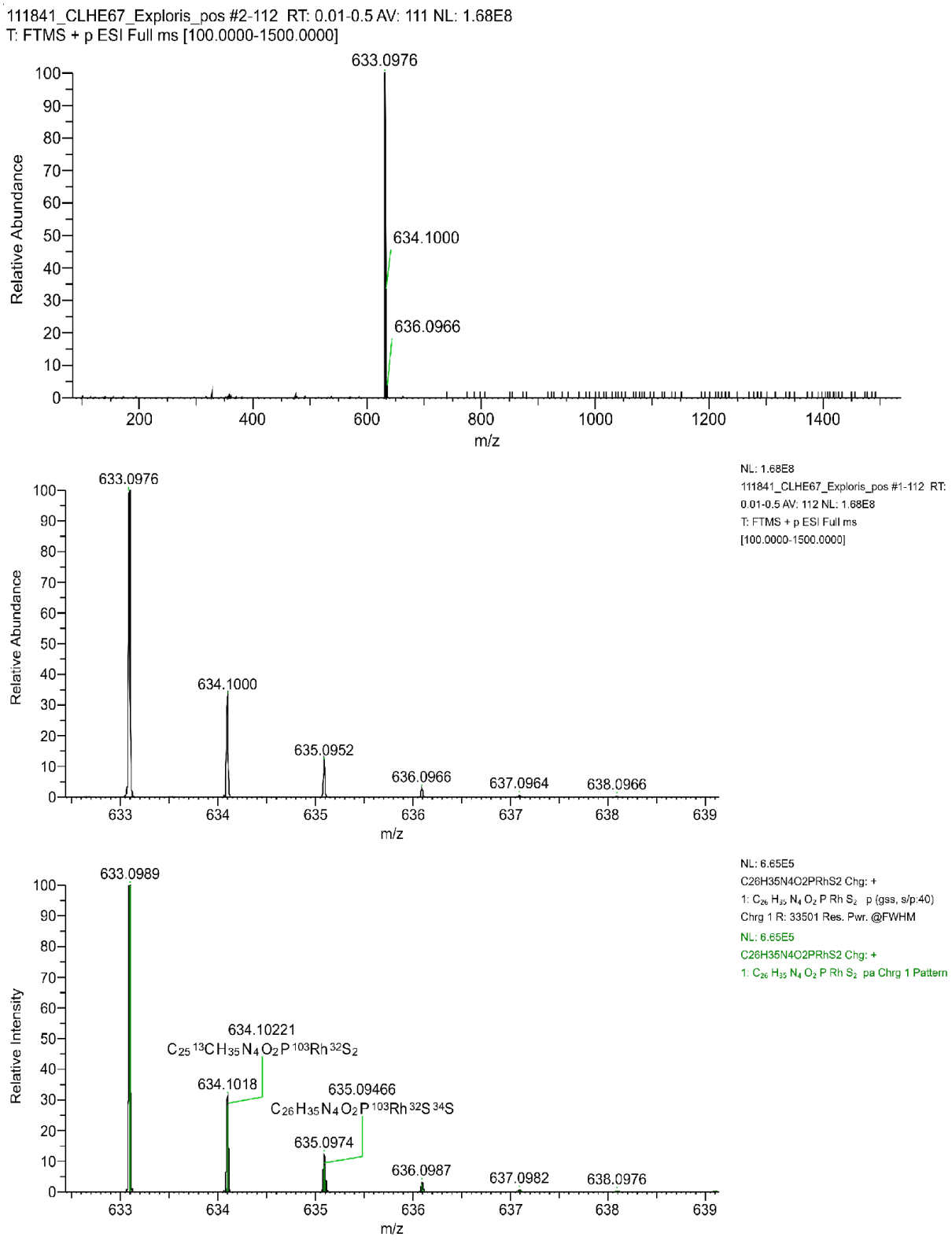

*Figure 32: ESI MS spectrum of complex **I**.*

Complex II

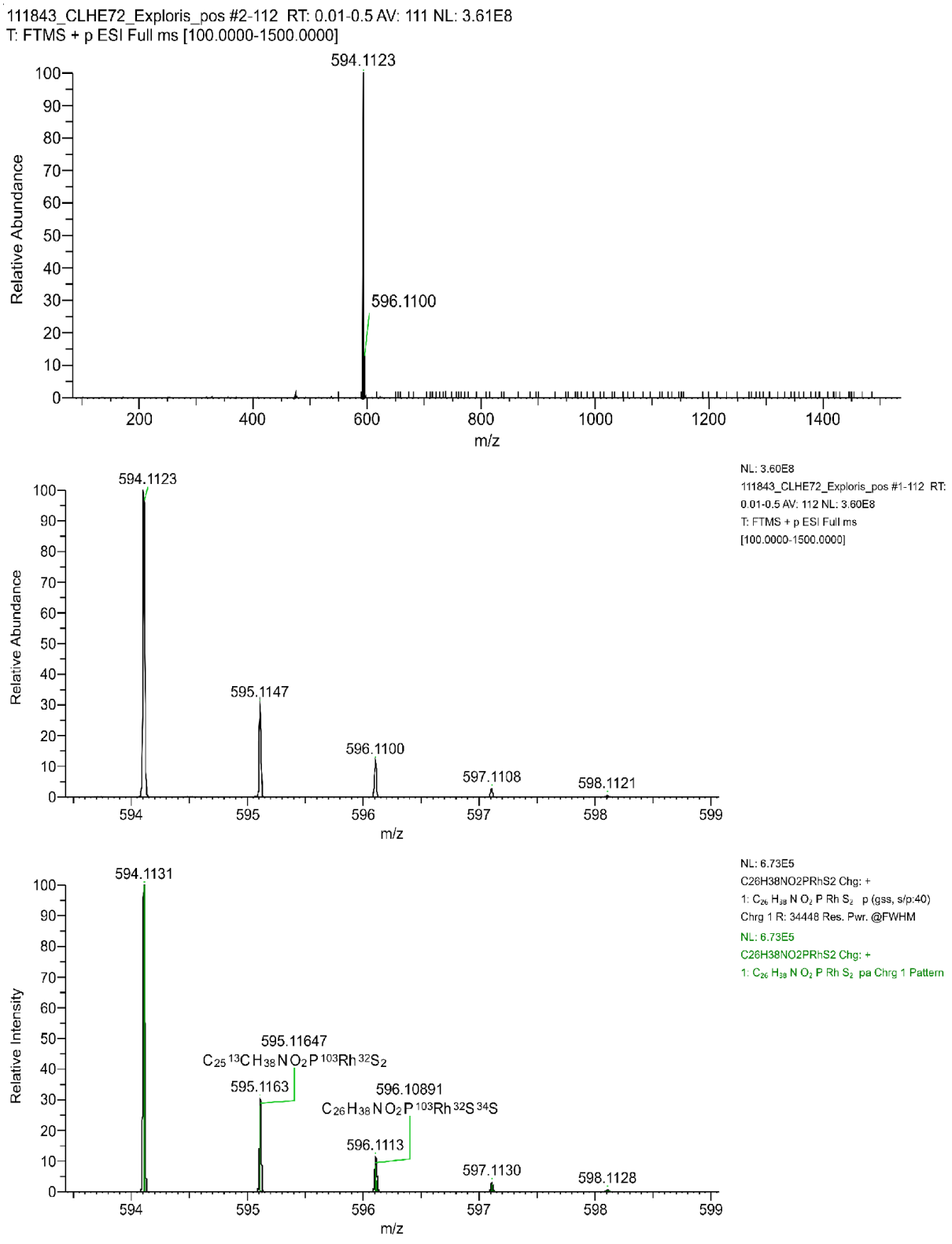

*Figure 33: ESI MS spectrum of complex **II**.*

Complex III

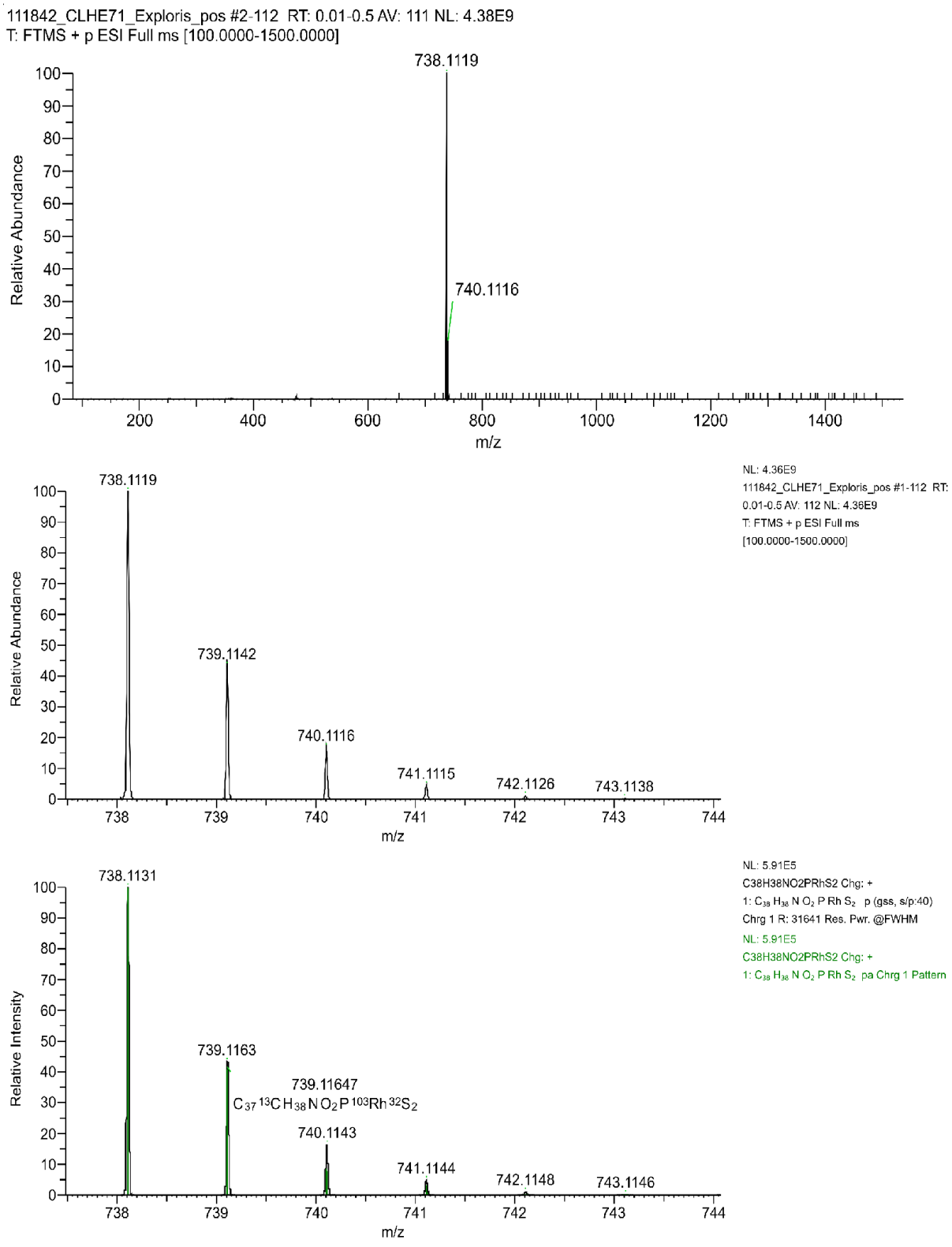

*Figure 34: ESI MS spectrum of complex **III**.*

Complex IV

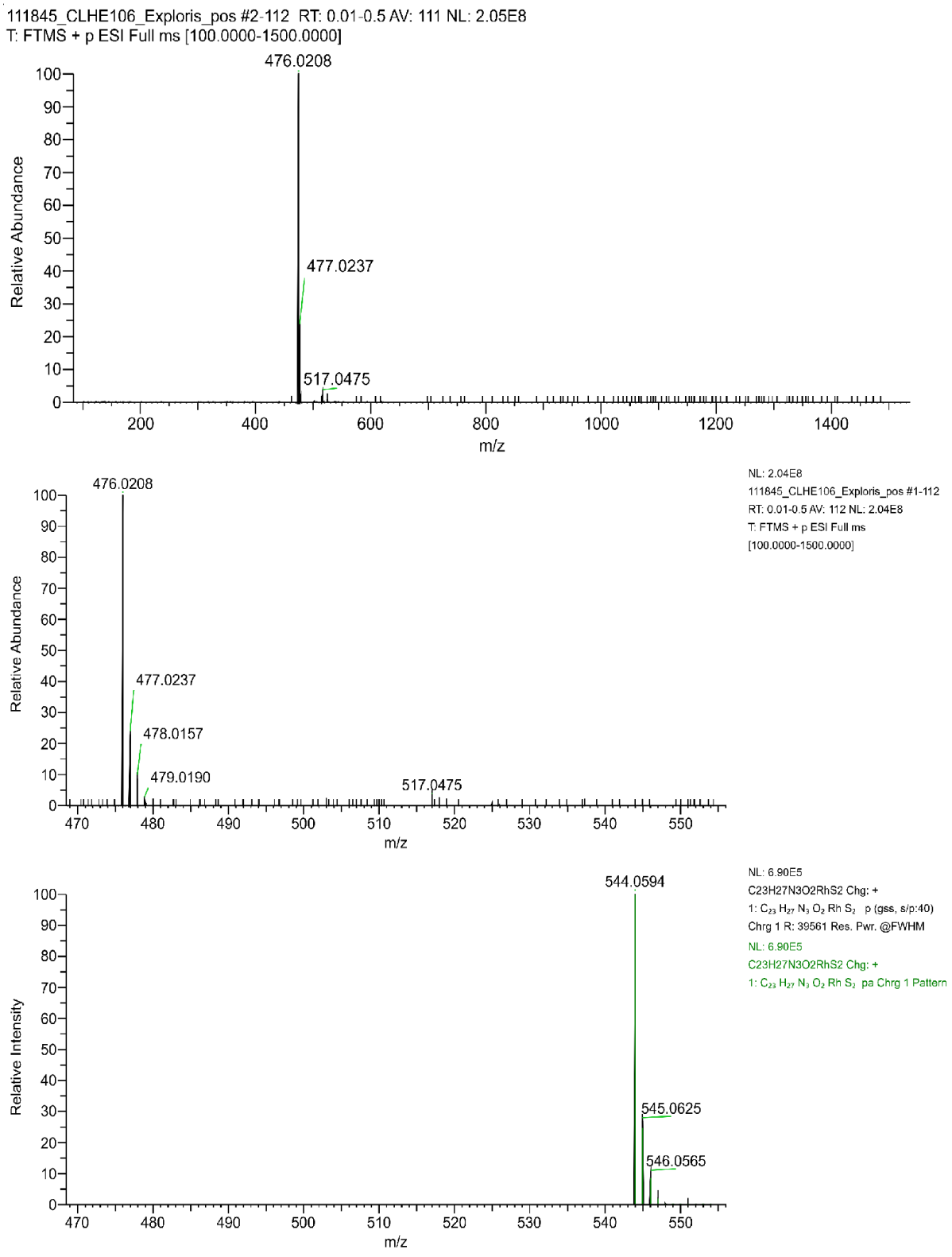

*Figure 35: ESI MS spectrum of complex **IV**.*

Complex V

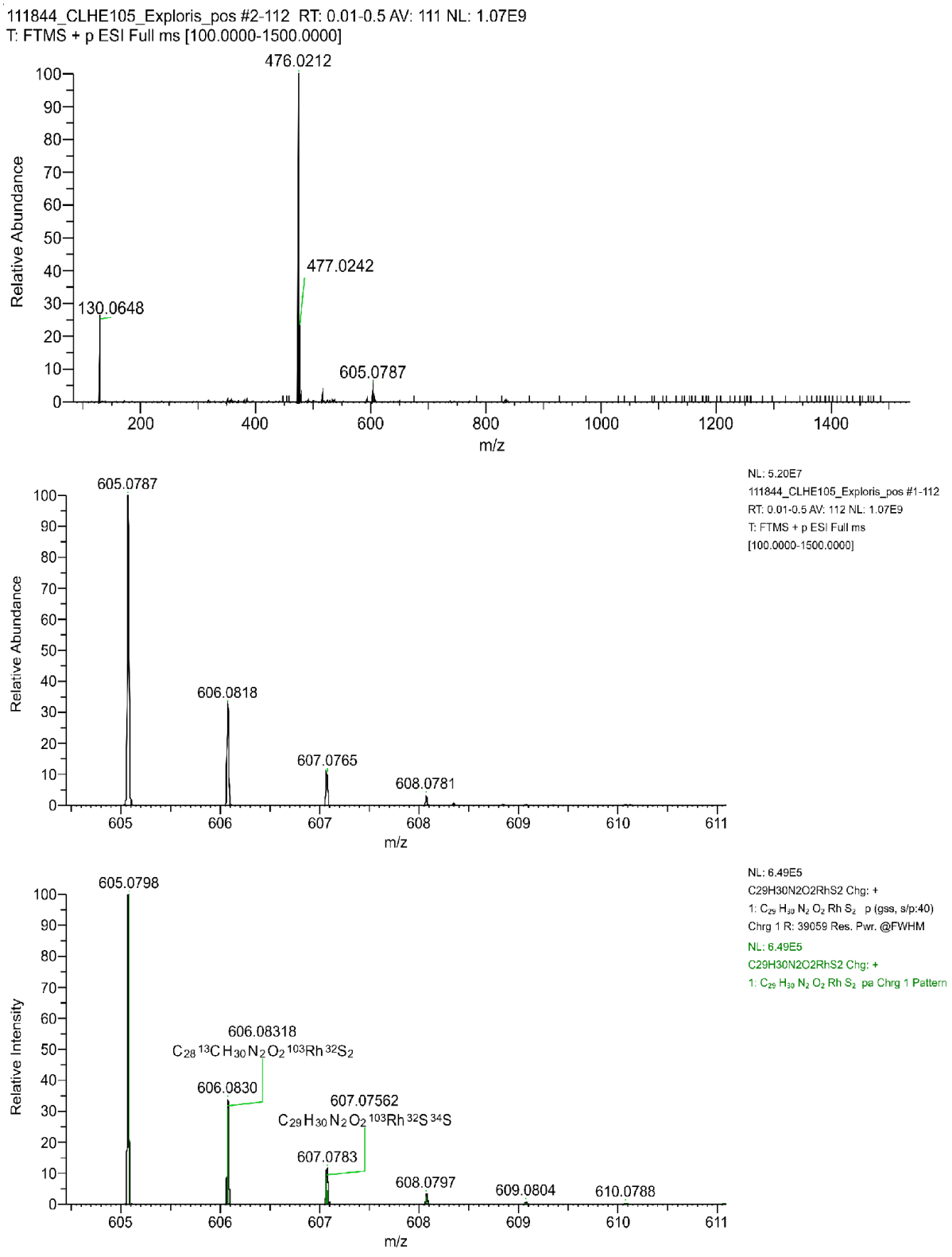

*Figure 36: ESI MS spectrum of complex **V**.*

Complex I

Bond precision: C-C = 0.0085 A Wavelength=0.71073

Cell: a=12.390(3) b=15.354(3) c=17.054(3)
alpha=86.43(3) beta=77.51(3) gamma=74.80(3)
Temperature: 100 K

	Calculated	Reported
Volume	3056.6(12)	3056.4(12)
Space group	P -1	P -1
Hall group	-P 1	-P 1
Moiety formula	C26 H35 N4 O2 P Rh S2, C H2 Cl2, Cl	C26 H35 N4 O2 P Rh S2, C H2 Cl2, Cl
Sum formula	C27 H37 Cl3 N4 O2 P Rh S2	C27 H37 Cl3 N4 O2 P Rh S2
Mr	753.96	753.95
Dx,g cm-3	1.638	1.638
Z	4	4
Mu (mm-1)	1.044	1.044
F000	1544.0	1544.0
F000'	1543.08	
h,k,lmax	16,19,22	18,21,24
Nref	14027	13796
Tmin,Tmax	0.920,0.939	0.983,0.987
Tmin'	0.920	

Correction method= # Reported T Limits: Tmin=0.983 Tmax=0.987
AbsCorr = MULTI-SCAN

Data completeness= 0.984 Theta(max)= 27.499

R(reflections)= 0.0660(7623) wR2(reflections)= 0.1628(13796)

S = 0.948 Npar= 733

Complex II

Bond precision: C-C = 0.0063 A Wavelength=0.71073

Cell: a=12.692(3) b=13.458(3) c=16.731(3)
alpha=90 beta=108.28(3) gamma=90
Temperature: 100 K

	Calculated	Reported
Volume	2713.6(11)	2713.6(10)
Space group	P 21/n	P 21/n
Hall group	-P 2yn	-P 2yn
Moiety formula	C26 H38 N O2 P Rh S2, Cl	C26 H38 N O2 P Rh S2, Cl
Sum formula	C26 H38 Cl N O2 P Rh S2	C26 H38 Cl N O2 P Rh S2
Mr	630.02	630.02
Dx,g cm-3	1.542	1.542
Z	4	4
Mu (mm-1)	0.965	0.965
F000	1304.0	1304.0
F000'	1301.86	
h,k,lmax	17,18,23	18,19,24
Nref	7904	7867
Tmin,Tmax	0.933,0.944	0.965,0.974
Tmin'	0.926	

Correction method= # Reported T Limits: Tmin=0.965 Tmax=0.974
AbsCorr = MULTI-SCAN

Data completeness= 0.995 Theta(max)= 29.999

R(reflections)= 0.0533(3982) wR2(reflections)= 0.1298(7867)

S = 0.988 Npar= 316

Complex III

Bond precision: C-C = 0.0051 A Wavelength=1.54178

Cell: a=16.623(3) b=16.363(3) c=27.809(6)
alpha=90 beta=90 gamma=90
Temperature: 100 K

	Calculated	Reported
Volume	7564(3)	7564(3)
Space group	P b c a	P b c a
Hall group	-P 2ac 2ab	-P 2ac 2ab
Moiety formula	C38 H38 N O2 P Rh S2, C H2 Cl2, Cl	C38 H38 N O2 P Rh S2, C H2 Cl2, Cl
Sum formula	C39 H40 Cl3 N O2 P Rh S2	C39 H40 Cl3 N O2 P Rh S2
Mr	859.07	859.07
Dx,g cm-3	1.509	1.509
Z	8	8
Mu (mm-1)	7.314	7.314
F000	3520.0	3520.0
F000'	3544.05	
h,k,lmax	20,20,34	20,20,34
Nref	7322	7263
Tmin,Tmax	0.620,0.746	0.618,0.786
Tmin'	0.531	

Correction method= # Reported T Limits: Tmin=0.618 Tmax=0.786
AbsCorr = MULTI-SCAN

Data completeness= 0.992 Theta(max)= 71.067

R(reflections)= 0.0448(6141) wR2(reflections)= 0.1186(7263)

S = 1.041 Npar= 447

Complex IV

Bond precision: C-C = 0.0059 A Wavelength=1.54178

Cell: a=10.400(5) b=8.497(3) c=31.769(17)
alpha=90 beta=91.07(3) gamma=90
Temperature: 100 K

	Calculated	Reported
Volume	2807(2)	2807(2)
Space group	P 21/c	P 21/c
Hall group	-P 2ybc	-P 2ybc
Moiety formula	C23 H27 N3 O2 Rh S2, F6 P [+ solvent]	?
Sum formula	C23 H27 F6 N3 O2 P Rh S2 [+ solvent]	C23 H27 Cl0 F6 N3 O2 P I S2
Mr	689.48	689.47
Dx,g cm-3	1.632	1.632
Z	4	4
Mu (mm-1)	7.456	7.456
F000	1392.0	1392.0
F000'	1400.41	
h,k,lmax	12,10,39	12,10,39
Nref	5625	4843
Tmin,Tmax	0.836,0.861	0.616,0.755
Tmin'	0.689	

Correction method= # Reported T Limits: Tmin=0.616 Tmax=0.755
AbsCorr = EMPIRICAL

Data completeness= 0.861 Theta(max)= 73.222

Complex V

Bond precision: C-C = 0.0040 A Wavelength=1.54178

Cell: a=13.793(6) b=21.143(8) c=22.990(12)
alpha=90 beta=90 gamma=90
Temperature: 100 K

	Calculated	Reported
Volume	6705(5)	6705(5)
Space group	P b c a	P b c a
Hall group	-P 2ac 2ab	-P 2ac 2ab
Moiety formula	C29 H30 N2 O2 Rh S2, F6 P, C H2 Cl2	?
Sum formula	C30 H32 Cl2 F6 N2 O2 P Rh S2	C30 H32 Cl2 F6 N2 O2 P Rh S2
Mr	835.48	835.47
Dx,g cm-3	1.655	1.655
Z	8	8
Mu (mm-1)	7.786	7.787
F000	3376.0	3376.0
F000'	3399.51	
h,k,lmax	17,26,28	17,26,28
Nref	6757	6640
Tmin,Tmax	0.628,0.704	0.508,0.657
Tmin'	0.420	

Correction method= # Reported T Limits: Tmin=0.508 Tmax=0.657
AbsCorr = EMPIRICAL

Data completeness= 0.983 Theta(max)= 73.481